Kazakh-British Technical University

UDC 517.972.7 On the manuscript rights

ARTEM VITALIEVICH SINITSA

Analytical Expressions for a Solution of Inverse Convective Heat and Moisture Transfer Equations in The Frequency Domain for Layered Media

8D06103 – Mathematical and Computer Modeling

A dissertation submitted in partial fulfillment of the requirements for the degree of Doctor of Philosophy (PhD)

Supervisor:
Doctor of physical and mathematical sciences
Professor Rysbaiuly B.R.

Abroad Supervisor:
PhD
Professor Capsoni A.
Polytechnic University of Milan

Republic of Kazakhstan
Almaty, 2023

CONTENT

NORMATIVE REFERENCES

This dissertation uses references to the following standards:

1. SN RK 4.04-04-2013, Street lighting of urban communities and rural settlements.
2. Rules for awarding academic degrees dated March 31, 2011 No. 127.
3. GOST 7.32-2001 (changes from 2006). Research report. Structure and rules of registration.
4. GOST 7.1-2003. Bibliographic record. Bibliographic description. General requirements and rules for compilation.

INTRODUCTION

The relevance of the work. The theory of inverse problems is one of the most frontier techniques in non-destructive control analysis approach that allows to study the state of dynamical system without any exploitation termination. However, the lack of analytical solutions in mentioned theory depends on primary issue connected with inverse problems which is ill-posedness of the proposed algorithms. Due to that fact most of numerical investigations also lead to an increase of technical complications in terms of perseverance of the solution at desired accuracy level and convergency rate. In presented study we investigate layered medium terrain via convective heat and moisture transfer analysis with the inverse theory approach that eventually should be utilized for ecological state explorations, but not limited only by that area of use as we will show further. In fact, the appliance of multi-physical model leads to possibility of finding inter-connections among various identification problems. We may identify set of parameters, geometrical domain, boundary, or initial conditions with the help of inverse theory approach, while presented case study with multilayered domain considered as soil demonstrates some typical peculiarities of the suggested methodology and it's both practical relevance and significance. In any environment system soil is presented by the multilayered non-homogeneous structure which works as an indicator factor of the air pollution and ground water purity level. However, to study the deterioration of the air-soil interaction system often requires both investigations on site and laboratory experiments that leads to increase of time and production cost needed for exploitation. With the help of inverse analysis methodologies, we strive to save both types of resources increasing the precision of received results. Although the theory of inverse problems is undergoing rapid development in both numerical and analytical exploitations, most of existed methods are still requiring comprehensive algorithmic implementations.

Accelerated industrial and urban expansion in both developed and developing countries leads to an increase in number of contaminated sites and thus the necessity of keeping the soil pollution rate under constant monitoring. Since the deterioration state of soil structures depends on numerous factors such that porosity level, conductibility rate, ground slope, vegetation and various erosions, there is a set of parameters that should be controlled through the modeling via multi-physical process investigation that is considered in current work.

The inverse analysis methodology for multi-physical models leads to possibility of determination of cross-related parameters that allow us to determine the current state of dynamical system by non-destructive method and keep it under control via constant monitoring, that eventually should be automized. Analytical approach allows to simplify the suggested algorithms, to derive additional tools useful for analyzing complementary non-primary parameters, those which are not terms of the governing equation of the model or take implicit form of action.

Practical significance. In practice it is of high importance to be able to operate with highly trusted data, having precise measurements of parameters for exploration of

any dynamical system. Small error in measurement may lead to disastrous circumstances during the control stage of considered domain. We may consider the design stage of artificial structure or the soil state exploitation, however in both cases there is a necessity to operate with some metrological techniques and involve the measurement of a priory data, which highly affect our posterior judgments over the estimation. Lack of stabilization factors in most cases leads to unpredictable results while implying the inverse analysis methodology. Therefore, analytical investigations should be a useful mathematical apparatus for estimation of key physical parameters and in some cases even fields itself. In almost all cases inverse problems are ill posed problems and numerical investigations lead to complications related to dealing with regularization or strict stability criteria conditions. At the same time the destructive control investigations usually leading to termination of exploitation of the considered process in dynamical system is not preferable by most industries. Sampling of the ground measurements in terms of environmental hazardous circumstances should not be neglected too. In such perspectives suggested methodology of non-destructive control identification acts as useful expertise tool.

Thesis objective. The primary goal of presented dissertation thesis is to design an analytical approach for inverse analysis methodology utilized for exploitation of multilayered medium terrain state by identifying key physical parameters of the considered dynamical system. Such system may be modeled as multilayered soil or key plate structural elements of artificial structures. The methodology designed should be universal regardless of the appliance area, weather it is an environmental or industrial dynamical system and bring new prospective in the study of inverse problems theory applications.

Dissertation work novelty. Suggested state of the art methodology unifies sampled postulates of the theory of inverse problems, operational and variational calculus, selected elements of functional analysis and dimensionality reduction techniques seeking for analytical expressions by observing derived integral relations from the posed general equations that describe multi-physical processes key parameters set identification. Most of inverse theory approaches imply numerical algorithms that give only prescribed error-tolerance as the resulting terms. At the same time existing algorithms mostly deal with one-dimensional cases due to the complexity of posed strict stability conditions or regularization parameters. Although there are useful numerical exploitations that provide smoothed numerical results, in most cases there is an immense demand in such resources as computational cost and time for such algorithms.

Presented methodology allows to reduce three-dimensional case to one dimensional preserving the properties of initial state and give opportunity to expand the area of its application to more than conductivity phenomena, for instance elasticity analysis or vibration theory and electromagnetism by studying quasi-linearized analogues of original problems. The problem of parameters and domain identifications are studied, however the posed functionals may be applied for boundary conditions identification as well with minor alterations. Posed coefficients matrixes of derived systems of linear equations play special role as fertile foundation for further theoretical

investigations as well as the received analytical expressions in frequency and time-dependent domains. Utilization of the spectral analysis exploitations of posed operators has high potential relation to compactness properties investigations of the operator theory.

Personal contributions of doctoral student. Design of computational algorithm for the derived analytical expression and software construction, writing and publishing research papers in international reviewed scientific journals with impact factor included in both Scopus and JCR databases, participation in popular-science faculty seminars and international scientific-practical conference.

Approbation of results. The dissertation work results were reported on:

- Popular-science seminars of Faculty – School of Applied Mathematics at Kazakh-British Technical University.
- Semestrial research work of doctoral students reporting meetings.
- Materials of VIII international scientific-practical conference: «Science and education in the modern world: challenges of the xxi century» - 2021, April.
- Published research article in first quartile journal according to Journal Citation Report and 96 Journal Impact Factor percentile according to Science Citation Index Expanded following up to date JCR issue.
- Published research article in first quartile journal according to Journal Citation Report and 79 Journal Impact Factor percentile according to Science Citation Index Expanded following up to date JCR issue.
- Experimental case study comparison with computational algorithm results derived by analytical investigations for conductivity posed problem.
- Research internship collaboration at Polytechnic University of Milan, department of mathematics, Milan, Italy.

Provisions submitted for defense.

1. Derived analytical expressions and designed computational algorithm for inverse problem of multi-physical processes of thermoelastic deformation and heat and moisture transfer.
2. Expanded designed methodology towards quasi-linearized dimensional reduction of thermoelastic stress analysis model along with the exact expressions of mathematical model explorations.
3. Discovered properties of the transformed operators in the frequency domain in terms of the nulls identification of characteristic polynomials around attenuation parameter and further construction of transformation decomposition for construction of transcendental equations.

Dissertation work structure. The presented thesis consists of 104 pages, 27 figures, 4 tables, introduction, three main parts, conclusion, references and 3 appendixes.

In the **first part** there is a description of main postulates, formulations of the inverse problems theory and literature review of the existed investigations on discussed

topic along with discussed peculiarities of posed models investigated in presented work.

The **second part** of presented thesis provides general mathematical formulation of the posed problem, main derivations, and proofs along with the algorithm description and some aspects of the analytical expressions and posed experimental measurements for the practical part.

The **core** of the thesis is located in the **third part** of the work and intended to give general overview of the obtained results and their analysis for variety of the posed models.

1 INVERSE ANALYSIS METHODOLOGY APPLIED FOR EQUATIONS OF MATHEMATICAL PHYSICS GENERAL OVERVIEW

This chapter presents general overview of the methodology for inverse theory problems applied for the partial differential equations, it contains main peculiarities, some historical overview of existed approaches along with the previous theoretical investigations. It also describes variations of the posed models with discussions over advances for each of them.

1.1 The development of the theory of inverse problems methodology

Although the basis mathematical formulation of the inverse problems theory was firstly introduced in the second quarter of the XX century by Soviet-Armenian physicist Viktor Ambarzumian [1] during his examination of the inverse Sturm-Liouville problem for determination of the vibration string equation, most of the implementations of the theory were conducted intuitively throughout the history of the humankind. The conceptual idea of the inverse problem theory lies in inversion of the cause-and-effect relationships. Initially, we should describe the idea of the direct problem, when for obtained set of input parameters, well-defined geometrical characteristics and continuously posed initial-boundary conditions we aiming to determine the field or some other quantity of interest via sequentially received solution or numerical algorithm. In this case from the given causes, we determine their effects over investigated domain and the relationship is direct in such case. Whereas in the case of the inverse problems, we are determining the causes by observing the effects that they are producing. Therefore, we may declare that such analogues of the inversely posed problem were always processed by individuals who were aiming to determine the reasons for observable phenomena at some point. For instance, around 375 BC the Greek philosopher Plato in his work Republic described a famous allegory of the cave [2], where people were reconstructing an image of the object by observing its shadows on the cage's wall, this is a typical example of the inverse problem. Another ancient philosophical epistemology that produced a great usage of the inverse analysis methodology was presented by Aristotle's arguments for the sphericity of the earth [3], where he provided evidence both theoretical and empirical. One of the arguments was made by observing the segments of the shape of the moon's eclipse, stating that it always preserves a convex form. Another fruitful proposition Aristotle derived by observing the night sky, stating that by changing position on Earth surface, some spectator will discover different allocations of stars, that is not possible in a planar shape case. More advanced philosophical formulations of the inverse theory problems were enriched by Immanuel Kant in his Critique of pure reason transcendental psychology revising epistemology and metaphysics of a priory conditions of the human cognition [4]. Such formulations gave basis for defining the nonlinear connections between posterior epistemology and preliminary estimations over the studied object or process, which lied in the foundation of inverse problem classical formulation. Such formulation always operates with additionally given data, that is a priory epistemology,

and that is the key element which is necessary for obtaining solution of the inverse problem, which itself is a posterior estimation over investigated matter. From engineering perspectives, first general contributions to the study of the theory of inverse problems were done by mathematician and physicist John William Strutt [5], when he was making experiments with string vibrations and by the frequency of its oscillations determined the strength and other elastic parameters of that string performing purely inverse analysis methodology. Around the same time Konrad Schlumberger performed his experimental resistance method, when by electric propulsion injected through the soil medium, he measured an electric potential of the ground [6]. These illustrative examples represent how throughout the development of technological stage, the theory of inverse problems was undergoing dynamical and rapid historical evolution. Depending on the increase in necessities of engineering industries different classes of the inverse theory appeared. The inverse coefficients problems are setting in order to determine the coefficients involved either in governing equations or initial-boundary conditions for considered process. Other classes of inverse problems like identification problems are dealing with the domain reconstruction by determining the geometrical properties of considered boundaries. In some cases, it is possible to identify the boundary condition itself and by solving the retrospective inverse problem we may obtain initial conditions of considered dynamical system.

Principal property of mostly all inverse problems is the ill-posedness due to sensitivity of obtained solution regarding the input parameters. Initially introduced by Hadamard [7] in the beginning of the XX century notion of well-posedness for mathematical models describing physical phenomena, requires existence and uniqueness of the solutions along with continuous dependence on the data, - the former requirement closely connected to stability concept. In case of inverse problems all three criteria could be violated. However, for most cases the inverse problems require regularization procedure in order to overcome the third criterion. Various approaches appeared throughout the evolutionary development of the inverse problems. For instance, the automatic selection of regularization parameter in Tikhonov regularization, based on the generalized cross-validation method [8] and appear to be a numerical optimization algorithm. Meanwhile the convergence issues near the global minimum are addressed by the changing the variables in optimization problem or modifying the least-square problem. However, the obtained estimates effectiveness is typically presented by conducted numerical experiments and this is another feature of inverse problem evaluation procedure. In recent times, different modern methods have been developed to solve inverse transfer problems, such as heuristic search method [9], neural network-based method [10], and dynamic Bayesian network method [11]. The numerical computations, even though it may be quite efficient for determination of inverse problems key goals, are not supplying us with functional relationship between characteristics and effects of influencing factors and the time for analytical computations in most cases is rather short. However, the analytical estimators require simplified geometrical configurations and should be explicit as was revealed in [12].

Some additional methods to deal with the irregularities were actively investigated in recent time. One of such examples is the machine learning based approach for inverse identification of heat flux demonstrated in [13], where authors presented an efficient and robust inverse approach to obtain the heat flux distribution on the tool rake face in a case of oblique cutting, which was including the tool nose radius investigations, studying the dependency of the proposed algorithm on the number of input data, the optimization strategy sampling, and the general performance of the selected ML-based approach. Another example is an inverse estimation of boundary heat flux using particle swarm optimization method is described in [14], where authors apply different Artificial Neural Network models to facilitate faster computations and perform the Particle Swarm Optimization combined Bayesian framework to quantify modeling error. At the same time, good example of empirical data utilization could be found in [15], where authors present a study of inverse natural convection-conduction heat transfer for in-line tube heat exchanger in a hot box with experimental data, stating that the accuracy of the chosen flow model as well as the near-wall treatment requires detailed experimental verification, since it can affect the accuracy of the numerical results obtained. Thus, authors conclude that the selection of an appropriate flow model is important. There are also some Bayesian models used to solve a two-dimensional inverse heat transfer problem of gas turbine discs described in [16]. Authors state that Bayesian method could be built to calculate heat transfer on both the upstream and downstream surfaces of discs from simulated temperature measurements, reducing the ill-posedness of the inverse problem. In such case, the accuracy of the Bayesian method depends on the sampling of the standard deviation in the prior distribution, and according to findings, the best accuracy is obtained when it is twice the maximum of posed Biot number. Solution of an inverse heat conduction problem with third-type boundary conditions well reflected by [17], where the authors developed an algorithm to solve inverse conduction problems by matrix inversion. The posed algorithm was applied to a slab with Robin boundary conditions on one wall, in a case when the tests were conducted for both simulated and experimental temperature distributions. Overall, authors verified that the algorithm is indeed accurate and tolerant of noise when the sampled data are adequately filtered. Some inaccuracies in the inverse heat conduction problem solution and their effect on the estimation of heat fluxes were described in [18], where the authors demonstrated that there are unavoidable issues that inherent to quenching experiments that may lead to significant overestimation of the surface temperature in the initial instants of the experiment, stating that is undesirable to relate the surface temperature estimation with boiling regime at initial conditions. Inverse analysis of mould-casting interfacial heat transfer towards improved castings could be found in [19], where the authors present a correct information about the interfacial heat transfer coefficient (IHTC) at the mould-casting interface, while the quality of caste materials is crucially dependent on the rate of change of heat transfer across the mould-casting interface during the process of solidification and cooling of the investigated casting materials. In some cases, the utilization of the special function is applied, like the Trefftz numerical functions used for solving inverse heat conduction problems, that are widely discussed in [20].

Authors present a concept of solving the inverse heat conduction problem with the utilization of a linear combination of functions that satisfy the differential equation in terms of identity property. It was proved that sampled Trefftz functions construct a complete system of functions necessary to develop the solution to the heat conduction equation. However, in a case of radiative heat transfer the governing equation is ill-conditioned and requires a special technique called regularization to make it amenable to stable numerical solution. For instance, some well-known techniques, such as Tikhonov regularization, and truncated singular value decomposition are discussed for such inverse problem in [21], where the authors discuss the results on methods based on metaheuristics, namely simulated annealing as well as some machine learning techniques based on neural networks. Ther are also discussion over numerical and experimental verification of the single neural adaptive technology with real-time inverse method for solving inverse heat conduction problems in the study [22], where authors show that the derived algorithm has stronger anti-interference ability and adaptability, based on ingenious experimental platform that was designed. In mentioned study, authors estimate unsteady boundary heat flux of one-dimensional heat conduction problem via the numerical and experimental tests, which verifies the effectiveness of the proposed inverse method. At the same time, in [23] authors discuss the forward problem data, interpolating functions that are developed to relate source heat input and location to temperature samples on the wall, downstream of the source. Advancing the posed problem, by posing the prediction of 3D natural convection heat transfer characteristics in a shallow enclosure with experimental data, authors discuss suitable flow model in [24], stating that obtained estimates are consistent with the existing correlation. It was also observed that thermocouple response time affects the heat flux estimates with inverse methods in [25], where authors proposed new correction method for applications with fast cooling or heating by using simplified model and a calibration test to estimate the response time, evaluating the effects of the thermocouple noise, data filtering and heat loss. In some cases, for stable sequential solution of inverse heat conduction problem, the optimal hybrid parameter sampling could be applied. For instance, the proposed ridge estimator in [26], which is based on the sum of the bias and variance errors of the heat flux, where authors derived new stability condition for sampling the governing coefficient by separate control of the stability of input and initial errors data in order to deal with the ill-posed nature of the inverse heat conduction problem. There were also successful examples of using exact solution of the heat conduction equation, presented in [27], when authors were investigating the surface heat flux in planar water-jet cooling of moving hot solid and obtained the heat flux profile of thin plate along with the high spatial resolution. It also correlates with the implementation of the Fourier's inverse problem when it could be supervised by the optimization problem for determination of the thermal diffusivity [28] by minimizing the residual function between the model predictions and the experimentally sampled data. Another study presents a novel approach for solving inverse heat conduction problems in case of one-dimensional domain by considering the moving boundary and temperature dependent material properties, where authors described in [29] two thermocouples that were used to measure temperature at two

interior locations inside the considered medium while the front boundary used to experience a recession process, that is moving towards the back surface. They have concluded that the developed method can be applied for calculating the surface heat flux in applications that involve case with moving boundary and large temperature variations such as the ablative thermal protection system. The local heat transfer investigation could be also utilized for characterization of thermal behavior of a micro pulsating heat pipe as was shown in [30], where authors described the temperature distribution of condenser by measuring data using the infrared camera and by solving the inverse heat conduction problem estimated the local heat flux discussing the variations of input data. While modulating heat transfer characteristics, it could be shown that some effect of rotating fluid with Taylor column phenomenon may occur, as was discussed in [31], where researchers presented a comparative study made between low Reynolds number heat transfer and steady high Reynolds number heat transfer revealing a broad perspective into the flow-physics of the problem. At the same time, there are cases when the inverse problem approach was used for investigation of solid concentration in solid–liquid two-phase flow, like the authors in [32] demonstrated for the case with horizontal pipeline, using the correction method for estimations based on forward problem error and estimating the solid concentration rate. Meanwhile the another aspects of inverse problem posedness, like the impulse response methods can be used to quantify the surface heat flux in multi-layer materials as was described in [33], where authors presented results over case study for components in which there are limited subsurface (internal) temperature measurements providing a foundation for deducing the heat flux estimators from a subsurface heat flux sensor, maintaining a high-frequency response. The non-iterative inversion of loadings could be utilized in case of isogeometric boundary elements as widely discussed in [34] when considering the transient heat transfer problems in cases of inhomogeneous materials. The authors investigate application of the implementation of basis function expansion and regularization scheme improving the accuracy and noise resistance of boundary condition inversion. It also correlates with thermal boundary condition modeling via the inversion modeling based on Green's function and regularization method as was presented in [35] where authors considered commercial aircrafts, precisely the inner wall of aircraft cabin, presenting additionally the model validation through the experimentally received data. Regardless of the numerical approach, an analytical methods of the inverse problem utilization could be also applied for empirical investigations, as was presented in [36], where authors investigated the periodical heat transfer problems of multilayer rocks calibrating the thermal energy storage in case of underground mines, revealing some crucial aspects of applicability and accuracy of the proposed analytical solution and valuable guidance for proper layer sampling. Beside that, some topological designs could be also utilized for forced convection heat transfer problems, as was presented in [37] by considering the deep generative model or solving complex topology optimization problems regarding the laminar and turbulent heat transfer problems solutions. Along that, the cooling configurations could be determined via the local heat transfer characteristics by experimental approach as described in [38], where the authors reveal results over analysis of inverse heat

conduction problem by discrete energy balances considering transient heat transfer measurements. Meanwhile another methodology such as the element differentiation method could be utilized transient heat transfer problems with phase change, as well studied in [39] for the phase change case, when the interface nodes and the outer boundary nodes were correlated with the flux equilibrium condition that resulted in estimator derivation for the validation of the effectiveness and accuracy of proposed methodology. Some other variations of the posed problem could be found in [40], where authors present a valuable result by considering the mechanism of heat transfer in two-layer porous materials with the heat generation stating that the total energy balance in system becomes zero according to thermodynamic law. Although, the study was conducted by purely numerical approach, authors have revealed some useful aspects for the proposed approximation algorithm, such as the sensitivity to the input data. Another coefficient identification problem solved by the integral local parameters identification coupled with the least squares method was studied in [41], where authors determined fluid specific heat capacity and heat transfer coefficient based on multiple-case joint analysis in heat exchangers proposing a novel methodology and computing the relative identification errors. Physically different type of proposed problem in terms of circumferentially non-uniform heat flux was investigated over the effect of flow boiling heat transfer in a horizontal tube and described in [42], where authors determined heat transfer coefficients via an inverse problem model and concluded that pressure drop was not affected by the heat flux condition. The heat and mass transfer in micropolar nanofluids flow numerically analyzed in [43] by the finite volume approach. The authors have revealed that a high vortex viscosity parameter value produces a weak rate of concentration field and has significant behavior in a case when thermophoresis parameter. Interesting findings of the heat transfer of single-jet impingement cooling may be found in [44], where authors have discussed an experimental case study, revealing conditions for obtaining macroscale data of the cooling process, while the dissipated heat flux was estimated by solving a 2D inverse heat conduction problem. Another application of the eigenfunction-based solution could be found in [45], where the authors presented one-dimensional solid-liquid phase change heat transfer problems solution with advection considering variety of the problem parameters, including Stefan and Peclet numbers, improving the theoretical understanding of phase change heat transfer in the presence of advection.

Another important aspect is the nonlinearity, which also affects the posedness procedure of inverse problem methodology. Such an example of investigations may be found in [46], where authors propose a surrogate model based with active interval densifying method provided for solving the uncertain nonlinear inverse problem. The study also presents a numerical experiment with its feasibility, computational accuracy, and efficiency level. Alternate research [47] shows the direct and inverse reconstruction of the heat flux via the multiresolution formulation with temperature measurement devices located over multidimensional solid in hypersonic flow. The approach is based on development of quadrature formulas for the convolution product construction between special wavelets and Green's function basing on iso-parametric mapping of three-dimensional geometries. Another example is the heat and mass

transfer of nanoparticles on mixed convective flow studied along with the impact of Richardson number in [48], where authors considered non-Newtonian liquid, revealing the existence of the solutions for the critical values of governing parameter. The establishment of the heat transfer model of solid rocket motor nozzle expansion section based on roughness wall with the help of empirical and numerical computations is presented in [49], where researchers demonstrate that the proposed segment method gives the error between computed parameter by the proposed heat transfer model and numerical experiment is controlled within 21% and 13% in the first and second segments respectively, and that he increase of the depth of temperature measuring devices in different segments accelerates the corresponding time response. Another experimental study on heat transfer performance and pressure drop characteristics is discussed by group of scientists in [50], where presented results demonstrated that the pressure gradients and friction factors with the standard Shah and Darcy's correlations are in good agreement with the local and average heat transfer coefficients. The question of the inverse transfer function identification studied for high-frequency pressures in [51] by the special pressure generators with different geometric parameters for the proposed methodology. The conductance of the multidimensional simulations of the heat transfer problem over the rectangular cylinders discussed in [52], where authors discussed the relationship between the Nusselt numbers with flow regimes. It was revealed that aspect ratios amplify the total heat transfer due to an enlargement in the heat transfer surfaces in a case of forced convection around isothermal cylinders. Another inverse improvement of the thermal performance was suggested in discussion of numerical experiments in [53] performed by authors for the ribbed channel in a case of pentagonal geometry with V-shapes. It was derived that the pentagonal V-shape geometry of a rib has higher thermal-hydraulic performance along with a slight high the pressure loss penalty rate. The analysis of heat transfer at polymer interface during over-molding was developed via study of thermoplastic elastomers discussed in [54], where authors used an inverse heat conduction problem to derive the time evolution of the surface temperature for the inserted and the injected material while computations were done by unidirectional scheme with the boundary conditions determined empirically. The singularly perturbed stationary models of heat and mass transfer implemented with a nonlinear thermal diffusion coefficient studied for multidimensional thermal structures in [55]. The new approach was presented by implementation of the asymptotic analysis methods and solving the inverse problem of reconstructing the temperature dependences. While the distributed heat transfer coefficient was investigated in a case study of CPU cooling in [56], where the authors presented optimizing integrated heat spreaders and revealed that the multi-objective optimization schemes produced the best overall heat transfer coefficient derivation. Another special Darcy Forchheimer flow of hybrid nanofluid was analyzed in heat transfer analysis study of a group of researchers in [57], where authors performed the analysis for the multiple shape effects over a curved stretching surface by transforming the equations into a collection of first-order problems using the shooting method. The phase-field methodology for interfacial heat and mass transfer in two-phase flows was described in [58] ,where authors demonstrated the computational model and found that

two-scalar model is much more accurate for realistic problems with large diffusivity ratios numerically predicting the evolution of heat and mass transfer rates. The falling film sensible heat transfer in a case of round horizontal tubes was numerically simulated in [59], where the authors also compared the local heat transfer coefficient distribution with the analytical heat transfer models in order to predict the heat transfer performance over horizontal tube surfaces. The study of flash pulse infrared thermal wave testing presented in case of three-dimensional ice shape detection was completed in [60] with the help of Levenberg-Marquardt (LM) method based on the inverse heat transfer problem leading to further discoveries in exploration of effective accurate and quantitative identification methodology. Some comprehensive correlation performed for the prediction of the heat transfer rates were numerically simulated in [61] for a case of a single droplet in dropwise condensation regime in order to determine the conduction heat transfer parameter in a sessile droplet geometry for a large range of dynamic contact values angle and Biot number parameter. The performance of the mini channel heat sinks was enhanced by utilizing the corona winds and investigated numerically in [62] via a full-scale three-dimensional model. The authors deduced that the electric field creates a vortex which in turn also causes the flow of mixing in the vicinity of the heated surface, disturbing the thermal boundary layer, which results in consequently increase of the heat transfer rate due to parameters configuration altering. Another novel inverse analysis methodology was presented in [63], where authors solve inverse identification problem for determination of the temperature-dependent thermal conductivity in transient heat conduction problem with the help of element differential method combining it with the Levenberg-Marquardt algorithm. Authors results show that the proposed method gives good accuracy level, efficiency and robustness in identifying the temperature-dependent thermal conductivity dealing with non-linearity with the help of special function iteratively optimizing the objective function optimizing the unknown thermal parameter. Successful utilization of the integral transform could be found in [64] in a case of heat transfer analysis of compressible laminar flow regime in a parallel-plates channel geometry for a coupled nonlinear mathematical model via the Generalized Integral Transform Technique (GITT) that is the hybrid numerical-analytical method. The [65] presents study over derivation of an inverse problem solution in a case of vertical plate cooling in air as a comparative study, where authors deduced new formula for the Nusselt number via the temperature measurement methodological approach. Some classical results are modernized by implementing the novel adjustments, such as the fractional Caputo-Fabrizio derivatives studied in [66], in terms of analysis of heat mass transfer of generalized second grade fluid, where authors solve the system of governing equations through Laplace transform including in study the effects of chemical reaction, heat source and porous media. It could be also observable that turbulent mixed convection flows inverse problem can be solved via the surrogate optimization approach, as demonstrated in [67] by researchers, where they utilize the space-time Riemannian barycentric interpolation and deduce genetic algorithm approach for inverse parameter identification showing delivery of good approximations of the optimal solutions within less than two minutes. The heat transfer performance of the conjugate heat dissipation

effect in high-speed rotating free-disk system of aero-engines was comprehensively evaluated in [68], where authors deduced that the heat transfer temperature and Nusselt number parameter of the free disk are strongly correlated along with the rotating Mach number and rotating Reynolds number parameters values, revealing by the analysis that the heat dissipation is a critical factor that affect the accurate determination of the heat transfer performance for the turbine disk. Alongside, the carbon nanotubes under an electric field heat transfer performance due to natural oil convection was investigated in [69], where researchers found useful multiparameter correlation for better understanding of the impact of variety of physical coefficients on the heat transfer in annular spaces, revealing also that it may help to predict exact values of the Nusselt number. The reliability assessment for non-stationary random thermal load was analyzed by stochastic heat transfer model via the explicit time-domain method in [70], where it was deduced that suggested approach may be extended for general stochastic problems governed by various physical laws, and with the help of explicit expressions, the statistics of the considered random system responses could be efficiently determined. Some benchmark solutions are presented in [71] ,where the authors considered the heat and mass transfer model for nanofluid flow over porous domain of cylinder geometry with chemical reaction participation and viscous dissipation effects performing a parametric study and deducing that the curvature parameter value directly affects the local skin friction coefficient and velocity value as well. The inverse uncertainty quantification problem in transient models solution has correlation with the effects of mesh refinement, as was investigated in [72] by a group of researchers, where they have revealed that the computed relative absolute error between empirically sampled data and code prediction results was critically decreased upon incorporating the input parameter uncertainties that were determined with the help of maximum likelihood estimate and the maximum a posterior methodologies. Some useful review on the heat transfer in a case of asphalt pavements along with urban heat island mitigation methods could be found in study [73], where it was demonstrated that insulation materials also increase the surface temperature of the asphalt mixture, meanwhile in a case when the higher thermal emissivity is available, a lower surface temperature could be observed by altering the thermal conductivity parameter value. The inverse analysis could be also utilized for determination of temperature distribution in cold forging as was shown in [74], where authors demonstrate that it is recommended to obtain the proper value of Taylor-Quinney coefficient from an inverse procedure since it may vary due to material and processing condition. The coupling of the finite difference and Monte-Carlo methods in the direct simulation could be utilized for moving impingement heat transfer in a case of three-dimensional rarefied hydrogen gas jet as presented in [75], where the researchers deduced the structural parameters that satisfy the temperature control requirements in the substrate by determination using the proposed comprehensive model revealing the inverse correlation of the impingement distance. At the same time, the thermal conductivity dependence on temperature, this is inversely proportionally by the linear functions of temperature fields are well studied in [76], where the authors examined the free convective flow of viscous fluid regime through the heated uniform and perpendicular wavy surface by

numerical investigations, revealing the rate of heat transfer, the skin friction coefficient, the isotherms and streamlines, while the system of nonlinear partial differential equations solved via implementation of the finite difference implicit scheme coupled with the Keller-box technique. Overall, the presented above review, demonstrates active interest of the utilization of inverse methodological approaches in heat transfer problems coupled with various physics in recent times, base on combination of classical methods and novel findings in computational and analytical investigations on the topic discussed in current work.

1.2 The principal peculiarities of inverse problems formulation

Practically most of inverse problems are set in opposite to the direct problems formulation, which depicts functional transformation of element from space of input data to another functional space, i.e.:

$$A: Q \to F: \forall f \in F,\ \exists q \in Q,\ Aq = f. \tag{1}$$

The former notation typically means that by acting via operator A over some element q from observable space of input configuration state of considered dynamical system, we obtain the field distribution from the functional space F, so called model response, and such solution should exist, be unique and preserve continuous dependence on the initial distribution. However, since in the case of inverse methodology we are aimed to determine elements q from received observations f, and such approach could result in infinitely many solutions or lack of the solution at all, while the initial data in such case critically depends on observations, resulting in unstable solution, that all depends on whereas the operator A is invertible or not. In most cases, we should set up the norm with existing global minimum, depicting the variation between observable and predicted responses, i.e.:

$$J(q) = \|Aq - f\|^2 \to min. \tag{2}$$

We treat (2) as the functional minimization problem, where $J(q)$ possesses several necessary properties that usually allows us to solve the inverse problem for identification of the model parameters. Meanwhile, for the regularization reasons, some altitude parameter should be also introduced, i.e.:

$$\alpha\|J\|^2 + J(q) = T_\alpha(q) \to min. \tag{3}$$

For instance, the Tikhonov regularization (3), where the parameter α could be sampled empirically or by some autonomous approach. In the case of inverse problem, the input data is taken as the observed or measured distribution of considered field or the initial approximations or guesses of either Neumann or Robin coefficients, initial data functional relationship, or the geometrical characteristics, while the problem is

formulated to estimate or determine exact or more precise values for initial approximations for such data. In this case, we may encounter several scenarios. The first scenario is that the number of data could be more than the number of unknown variables and in such case the solution may not exist. In another scenario, the number of unknown variables may be above than the number of initial data points, and that may lead to the case, when we have infinitely many solutions or again it may not exist. In the case, when initial data was sampled with some perturbation, i.e., error due to measurement device accuracy, we gain unstable solution due to the crucial dependency of inverse problem solution on input parameters. In the case of analytical approach many issues posed by numerical methodology are disappearing. In (1) an element q may be regarded as a model and A as the forward map, while f_{obs} is produced observable data and the left part as model response to input data q. We may convert the measurements into our model parameters by inverting the map A as:

$$q = A^{-1} f_{obs}. \tag{4}$$

Our observations may not contain enough information and additional data could be required, that may come from physical prior information on mutual dependence of parameter values. Even if A is considered as being a square matrix, it can have no inverse, being rank deficient, so that solution of (4) will be not unique. In such case the solution of posed inverse problem will be undetermined. If we will have more equations than unknown the solution will be represented by overdetermined system. If the noise corrupts obtained observations so that f_{obs} will lie outside the space F of possible responses to our model parameters, the solution to (4) may not exist. Another comprehensive issue appears when we are aiming to determine several parameters of model inputs at the same time, especially of different nature, such as the physical and geometrical characteristics of the model. In such case some crucial limitations regarding an incompleteness in observable data are limiting this possibility. Meanwhile the issues described for the formulation (1) – (4) are considered for single forward map, i.e., when the operator acting over field has homogeneous nature, saying that we observe single physical process. However, most physical processes are occurring in combined nature, for instance, heat and moisture transfer, or the thermoelastic bending, where investigated fields are in mutual, often non-linear, dependencies. Since the numerical approaches for former formulations will lead to unpredictable complexity, analytical investigations play more important role here. By using the functional derivation technique, based on considered minimization approach above, the iterative algorithm includes construction of the linear metric space that allows us to derive the conjugate problem and further obtain necessary computational formulas. Initially, we investigate the posed model with our approximated parameter values, sampled for initial iteration, then we observe the difference of model response with re-evaluated set of parameters:

$$\Delta(Aq) = A_{n+1} q_{n+1} - A_n q_n = \Delta f = f_{n+1} - f_n. \tag{5}$$

Constructing the self-adjoint operator for ΔA, we should obtain the conjugate problem, which analytical or numerical solution provides us necessary elements for derivation of Δq.

1.3 The principal peculiarities of considered formulations for direct multi-physical problems.

In our work, we were aimed to consider coupled equations of mathematical physics and through investigations over analytical solutions derivations, solve an inverse problem to obtain model parameters, physical coefficients, and geometrical characteristics. For this reason, firstly, we considered posed heat and moisture transfer as a model coupled equation of mathematical physics with various formulations of boundary conditions: I (Dirichlet), II (Neumann) and III (Robin) types. Afterwards, we observed different geometrical formulations of the problem, considering one-dimensional, two-dimensional, and three-dimensional cases, including non-homogeneous multilayered structures. Finally, our aspirations were aimed on expansion of derived methodology towards different physical fields, analogically varying dimensions, boundary conditions and homogeneity of posed structure. We will start our explanation by demonstrating general posed problems below that were considered in this work and discussing their peculiarities depending on the derived methodology.

As was mentioned above, our initial approach was to consider the convective heat and moisture transfer model for homogeneous structure. The approach was to model multi-physical process via the coupled system of partial differential equations in multi-layered system. For that reason, we have considered the model discussed in our main reference [77]. The paper studies N-layered structure with general thickness H, boundary points $z_k(k = \overline{0,N}), z_0 = 0, z_N = H$ with k-th layer considered as the interval $[z_{k-1}, z_k], h_k = z_k - z_{k-1}$ considered as the thickness of the layer and the governing equation as:

$$\rho(z)c_p(z)\gamma(z)\frac{\partial T}{\partial t} - \frac{\partial}{\partial z}\left(\alpha(z)\frac{\partial T}{\partial z}\right) = C_b(z)\left(\frac{\partial}{\partial z}\left(\eta(z)\frac{\partial \Omega}{\partial z}\right) + \frac{\partial}{\partial z}\left(\mu(z)\frac{\partial T}{\partial z}\right)\right). \tag{6}$$

Here we investigate two fields simultaneously. The first one is the non-stationary temperature field, $T(z,t)$ measured in kelvins, which reflects amount of heat passing through the unit volume of considered layer thickness at given instance of time. Another major field is the moisture field $\Omega(z,t)$, which depicts the moisture level and generally depends on the same spatial and time parameters as the temperature field and could be measured in specific humidity unit, that is the weight of water vapor per unit weight of air or the grams of water vapor per kilogram of air. Other physical properties acting in governing equations are $\rho(z)$ – the soil density, $c_p(z)$ – specific heat capacity of soil, $\gamma(z)$ – specific gravity of soil, $\alpha(z)$ – thermal conductivity of soil, $\eta(z)$ – soil

moisture diffusion, $\mu(z)$ – thermal transfer coefficient of soil, $C_b(z)$ – coefficient of convective heat transfer of soil. As could be seen from the definitions of the governing coefficients, all of them are depending on spatial parameter, however we should also note their dependency on the temperature and moisture fields, that results in nonlinear posedness of the considered problem. The structure under consideration may also be anisotropic and nonhomogeneous, which provides us with tensor form equation posedness, in case if we would consider the three-dimensional real case, i.e., $\bar{z} = [x_I, x_L] \times [y_I, y_L] \times [z_I, z_L]$, where $\{x, y, z\}$ being the orthonormal standard basis set coordinate system. As for the boundary and initial conditions, our main reference studies following open boundaries and continuity conditions for the fluxes between the layers represented by the system of equations:

$$\begin{cases} T(z,0) = T_0(z), \Omega(z,0) = \Omega_0(z), \\ \left(\alpha(z)\frac{\partial T}{\partial z} + h(T - T_a)\right)_{k=0} = 0, \\ \left(\eta(z)\frac{\partial \Omega}{\partial z} + \beta(\Omega - \Omega_a\right)_{k=0} = 0, \\ T|_{k=N} = T_H(t),\ \Omega|_{k=N} = \Omega_H(t), \\ \left[\alpha(z_k)\frac{\partial T}{\partial z}\right]_{z_k} = \left[\eta(z)\frac{\partial \Omega}{\partial z} + \mu(z)\frac{\partial T}{\partial z}\right]_{z_k} = 0, \\ [T]_{z_k} = [\Omega]_{z_k} = 0. \end{cases} \tag{7}$$

Typical set of conditions with measured temperature and moisture values on the outlet of domain and initial conditions chosen as continuous functions, could be also sampled via the following approximations:

$$\begin{cases} T(z,0) = \frac{1}{2}a_T^k(z - z_{k-1})^2 + \frac{1}{2}b_T^k(z - z_{k-1}) + c_T^k, \\ \Omega(z,0) = \frac{1}{2}a_\Omega^k(z - z_{k-1})^2 + \frac{1}{2}b_\Omega^k(z - z_{k-1})^2 + c_\Omega^k. \end{cases} \tag{8}$$

Where the set of coefficients $\left\{a_T^k, b_T^k, c_T^k, a_\Omega^k, b_\Omega^k, c_\Omega^k\right\}$ are the subject for determination via inverse problem methodological approach, – in such case we would pose the retrospective inverse problem, however we may also suggest such approximation for the boundary conditions sampled measurements $T_H(t)$ and $\Omega_H(t)$. The analytical solution of the posed system (6) – (8) was obtain via the differential matrix Riccati equation in the frequency domain. Obviously, we may solve problems of heat and moisture transfer separately by introducing the transition functions, consequently homogenizing the sampled measurements. For instance, the following direct problem with the boundary condition of the third kind, that is the convective heat exchange between the surface and the environment, i.e., heating or cooling by the fluid flow around the domain, also known as linear homogeneous boundary conditions and the same initial conditions as in the system (7):

$$\frac{\partial T}{\partial t} = \alpha \frac{\partial^2 T}{\partial z^2} + \omega(z,t). \quad (9)$$

$$\omega(z,t) = P(z)Q(t). \quad (10)$$

$$\left(\alpha_1 \frac{\partial T_1}{\partial z} + \beta_1[T - T_a]\right)_{k=0} + \aleph_1 j_1(t) = 0. \quad (11)$$

$$\left(\alpha_2 \frac{\partial T}{\partial z} + \beta_2[T - T_a]\right)_{k=N} + \aleph_N j_N(t) = 0. \quad (12)$$

Here both the (11) and (12) equations we may consider as the Newton's law or the Newton's equation of convection, whereas it is also possible to consider for accuracy and thermal slip - the speed of the gas on the surface, together with the Navier-Stokes system and continuity equations. As could be observed the decomposed source $\omega(z,t)$ represented by separate functions (10) could be rewritten only in terms of the homogenized sampled measurements and in such case non-homogeneous (11) and (12) equations we may rewrite using the transition function:

$$u(z,t) = T(z,t) - \psi(z,t). \quad (13)$$

That will lead us to the homogeneous system:

$$\alpha \frac{\partial \psi(z,t)}{\partial z} = -\aleph j(t). \quad (14)$$

$$\begin{cases} \psi_1(0,t) = T_{a_1}, \\ \psi_N(l_N,t) = T_{a2}, \\ \psi_k(l_k,t) = \psi_{k+1}(l_{k+1},t), \\ \alpha_k \frac{\partial \psi_k(l_k,t)}{\partial z} = \alpha_{k+1} \frac{\partial \psi_{k+1}(l_{k+t},t)}{\partial z}. \end{cases} \quad (15)$$

The advanced peculiarity of such problem formulation is that the analytical determination of nonstationary transfer potential fields in multilayer systems could obtained using transformations with the Green's function as demonstrated in [78], which is determined in accordance with the boundary conditions (15) or without the Green's function as shown in [79] and via the Fourier variables decomposition method. In our work we will demonstrate the received solution in frequency domain via Laplace direct and inverse transforms and derivation of the inverse problem for coefficients determination via the conjugate problem formulation and its analytical solution consequential deduction.

In our work we have considered several variations of posed boundary conditions for system (9) – (12) and their solution. For instance, when we have both sides as isolated boundaries, or one of the side open with second boundary being isolated, or

the mixed boundary conditions, such as that on one side of our domain we have the heat flux, and another side is the open boundary. For the former formulated problem, we have sampled empirically received experimental design data. In each case of the posed models, it was possible to evaluate certain number of parameters simultaneously via the inverse problems methodological approach due to special peculiarities of each model that we will discuss in the main part of the presented thesis.

Another principal peculiarity that we may distinguish was noted from considering the expansion of the designed methodology towards connections with various physical fields. For instance, presented in our work thermoelastic heat transfer of the three dimensional horizontally bend plate with thickness h. In that case, we observed the Sophie Germain equation:

$$\rho h \frac{\partial^2 W}{\partial t^2} = -D\Delta\Delta W - \Delta M_T + q. \quad (16)$$

Where last term q is load per unit area of plate, M_T is the bending moment, induced by the thermal effect, that we will relate via another system of the heat transfer posed model, the coefficient D – cylindrical stiffness, related by the expression:

$$D = \frac{Eh^3}{12(1-\nu^2)}. \quad (17)$$

Here we also have elasticity parameters: E – the Young's modulus, ν – the Poisson coefficient. When the heat is induced through the medium, material of the observed domain starts to resist, and internal forces aroused inside the observed domain could be summed via the integral expression:

$$M_T = 2\mu\alpha \int_{-h/2}^{h/2} T(x, y, z) z dz. \quad (18)$$

In the last expression, we obtain another set of elasticity parameters, such as α – the coefficient of the linear expansion, and μ – the Lame's coefficient, being independent of temperature and expressed as:

$$\mu = \frac{E}{2(1+\nu)}. \quad (19)$$

Furthermore, have the temperature field, that depends on three spatial parameters, being non-stationary, we pose the following model to relate the stress-energy dissipation quantities with thermal term by the introduced heat flux $\sigma = k\nabla T$:

$$\frac{\partial T}{\partial t} = k\nabla^2 T. \quad (20)$$

$$T|_{t=0} = T_{init}. \quad (21)$$

$$T|_{\Gamma} \propto t. \quad (22)$$

$$\sigma|_{Z=-\frac{h}{2}} = \sigma|_{Z=\frac{h}{2}} = h\omega_{1,2}. \quad (23)$$

Since the posed system (20) – (23) has dimension R^3, it is necessary to present reduction, that we will demonstrate by using the locally one-dimensional splitting scheme, reducing multidimensional problem to the sequence of one-dimensional equations. Further peculiarities of the discussed above problems will be noted during the presented inverse analysis methodology derivation process in the main part of current thesis.

2 ANALYTICAL EXPRESSIONS DERIVATION TECHNIQUES APPLIED FOR INVERSE ANALYSIS OF MATHEMATICAL PHYSICS EQUATIONS

Current section presents main postulates formulated for the derivation stages of analytical expressions obtained for inverse problems posed for multi-physical processes. It also presents discussion on formulation of variations of the posed direct models along with their analytical solutions derivation methodologies, experimental posed design for sampling the measurements utilized for homogenized models, solved in both real and frequency-time dependence, multilayered domain.

2.1 Homogenization of the direct multiphysical mathematical model in both real and frequency time domains.

The discussed system (6) – (7) from the first part of current thesis postulates with relation between two physically governed fields. Due to that reason the homogenized solution, presented in [77] suggests introducing the transition functions for both fields as:

$$\begin{cases} \tau(z,t) = T(z,t) - T_0(z), \\ \omega(z,t) = \Omega(z,t) - \Omega_0(z). \end{cases} \tag{24}$$

Which allows us further to utilize the layer stripping method towards the Laplace transform of $\tau(z,t)$ and $\omega(z,t)$ and then to obtain the solution to received differential matrix Riccati equation. The (24) substitution provides:

$$\begin{cases} \rho c_p \gamma \frac{\partial \tau}{\partial t} - C_b \frac{\partial \omega}{\partial t} = \frac{\partial}{\partial z}\left(\lambda \frac{\partial \tau}{\partial z}\right) + f_T, \\ \frac{\partial \omega}{\partial t} = \frac{\partial}{\partial z}\left(\eta \frac{\partial \omega}{\partial z} + \mu \frac{\partial \tau}{\partial z}\right) + f_\Omega. \end{cases} \tag{25}$$

With the following initial-boundary conditions:

$$\begin{cases} \left(\lambda \frac{\partial \tau}{\partial z} + \alpha(T - T_a)\right)_{z=0} = \phi_T,\ \tau_{z=H} = \tau_H,\ \tau_{t=0} = 0, \\ \left(\eta \frac{\partial \omega}{\partial z} + \beta(\omega - \Omega_0)\right)_{z=0} = \phi_\Omega,\ \omega_{z=H} = \omega_H,\ \omega_{t=0} = 0. \end{cases} \tag{26}$$

And the correspondingly posed continuity conditions for the introduced functions and their derivatives:

$$\begin{cases} \left[\lambda\frac{\partial\tau}{\partial z}\right]_{z_k} = [\tau]_{z_k} = 0, \\ \left[\eta\frac{\partial\omega}{\partial z} + \mu\frac{\partial\tau}{\partial z}\right]_{z_k} = [\omega]_{z_k} = 0. \end{cases} \tag{27}$$

Here the newly introduced expressions refer to coefficients sampled in (8):

$$\begin{cases} f_T = \lambda a_T, \\ f_\Omega = \eta a_\Omega + \mu a_T, \\ \phi_T = -\lambda b_T^1 - \alpha c_T^1, \\ \phi_\Omega = -\eta b_\Omega^1 - \beta c_\Omega^1, \\ \tau_H = T_H - \frac{1}{2}a_T^N(H - z_{N-1})^2 + \frac{1}{2}b_T^N(H - z_{N-1}) + c_T^N, \\ \omega_\Omega = \Omega_H - \frac{1}{2}a_\Omega^N(H - z_{N-1})^2 + \frac{1}{2}b_\Omega^N(H - z_{N-1}) + c_\Omega^N. \end{cases} \tag{28}$$

Such that f_T and f_Ω are the piecewise constant functions, while ϕ_T, ϕ_Ω, τ_H, ω_Ω are constants. These assumptions allow us further to transform introduced functions $\tau(z,p)$ and $\omega(z,p)$ to the frequency domain, finding their images of the Laplace transform:

$$\begin{cases} \mathcal{L}[\tau(z,t)] = \int_0^{+\infty} e^{-pt}\tau(z,t)dt = \tilde{\tau}(z,p)\,, \\ \mathcal{L}[\omega(z,t)] = \int_0^{+\infty} e^{-pt}\omega(z,t)dt = \tilde{\omega}(z,p)\,. \end{cases} \tag{29}$$

Where the complex number $p = \epsilon + i\varepsilon$ is the Laplace transform parameter with ϵ – attenuation parameter and ε – circular time frequency. Introducing the following matrix notations:

$$\begin{cases} U = \begin{pmatrix}\tilde{\tau}\\ \tilde{\omega}\end{pmatrix}, A = \begin{pmatrix}\lambda & 0\\ \mu & \eta\end{pmatrix}, D = p\begin{pmatrix}\rho c_p\gamma & -C_b\\ 0 & 1\end{pmatrix}, F = \frac{1}{p}\begin{pmatrix}f_T\\ f_\Omega\end{pmatrix}, \\ A_0 = \begin{pmatrix}\lambda & 0\\ 0 & \eta\end{pmatrix}, B_0 = \begin{pmatrix}\alpha & 0\\ 0 & \beta\end{pmatrix}, G_0 = \begin{pmatrix}\phi_T + \alpha\widetilde{T_0}(p)\\ \phi_\Omega + \beta\widetilde{\Omega_0}(p)\end{pmatrix}, G_H = \begin{pmatrix}\tau_H\\ \omega_\Omega\end{pmatrix}. \end{cases} \tag{30}$$

Where the functions $\widetilde{T_0}(p)$ and $\widetilde{\Omega_0}(p)$ are the corresponding images of the Laplace transform for boundary samples on the inlet for both temperature and moisture measurements, i.e., $T(0,t)$ and $\Omega(0,t)$. After sequentially applying the Laplace transform (29) towards received system (25) – (27), and applying the substitutions (30) we obtain the following system:

$$\begin{cases} \frac{\partial}{\partial}\left(A\frac{\partial U}{\partial z}\right) - DU = -F, \\ \left(A_0\frac{\partial U}{\partial z}x + B_0\right)_{z=0} = G_0,\ U_{z=H} = G_H, \\ \left[A\frac{\partial U}{\partial z}\right]_{z_k} = 0,\ [U]_{z_k} = 0. \end{cases} \quad (31)$$

As we mentioned above, analytical solution of the direct model (16) – (18) is obtained by introducing the square matrix X and the vector Y through the following correlation:

$$A\frac{\partial}{\partial z}U = XU + Y. \quad (32)$$

After substituting (32) to (31), the following statements for bot X and Y are obtained:

$$\begin{cases} X' + XA^{-1}X = D, X_{z=0} = -AA_0^{-1}B_0, [X]_{z_k} = 0, \\ Y' + XA^{-1}Y = -F, Y_{z=0} = AA_0^{-1}G_0, [Y]_{z_k} = 0. \end{cases} \quad (33)$$

That is the matrix Riccati equation, which solution is demonstrated in [77]. Now we will demonstrate the prescribed approach utilized for the second posed problem part, that is the thermoelastic bending model, heat transfer equation system for multilayered medium, by considering the system [84] – [87]. For that reason, we will reformulate the mentioned system by prescribing more detailed initial – boundary conditions in the one-dimensional form, two-layered domain, introduced by Ω: $(0, \xi) \cup (\xi, L) \times (0, t_{max})$:

$$\rho(x)c_p(x)\frac{\partial T}{\partial t} = \frac{\partial}{\partial x}\left(k(x)\frac{\partial T}{\partial x}\right), (x, t) \in \Omega. \quad (34)$$

$$k_1\frac{\partial T}{\partial x}|_{x=0} = h_{ins}(T - T_{ins})|_{x=0}. \quad (35)$$

$$k_2\frac{\partial T}{\partial x}|_{x=L} = -h_{out}(T - T_{out})|_{x=L}. \quad (36)$$

$$T(x, 0) = T_0(x). \quad (37)$$

$$T(\xi + 0, t) = T(\xi - 0, t) = T_\xi, k_2\frac{\partial T(\xi+0,t)}{\partial x} = k_2\frac{\partial T(\xi-0,t)}{\partial x}. \quad (38)$$

Above system depicts the heat transfer through one-dimensional two-layered string, when both inlet and outlet are open and subjected to the heat exchange with

environment, where T_{ins} and T_{out} are the inside and outside temperatures respectively and T_ξ – is the measured temperature over the contact region of two mediums that we will assume to be constant by considering the steady state of the heat transfer process. Although, there are variety of approaches utilized for the non-linear cases through quasi-linearization of received solutions, we will linearize the posed model via introducing the following piece-wise function:

$$\rho(x) = \begin{cases} \rho_1, x \in [0, \xi) \\ \rho_2, x \in (\xi, L] \end{cases}, c_p(x) = \begin{cases} c_{p_1}, x \in [0, \xi) \\ c_{p_2}, x \in (\xi, L] \end{cases},$$

$$k(x) = \begin{cases} k_1, x \in [0, \xi) \\ k_2, x \in (\xi, L] \end{cases}, \alpha(x) = \begin{cases} \alpha_1 = \frac{k_1}{\rho_1 c_{p_1}}, x \in [0, \xi) \\ \alpha_2 = \frac{k_2}{\rho_2 c_{p_2}}, x \in (\xi, L] \end{cases}. \quad (39)$$

Here we introduce continuously differentiable function $v(x,t)$, which is related to the temperature field via unknown coefficients γ and γ_1 that are subjects for determination and here $x \in [0, \xi]$:

$$\begin{cases} T(x,t) = v(x,t) + \gamma + \gamma_1 x, \\ \frac{\partial T}{\partial x} = \frac{\partial v}{\partial x} + \gamma_1. \end{cases} \quad (40)$$

Above substitution allows us to reduce the boundary conditions (36) towards:

$$k_1 \frac{\partial v}{\partial x}|_{x=0} = h_{ins} v|_{x=0} + h_{ins}\gamma - h_{ins} T_{ins} - k_1 \gamma_1. \quad (41)$$

The condition (41) is homogeneous only if the further identity is satisfied:

$$\begin{cases} h_{ins}\gamma - k_1\gamma_1 = T_{ins} h_{ins}, \\ \gamma + \gamma_1 \xi = T_\xi. \end{cases} \quad (42)$$

With the major and auxiliary determinants of the posed system being the following expressions:

$$\begin{cases} \Delta = \begin{vmatrix} h_{ins} & -k_1 \\ 1 & \xi \end{vmatrix} = \xi h_{ins} + k_1 > 0, \\ \Delta_1 = \begin{vmatrix} h_{ins} T_{ins} & -k_1 \\ T_\xi & \xi \end{vmatrix} = \xi h_{ins} T_{ins} + T_\xi k_1, \\ \Delta_2 = \begin{vmatrix} h_{ins} & h_{ins} T_{ins} \\ 1 & T_\xi \end{vmatrix} = h_{ins} T_\xi - h_{ins} T_{ins} = h_{ins}(T_\xi - T_{ins}). \end{cases} \quad (43)$$

By knowing above determinants, we may further determine the unknown coefficients by:

$$\begin{cases} \gamma = \frac{\Delta_1}{\Delta} = \frac{\xi h_{ins} T_{ins} + T_\xi k_1}{\xi h_{ins} + k_1}, \\ \gamma_1 = \frac{\Delta_2}{\Delta} = \frac{h_{ins}(T_\xi - T_{ins})}{\xi h_{ins} + k_1}. \end{cases} \tag{44}$$

Now, we may link initially posed problem with the introduced homogenized function as:

$$T(x,t) = v(x,t) + \frac{\xi h_{ins} T_{ins} + T_\xi k_1}{\xi h_{ins} + k_1} + \frac{h_{ins}(T_\xi - T_{ins})}{\xi h_{ins} + k_1} x. \tag{45}$$

From (45), we observe equivalent rates of functions changes with respect to time and the differential relations with respect to spatial variables hold, i.e.:

$$\begin{cases} \frac{\partial T}{\partial t} = \frac{\partial v}{\partial t}, \\ \frac{\partial}{\partial x}\left(k(x)\frac{\partial T}{\partial x}\right) = \frac{\partial}{\partial x}\left(k(x)\left(\frac{\partial v}{\partial x} + \gamma_1\right)\right) = \frac{\partial}{\partial x}\left(k(x)\frac{\partial v}{\partial x}\right). \end{cases} \tag{46}$$

Thus, the governing equation and the system of boundary and continuity conditions for the introduced function $v(x,t)$ is:

$$\begin{cases} \rho(x)c(x)\frac{\partial v}{\partial x} = \frac{\partial}{\partial x}\left(k(x)\frac{\partial v}{\partial x}\right), \\ k_1 \frac{\partial v}{\partial x}|_{x=0} = h_{ins} v|_{x=0},\ v(\xi,t) = 0, \\ T(\xi - 0, t) = T_\xi = v(\xi - 0, t) + \gamma + \gamma_1 \xi. \end{cases} \tag{47}$$

That is an equivalent problem for the posed (34 – 38) system, defined over sub-domain $x \in [0, \xi]$. The similar procedure we shall perform for the second layer by applying the corresponding substitution for $x \in [\xi, L]$ and taking into account the boundary conditions over outlet domain:

$$\begin{cases} T(x,t) = v(x,t) + \beta + \beta_1 x, \\ T(\xi,t) = v(\xi,t) + \beta + \beta_1 \xi = T_\xi, \\ k_2\left(\frac{\partial v}{\partial x} + \beta_1\right) = -h_{out}(v(L,t) + \beta + \beta_1 L - T_{out}). \end{cases} \tag{48}$$

Further in order to receive the homogenized expressions for (48), introduced unknown coefficients should satisfy following system of equation:

$$\begin{cases} \beta + \beta_1 \xi = T_\xi, \\ \beta h_{out} + \beta_1 (k_2 + h_{out} L) = h_{out} T_{out}. \end{cases} \tag{49}$$

Similarly, as to the previously determined coefficients γ, γ_1, we are applying the Cramer's method by evaluating the following determinants:

$$\begin{cases} \Delta = \begin{vmatrix} 1 & \xi \\ h_{out} & k_2 + h_{out} L \end{vmatrix} = k_2 + h_{out} L - h_{out} \xi > 0, \\ \Delta_1 = \begin{vmatrix} T_\xi & \xi \\ h_{out} T_{out} & k_2 + h_{out} L \end{vmatrix} = T_\xi (k_2 + h_{out} L) - h_{out} T_{out} \xi, \\ \Delta_2 = \begin{vmatrix} 1 & T_\xi \\ h_{out} & h_{out} T_{out} \end{vmatrix} = h_{out} T_{out} - h_{out} T_\xi. \end{cases} \tag{50}$$

Therefore, the computational formulas for homogenized coefficients are:

$$\begin{cases} \beta = \frac{\Delta_1}{\Delta} = \frac{T_\xi k_2 + h_{out}(T_\xi L - T_{out} \xi)}{k_2 + h_{out}(L - \xi)}, \\ \beta_1 = \frac{\Delta_2}{\Delta} = \frac{h_{out}(T_{out} - T_\xi)}{k_2 + h_{out}(L - \xi)}. \end{cases} \tag{51}$$

Further we construct the system for the introduced function $v(x,t)$ towards the second sub-domain, when $x \in [\xi, L]$:

$$\begin{cases} \frac{1}{\alpha_2^2} \frac{\partial v}{\partial t} = \frac{\partial^2 v}{\partial x^2}, \ \ x \in (\xi, L) \ t \in (0, t_{max}), \\ v(\xi, 0) = 0, \ k_2 \frac{\partial v}{\partial x} + h_{out} v|_{x=L} = 0. \end{cases} \tag{52}$$

2.2 Reduction of dimensionality of the direct multiphysical mathematical model in the real time domain

Concerning the thermoelastic model given by (16 – 23), it is necessary to note that in the considered model the displacement and velocity initially take zero values, such that:

$$\begin{cases} W(x, y, 0) = 0, \\ \frac{\partial W(x,y,0)}{\partial t} = 0. \end{cases} \tag{52}$$

We also shall indicate the rigid joint conditions, stating that considered plate has fixed supports at the upper boundary of the plate Γ:

$$\frac{\partial W(x,y,t)}{\partial n}|_{(x,y) \in \Gamma} = W(x, y, t)|_{(x,y) \in \Gamma} = 0. \tag{53}$$

Furthermore, we apply the locally one-dimensional splitting scheme towards the equation (20) and reduce the initially posed multidimensional thermoelastic model to the sequence of one-dimensional equations, considering the case of linear heat transfer coefficients without any heat source inside the domain. For that reason, we depict the boundaries of investigated domain as a parallelepiped by $P: \left[x = (x, y, z) = (x_1, x_2, x_3), 0 \le x_j < S_j,\ \left(0 < S_j < \infty, j = 1,2,3\right)\right]$, then we may introduce the following terms:

$$\begin{cases} R_{(j)}V_{(j)} = k\frac{\partial^2 T}{\partial x_j^2}, j = \overline{1,3}, t \in (0, t_*), \\ \frac{\partial V_{(1)}}{\partial t} = R_{(1)}V_{(1)},\ V_{(1)}(0,x) = T_{init}(x),\ V_{(1)}|_{\Gamma} = h\omega_1, \\ \frac{\partial V_{(2)}}{\partial t} = R_{(2)}V_{(2)},\ V_{(2)}(0,x) = V_{(1)}(t_*,x),\ V_{(2)}|_{\Gamma} = h\omega_2, \\ \frac{\partial V_{(3)}}{\partial t} = R_{(3)}V_{(3)},\ V_{(3)}(0,x) = V_{(2)}(t_*,x),\ V_{(3)}|_{\Gamma} = h\omega_3. \end{cases} \tag{54}$$

Solutions of (54) are easily received by the Fourier method, since both spatial and time variables are separable due to the well posed initial boundary conditions for the sequence of posed equations. The solutions take the following form:

$$\begin{cases} V_{(1)}(x,t_*) = \frac{2}{S_1}\sum_{n_1=1}^{\infty}\int_0^{S_1} T_{init}(\xi, x_2, x_3)\sin\left(\frac{n_1\pi\xi}{S_1}\right)d\xi \times e^{-t_* k\frac{n_1^2\pi^2}{S_1^2}}\sin\left(\frac{n_1\pi x_1}{S_1}\right), \\ V_{(2)}(x,t_*) = \frac{2}{S_2}\sum_{n_2=1}^{\infty}\int_0^{S_2} V_{(1)}(t_*, x_1, \eta, x_3)\sin\left(\frac{n_2\pi\eta}{S_2}\right)d\eta \times e^{-t_* k\frac{n_2^2\pi^2}{S_2^2}}\sin\left(\frac{n_2\pi x_2}{S_2}\right), \\ V_{(3)}(x,t_*) = \frac{2}{S_3}\sum_{n_3=1}^{\infty}\int_0^{S_3} V_{(2)}(t_*, x_1, x_2, \gamma)\sin\left(\frac{n_3\pi\gamma}{S_3}\right)d\gamma \times e^{-t_* k\frac{n_3^2\pi^2}{S_3^2}}\sin\left(\frac{n_3\pi x_3}{S_3}\right). \end{cases} \tag{55}$$

Subsequently plugging expression of $V_{(1)}$ to $V_{(2)}$ and $V_{(2)}$ to $V_{(3)}$, we obtain following terms for the direct thermoelastic model in the following form:

$$V_{(2)}(x,t_*) = \frac{4}{S_1 S_2}\sum_{n_2=1}^{\infty}\sum_{n_1=1}^{\infty}\exp\left[-t_* k\left(\frac{n_1^2\pi^2}{S_1^2} + \frac{n_2^2\pi^2}{S_2^2}\right)\right]\int_0^{S_2}\sin\left(\frac{n_2\pi\eta}{S_2}\right)\times$$

$$\times\left[\int_0^{S_1} T_{init}(\xi,\eta,x_3)\sin\left(\frac{n_1\pi\xi}{S_1}\right)d\xi\right]d\eta\sin\left(\frac{n_1\pi x_1}{S_1}\right)\sin\left(\frac{n_2\pi x_2}{S_2}\right). \tag{56}$$

$$V_{(3)}(x,t_*)=\frac{8}{S_1S_2S_3}\sum_{n_3=1}^{\infty}\sum_{n_2=1}^{\infty}\sum_{n_1=1}^{\infty}\int_0^{S_3}\sin\left(\frac{n_3\pi\gamma}{S_3}\right)\{\int_0^{S_2}\sin\left(\frac{n_2\pi\eta}{S_2}\right)\times$$

$$\times\left[\int_0^{S_1}T_{init}(\xi,\eta,\gamma)\sin\left(\frac{n_1\pi\xi}{S_1}\right)d\xi\right]d\eta\}d\gamma\times$$

$$\times\exp\left[-t_*k\left(\frac{n_1^2\pi^2}{S_1^2}+\frac{n_2^2\pi^2}{S_2^2}+\frac{n_3^2\pi^2}{S_3^2}\right)\right]\prod_{i=1}^{3}\sin\left(\frac{n_i\pi x_i}{S_i}\right)=T(t_*,x). \quad (57)$$

The ideas that were illustrated in the 2.1 and 2.2 parts outline the general springboard that lied in the foundation of our analytical investigations of the inverse analysis methodology, that we have utilized for the derivation of analytical expressions for simultaneous determination of several parameters of multi-physical processes.

Further chapters of the current thesis part will be concentrated on the derivation of the mentioned expressions and discussion of the major peculiarities for variations of direct model statement considered as selected case studies.

2.3 Analytical expressions for inverse analysis methodology derivation procedure for homogenized multiphysical process

In current section, we will depict main postulates for the derivation of analytical expressions for both direct and inverse analysis methodological approach utilized for homogenized models (47) and (52), which are split equivalences for the system (34 – 38).

Initially, we will demonstrate the analytical solution derivation for the system (47), which we are seeking in the form of $v(x,t)=X_0(x)T_0(t)$. By plugging the suggested substitution into (47), and introducing the root of characteristic equation of the proposed form as λ we will obtain:

$$\frac{1}{\alpha^2}\frac{T_0'(t)}{T_0(t)}=-\lambda^2,\frac{X_0'(x)}{X_0(x)}=-\lambda^2, x\in(0,\xi), t\in(0,t_{max}). \quad (58)$$

First and second equations of the received system have following solutions:

$$\begin{cases} T_0(t)=T_0(0)e^{-\lambda^2\alpha^2t},\ t\in(0,t_{max}),\\ X_0(x)=Acos(\lambda x)+Bsin(\lambda x),\ x\in(0,\xi). \end{cases} \quad (59)$$

Above system allows us to obtain an exact form of the function $v(x,t)$ over the first sub-domain as:

$$v(x,t)=T_0(0)e^{-\lambda\alpha^2t}\big(Acos(\lambda x)+Bsin(\lambda x)\big). \quad (60)$$

Further we apply the boundary condition $v(\xi,t)=0$ and assume the non-triviality principal of seek solution, i.e.:

$$\begin{cases} T_0(0)e^{-\lambda\alpha^2 t}\big(Acos(\lambda x)+Bsin(\lambda x)\big)=0, \\ T_0(0)e^{-\lambda\alpha^2 t}\neq 0. \end{cases} \tag{61}$$

Taking into account (61), we may rewrite (60) as the general characteristic equation that should be solved via:

$$Acos[\lambda\xi]+Bsin[\lambda\xi]=0. \tag{62}$$

Furthermore, we use the first boundary condition of the model (47) and observe the value of unknown function $v(x,t)$ at origin, that is: $v(0,t)=AT_0(t)$. From this observation we will rewrite the Robin condition in the following consequential order:

$$\begin{cases} \frac{\partial v}{\partial x}|_{x=0}=T_0(0)e^{-\lambda\alpha^2 t}(-A\lambda sin[\lambda 0]+B\lambda cos[\lambda 0])=B\lambda T_0(t), \\ k_1 B\lambda T_0(t)=h_{ins}T_0(t)A. \end{cases} \tag{63}$$

Due to non-triviality of solutions, we have the inequality $T_0(t)\neq 0, t\in(0,t_{max})$, and it gives us the following formulas:

$$A=\frac{k_1 B\lambda}{h_{ins}}\rightarrow\frac{A}{B}=\frac{k_1\lambda}{h_{ins}}. \tag{64}$$

Afterwards, we transform the equation (62), and deduce the following relation between coefficients A and B in a form of the following equation:

$$\frac{A}{B}=-tg[\lambda\xi]. \tag{65}$$

Combining the equations (64) and (65), we get the following transcendental equation:

$$\frac{k_1\lambda}{h_{ins}}=-tg[\lambda\xi]. \tag{66}$$

We suggest that the transcendental equation above could be solved analytically by applying the suitable transformation, however it will not affect the general solution in terms of precision, therefore, we approach the solution of (66) numerically for parameter λ and obtain values for $\lambda_1,\lambda_2,\dots\lambda_n$. After that the solution (60) could be rewritten as:

$$v_n(x,t)=T_0(0)e^{-\lambda_n\alpha^2 t}(Acos[\lambda_n x]+Bsin[\lambda_n x]),\ n=1,2,\dots \tag{67}$$

Applying the boundary conditions (63), we may present the solution via unknown coefficient as:

$$v_n(x,t) = B_n T_0(0) e^{-\lambda_n \alpha^2 t} \left(\frac{k_1 \lambda_n}{h_{ins}} cos[\lambda_n x] + sin[\lambda_n x] \right). \quad (68)$$

For comfortable representation we are denoting from this step $B_n T_0(0)$ again by B_n, just for convenience, and rewrite (68) as:

$$v_n(x,t) = B_n e^{-\lambda_n \alpha^2 t} \left(\frac{k_1 \lambda_n}{h_{ins}} cos[\lambda_n x] + sin[\lambda_n x] \right), \; n = 1,2,\ldots \quad (69)$$

Due to linearity of initial equation, we may present the solution now in a form of the following series by superposition principle:

$$v(x,t) = \sum_{n=1}^{\infty} v_n(x,t) = \sum_{n=1}^{\infty} B_n e^{-\lambda_n \alpha^2 t} X_n(x). \quad (70)$$

Here $X_n(x)$ is a family of eigen functions of the governing equation for model (47) when spatial subdomain is $x \in (0, \xi)$. Taking into account above fact, we state the first lemma**.**

Lemma 1. If n $\neq m$, we have the following identity that postulates an orthogonality of the proposed system $X_n(x), \; \forall n, m \in Z$:

$$\int_0^{\xi} X_n(x) X_m(x) dx = 0. \quad (71)$$

Proof. The eigenfunctions are representing the solution of the governing equation for model (47), thus we have the following identities:

$$\begin{cases} X_n''(x) + \lambda_n^2 X_n(x) = 0, \\ X_m''(x) + \lambda_m^2 X_m(x) = 0. \end{cases} \quad (72)$$

Further, in order to sustain the proof, we perform the multiplication operation of the first equation in (72) by $\mathrm{X}_m(x)$, and the second equation by $X_n(x)$ and subtract the second expression from the first one, it will allow us to obtain the following identity:

$$X_n''(x) X_m(x) - X_m''(x) X_n(x) + (\lambda_n^2 - \lambda_m^2) X_n(x) X_m(x) = 0. \quad (73)$$

From general rules of differentiation calculus, we may imply the next expression:

$$X_n''(x) X_m(x) - X_m''(x) X_n(x) = \left(X_n'(x) X_m(x) - X_m'(x) X_n(x) \right)'. \quad (74)$$

By performing above manipulation, we receive the transformed form of (73) as:

$$\left(X_n'(x)X_m(x) - X_m'(x)X_n(x)\right)' + (\lambda_n^2 - \lambda_m^2)X_n(x)X_m(x) = 0. \quad (75)$$

The received expression (75) then is continuously summed along the spatial component x from 0 to ξ by the following integral, so we receive:

$$X_n'(\xi)X_m(\xi) - X_m'(\xi)X_n(\xi) - X_n'(0)X_m(0) + X_m'(0)X_n(0) = \\ = (\lambda_m^2 - \lambda_n^2)\int_0^\xi X_n(x)X_m(x)dx. \quad (76)$$

Analyzing both families of the functions $X_n(x)$ and $X_m(x)$, we may derive the boundary conditions for these systems as:

$$X_n(\xi) = 0,\ X_m(\xi) = 0,\ X_n'(0) = \frac{h_{ins}}{k_1}X_n(0),\ X_m'(0) = \frac{h_{ins}}{k_1}X_m(0). \quad (77)$$

The derived boundary conditions (77) allow us to set the left part of integral expression (76) to zero, so now we observe the following identity:

$$(\lambda_m^2 - \lambda_n^2)\int_0^\xi X_n(x)X_m(x)dx = 0. \quad (78)$$

Whenever we consider the cases $n \neq m, \lambda_n \neq \lambda_n$ we obtain an exact form of orthogonality of the functions $X_n(x)$ and $X_m(x)$ as:

$$\int_0^\xi X_n(x)X_m(x)dx = 0. \quad (79)$$

■

Additionally, we need to propose another lemma that will allow us to derive the computational formula of the norm of the eigenfunctions $X_n(x)$.

Lemma 2. The computational formula for the norm of the eigenfunction $X_n(x)$, $\forall n \in Z$ takes the following form:

$$\|X_n\|^2 = \int_0^\xi [X_n(x)]^2 dx = \frac{\alpha^2+\xi}{2} + \frac{\alpha}{2\lambda_n}, \alpha = \frac{k_1\mu_n}{h_{ins}}. \quad (80)$$

Proof. We will start the proof of proposed lemma by the direct computation of the suggested integral in a form:

$$\int_0^\xi \left(\frac{k_1\lambda_n}{h_{ins}}cos[\lambda_n x] + sin[\lambda_n x]\right)^2 dx. \quad (81)$$

In order to perform the evaluation of posed integral, we shall apply the decreasing order formula which has the following form:

$$\|X_n\|^2 = \frac{\alpha^2}{2}\int_0^{\xi}(1 + cos[2\lambda_n x])dx + \frac{1}{2}\int_0^{\xi}(1 - cos[2\lambda_n x])dx + \\ +2\alpha\int_0^{\xi}(cos[\lambda_n x]sin[\lambda_n x])dx. \quad (82)$$

Right after the direct computation of the received integral (82), we obtain an expression:

$$\|X_n\|^2 = \frac{\alpha^2}{2}\left(x + \frac{1}{2\lambda_n}sin[2\lambda_n x]\right)|_0^{\xi} + \frac{1}{2}\left(x - \frac{1}{2\lambda_n}\sin[2\lambda_n x]\right)|_0^{\xi} + \\ + \frac{2\alpha}{\lambda_n}\frac{\sin^2[\lambda_n x]}{2}|_0^{\xi}. \quad (83)$$

After plugging the limits in this expression, it will be transformed into:

$$\|X_n\|^2 = \frac{\xi}{2}(\alpha^2 + 1) + \frac{\sin[2\lambda_n\xi]}{4\lambda_n}(\alpha^2 - 1) + \frac{\alpha}{\lambda_n}\sin^2[\lambda_n\xi]. \quad (84)$$

Here, we may imply the following trigonometrical identities:

$$\begin{cases}\sin[2\lambda_n\xi] = \frac{2tg[\lambda_n\xi]}{1+tg^2[\lambda_n\xi]}, \\ \sin^2[\lambda_n\xi] = \frac{tg^2[\lambda_n\xi]}{1+tg^2[\lambda_n\xi]}.\end{cases} \quad (85)$$

From another point of view, we may get an equality $tg[\lambda_n\xi] = -\alpha$, thus our norm will be rewritten now as the following computational formula:

$$\|X_n\|^2 = \frac{\xi}{2}(\alpha^2 + 1) - \frac{\alpha}{2\lambda_n}\frac{(\alpha^2 - 1)}{1 + \alpha^2} + \frac{\alpha}{\lambda_n}\frac{\alpha^2}{1 + \alpha^2} = \frac{\xi}{2}(\alpha^2 + 1) + \frac{2\alpha^3 - \alpha(\alpha^2 - 1)}{2\lambda_n(\alpha^2 + 1)} \\ = \\ = \frac{\xi}{2}(\alpha^2 + 1) + \frac{\alpha}{2\lambda_n} = \frac{\xi}{2}\left[\left(\frac{k_1\mu_n}{h_{ins}}\right)^2 + 1\right] + \frac{k_1}{2h_{ins}} = A_n. \quad (86)$$

■

Now we observe initial instance of time for the equation (70) in order to deduce the computable and explicit form of the function $v(x,t)$:

$$v(x,0) = \sum_{n=1}^{\infty} v_n(x,0) = \sum_{n=1}^{\infty} B_n X_n(x). \quad (87)$$

At the same time, we are taking into account the identity (40) at initial time instance, i.e., $v(x,0) = u_0(x) - \gamma - \gamma_1 x$. Furthermore, here we are multiplying the both sides of the second equation of system (59) by the function $X_m(x)$ and integrate it along the spatial variable x from 0 to ξ. Afterwards we use the conclusions of the lemmas 1 and 2 in order to obtain the following identity:

$$\int_0^{\xi}(u_0(x)-\gamma-\gamma_1 x)X_m(x)dx = A_m B_m,\ m=1,2,\dots \tag{88}$$

The above expression gives us opportunity to derive the computational expression for B_n as the following explicit identity:

$$B_n = \frac{1}{A_n}\int_0^{\xi}(u_0(x)-\gamma-\gamma_1 x)X_n(x)dx,\ n=1,2,\dots \tag{89}$$

At this point we already demonstrated the solution derivation of the direct model (34) – (38) along the first sub-domain, when $x \in (0,\xi)$ for homogenized sampled measurements. Now we shall perform same procedure steps along the second portion of the domain, i.e., when $x \in (\xi, L)$. Since we have already demonstrated the homogenization process of the original model, we will start here by working with the model (52) via introduction of the following spatial variable substitution to receive more convenient form of the model. We introduce $\overline{x} = x - \xi$, and afterwards we substitute $x = \overline{x} + \xi$. By observing introduced relations we may derive the differential identity:

$$\begin{cases} \dfrac{\partial v}{\partial x} = \dfrac{\partial v}{\partial \overline{x}}\dfrac{\partial \overline{x}}{\partial x} = \dfrac{\partial v}{\partial \overline{x}}, \\ \dfrac{\partial^2 v}{\partial x^2} = \dfrac{\partial^2 v}{\partial \overline{x}^2}. \end{cases} \tag{90}$$

For convenience reasons we will use further the variable $\overline{x}$ denoted through the same variable x and our system (52) will obtain the following form:

$$\begin{cases} \dfrac{1}{\alpha_2^2}\dfrac{\partial v}{\partial t} = \dfrac{\partial^2 v}{\partial x^2}, x \in (0, l-\xi), t \in (0, t_{max}), \\ v(0,t) = 0, k_2 \dfrac{\partial v}{\partial x}\Big|_{x=l-\xi} + h_{out} v|_{x=l-\xi} = 0. \end{cases} \tag{91}$$

The solution to posed model (91) we will seek in the analogue approach to first sub-domain, as $v(x,t) = X_2(x)T_2(t)$. This substitution, will provide us the following system of differential equations:

$$\frac{1}{\alpha_2^2}\frac{T_2'(t)}{T_2(t)} = -\mu^2,\ \frac{X_2'(x)}{X_2(x)} = -\mu^2. \tag{92}$$

At the same time, we have the following general solution of the posed system, represented by roots of characteristic equations, μ and unknown coefficients:

$$T_2(t) = T_2(0)e^{-\mu^2\alpha_2^2 t},\ X_2(x) = C\cos(\mu x) + D\sin(\mu x). \tag{93}$$

We apply the boundary conditions of the system (91) for the eigen function $X_2(x)$ which take the following form:

$$X_2(0) = 0,\ k_2 X_2'(l-\xi) + h_{out} X_2(l-\xi) = 0. \tag{94}$$

Received boundary conditions are observed along with the following identity for eigenfunction derivative:

$$X_2'(x) = -C\mu \sin(\mu x) + D\mu \cos(\mu x). \tag{95}$$

So that our initial system could be rewritten as:

$$\mathrm{C} = 0,\ k_2 D\mu \cos\big(\mu(l-\xi)\big) + h_{out} D sin\big(\mu(l-\xi)\big) = 0. \tag{96}$$

Due to nontriviality principle, we consider the case when $D \neq 0$ for our solution. Thus, it follows that:

$$k_2\mu \cos\big(\mu(l-\xi)\big) + h_{out} sin\big(\mu(l-\xi)\big) = 0. \tag{97}$$

Rewriting the (97) into equivalent form, we obtain the following transcendental equation:

$$tg\big(\mu(l-\xi)\big) = -\frac{k_2\mu}{h_{out}}. \tag{98}$$

We may solve (98) numerically, in order to obtain the set of eigenvalues $\mu_1, \mu_2, \dots, \mu_n$, which will construct the following set of eigenfunctions

$$X_1 = \sin[\mu_1 x]\,, X_2 = \sin[\mu_2 x]\,, \dots \tag{99}$$

Therefore, the solution of (91) will take the following form:

$$v(x,t) = \sum_{n=1}^{\infty} D_n e^{-\mu_n^2 \alpha_2^2 t} \sin[\mu_n x]\,, x \in (0, l-\xi). \tag{100}$$

Furthermore, we pose our third lemma to verify if the constructed system of eigenfunctions $\{\sin(\mu_n x)\}$ will be orthogonal on $x \in (0, l-\xi)$.

Theorem of Rysbaiuly – Sinitsa. The eigenfunction system $X_n = \{\sin(\mu_n x)\}$ is orthogonal on $x \in (0, l-\xi)$, $\forall n, m \in Z$ provides convergency of the series (100).

Proof. We approach the proof of proposed lemma through the definition of $X_n(x)$ and $X_m(x)$, which state that they should satisfy to the following system of equations:

$$\begin{cases} X_n'' + \lambda_n^2 X_n = 0, \\ X_m'' + \lambda_m^2 X_m = 0. \end{cases} \tag{101}$$

Here we perform similar manipulation with obtained system, so that we multiply the first equation by $X_m(x)$, and the second equations by $X_n(x)$ and then we subtract second equation from the first one, which gives us the following identity:

$$(\lambda_n^2 - \lambda_m^2)X_n(x)X_m(x) = \lambda_m X_n'' - \lambda_n X_m''. \tag{102}$$

Equation above is equivalent to the following expression by analogy to the first sub-domain:

$$(\lambda_n^2 - \lambda_m^2)X_n(x)X_m(x) = (\lambda_m X_n' - \lambda_n X_m')'. \tag{103}$$

Furthermore, we integrate the equation (103) along the spatial variable x from 0 to $l - \xi$:

$$(\lambda_n^2 - \lambda_m^2)\int_0^{\xi} X_n(x)X_m(x)dx = (\lambda_m X_n' - \lambda_n X_m')|_0^{l-\xi} =$$

$$= X_m(l-\xi)X_n'(l-\xi) - X_n(l-\xi)X_m'(l-\xi) -$$

$$-X_m(0)X_n'(0) + X_n X_m'(0). \tag{104}$$

For both families of derived eigenfunctions $X_n(x)$ and $X_m(x)$ there are the following boundary conditions from initial system of equations (47), i.e.:

$$\begin{cases} X_n(0) = 0,\ X_m(0) = 0, \\ X_n'(l-\xi) = -\frac{h_{out}}{k_2}X_n(l-\xi), X_m'(l-\xi) = -\frac{h_{out}}{k_2}X_m(l-\xi). \end{cases} \tag{105}$$

By observing the integral relation (104) along with the boundary conditions (105), we will deduce the following identity:

$$(\lambda_n^2 - \lambda_m^2)\int_0^{\xi} X_n(x)X_m(x)dx = (\lambda_m X_n' - \lambda_n X_m')|_0^{l-\xi} =$$

$$= -X_m(l-\xi)\frac{h_{out}}{k_2}X_n(l-\xi) + X_n(l-\xi)\frac{h_{out}}{k_2}X_m(l-\xi) = 0. \tag{106}$$

Now, by considering the case when $\lambda_n \neq \lambda_m$ we will see that indeed the system is orthogonal and:

$$\int_0^{\xi} X_n(x)X_m(x) = 0. \tag{107}$$

■

Now, by using the last observations, we may evaluate this integral as the following norm:

$$\|X_n\|^2 = \int_0^{\xi} X_n^2(x)dx = \int_0^{l-\xi} \sin^2[\mu_n x]\, dx. \tag{108}$$

By analogy to the first sub-domain, we imply the order reduction formula, and deduce the following integral expression:

$$\|X_n\|^2 = \frac{1}{2}\int_0^{l-\xi} (1-\cos(2\mu_n x))dx = \frac{1}{2}\left(x - \frac{2}{2\mu_n}\sin(2\mu_n x)\right)|_0^{l-\xi} =$$
$$= \frac{1}{2}\left(l-\xi - \frac{1}{\mu_n}\sin\big(2\mu_n(l-\xi)\big)\right). \tag{109}$$

At this point, we shall take into account the following trigonometrical identity to express (109) in accordance with the transcendental equation (98):

$$\sin\big(2\mu_n(l-\xi)\big) = 2\sin\big(\mu_n(l-\xi)\big)\cos\big(\mu_n(l-\xi)\big) = \frac{2tg\big(\mu_n(l-\xi)\big)}{1+tg^2\big(\mu_n(l-\xi)\big)}. \tag{110}$$

By applying the (98) towards (110) we will derive the computational formula of the norm of $\|X_n\|^2$ as:

$$\|X_n\|^2 = \frac{1}{2}(l-\xi) + \frac{k_2}{k_2\left(1+\left(\frac{k_2\mu_n}{h_{out}}\right)^2\right)} = C_n,\ n = 1,2,\dots \tag{111}$$

Furthermore, in order to determine the coefficients D_n we shall use the identity (100) and take for consideration the case when $t = 0$, that will give us the following identity:

$$v(x,0) = \sum_{n=1}^{\infty} D_n \sin(\mu_n x)\,, x \in (0, l-\xi). \tag{112}$$

From another point of view, we recall our initial substitution $v(x,0) = u_0 - \beta - \beta_1 x$ and conclude that:

$$\int_0^{l-\xi} (u_0(x) - \beta - \beta_1 x)sin(\mu_n x)\, dx = C_n D_n. \tag{113}$$

That is the computational formula explicitly derived for the coefficient D_n as:

$$D_n = \frac{1}{C_n}\int_0^{l-\xi} (u_0(x) - \beta - \beta_1 x)sin(\mu_n x)\, dx\,,\ n = 1,2,\dots \tag{114}$$

Due to our substitution for spatial variable $\bar{x} = x - \xi$, we shall perform the backward substitution via $x = \bar{x} + \xi$,which will give us the following computational formula:

$$D_n = \frac{1}{C_n}\int_{\xi}^{l}(u_0(x) - \beta - \beta_1 x)sin(\mu_n x)\,dx\,,\ n = 1,2,\dots \tag{115}$$

Having the derived expressions, we may present further the algorithm for the analytical evaluation of the initial problem statement for temperature field.

Algorithm 1.

Step 1. Initially we shall perform the homogenization by computing the coefficients by the set of formulas:

$$\begin{cases} \gamma = \frac{\xi h_{ins}u_{ins} + T_\xi k_1}{\xi h_{ins} + k_1}, \\ \gamma_1 = \frac{h_{ins}(T_\xi - u_{ins})}{\xi h_{ins} + k_1}, \\ \beta = \frac{T_\xi k_2 + h_{out}(T_\xi L - u_{out}\xi)}{k_2 + h_{out}(L-\xi)}, \\ \beta_1 = \frac{h_{out}(u_{out} - T_\xi)}{k_2 + h_{out}(L-\xi)}. \end{cases} \tag{116}$$

Step 2. We are solving numerically the following transcendental equations and obtain two sets of eigenvalues $\lambda_1, \lambda_2, \dots, \lambda_n$ and $\mu_1, \mu_2, \dots, \mu_n$:

$$\begin{cases} tan[\lambda_n \xi] = -\frac{k_1\lambda_n}{h_{ins}}, \\ tan\big(\mu(l-\xi)\big) = -\frac{k_2\mu}{h_{out}}. \end{cases} \tag{117}$$

Step 3. We shall compute the norm of the eigenfunctions of the first and second problem via formulas:

$$\begin{cases} \|X_{1,n}\|^2 = A_n = \frac{\xi}{2}\left(\frac{k_1\lambda_n}{h_{ins}}\right)^2 + \frac{\xi}{2} + \frac{k_1}{2h_{ins}}, \\ \|X_{2,n}\|^2 = C_n = \frac{1}{2}(l-\xi) + \frac{k_2}{k_2\left[1+\left(\frac{k_2\mu_n}{h_{out}}\right)^2\right]}. \end{cases}, n = 1,2,\dots \tag{118}$$

Step 4. After that we shall compute the following coefficients by integral relations:

$$\begin{cases} B_n = \frac{1}{A_n}\int_0^{\xi}(u_0(x) - \gamma - \gamma_1 x)\left(\frac{k_1\lambda_n}{h_{ins}}\cos(\lambda_n x) + \sin(\lambda_n x)\right)dx, \\ D_n = \frac{1}{C_n}\int_{\xi}^{l}(u_0(x) - \beta - \beta_1 x)sin(\mu_n x)\,dx. \end{cases}, n = 1,2,\dots \tag{119}$$

Step 5. Afterwards, we are ready to evaluate the solutions for initial-boundary value problem (34) – (38) via the following computational formulas:

$$u(x,t) = \begin{cases} \sum_{n=1}^{\infty} B_n e^{-\lambda_n \alpha^2 t}\left(\frac{k_1\lambda_n}{h_{ins}}\cos(\lambda_n x)+\sin(\lambda_n x)\right)+\gamma+\gamma_1 x, & x\in(0,\xi), t\in(0,T_m), \\ \sum_{n=1}^{\infty} D_n e^{-\mu_n^2\alpha_2^2 t}\sin(\mu_n x)+\beta+\beta_1 x, & x\in(\xi,l)t\in(0,T_m). \end{cases} \quad (120)$$

After derivation of the analytical solution for the direct problem is finished, we may start the procedure of derivation for the inverse problem analytical solution. Since the key problem formulation is to determine the unknown parameters via measured response of the system, we will formulate the system of nonlinear equations as follows:

$$\begin{cases} T_1(t^k) - \sum_{n=1}^{\infty} B_n e^{-\lambda_n \frac{k_1}{\rho_1 c_{p_1}} t^k} X_n(0) + \gamma = f(\rho_1), \\ T_1(t^{k+1}) - \sum_{n=1}^{\infty} B_n e^{-\lambda_n \frac{k_1}{\rho_1 c_{p_1}} t^{k+1}} X_n(0) + \gamma = f\left(c_{p_1}\right), \\ T_1(t^{k+2}) - \sum_{n=1}^{\infty} B_n e^{-\lambda_n \frac{k_1}{\rho_1 c_{p_1}} t^{k+2}} X_n(0) + \gamma = f(h_{ins}), \\ T_1(t^{k+3}) - \sum_{n=1}^{\infty} B_n e^{-\lambda_n \frac{k_1}{\rho_1 c_{p_1}} t^{k+3}} X_n(0) + \gamma = f(k_1). \end{cases} \to min \quad (121)$$

Where $t^k \in (t_i, t_{i+1})$ is the time partition for our received measurements, which at the same time could be observed in the frequency domain. By prescribing the corresponding accuracy and measurement device position, - that is also could be subject for determination via the optimal experiment design approach. The system (121) shall perceive the local convex properties, otherwise, we may apply the least square method. Right after evaluation of the first set of parameters, π_1 we clarify them additionally by another optimization problem from the system with second device measurements:

$$\begin{cases} T_2(t^k) - \sum_{n=1}^{\infty} B_n e^{-\lambda_n \frac{k_1}{\rho_1 c_{p_1}} t^k} X_n(x_2) + \gamma + \gamma_1 x_2 = f(\rho_1), \\ T_2(t^{k+1}) - \sum_{n=1}^{\infty} B_n e^{-\lambda_n \frac{k_1}{\rho_1 c_{p_1}} t^{k+1}} X_n(x_2) + \gamma + \gamma_1 x_2 = f\left(c_{p_1}\right), \\ T_2(t^{k+2}) - \sum_{n=1}^{\infty} B_n e^{-\lambda_n \frac{k_1}{\rho_1 c_{p_1}} t^{k+2}} X_n(x_2) + \gamma + \gamma_1 x_2 = f(h_{ins}), \\ T_2(t^{k+3}) - \sum_{n=1}^{\infty} B_n e^{-\lambda_n \frac{k_1}{\rho_1 c_{p_1}} t^{k+3}} X_n(x_2) + \gamma + \gamma_1 x_2 = f(k_1). \end{cases} \to min \quad (122)$$

Here, x_2 – is the position of second device, that will be illustrated in validation part. Going further towards the third measurement device, we construct another system to perform the same procedure with x_3 being the position of the third device:

$$\begin{cases} T_3(t^k) - \sum_{n=1}^{\infty} D_n e^{-\mu_2 \frac{k_2}{\rho_2 c_{p_2}} t^k} \sin(\mu_2 x_3) + \beta + \beta_1 x_3 = f(\rho_2), \\ T_3(t^{k+1}) - \sum_{n=1}^{\infty} D_n e^{-\mu_2 \frac{k_2}{\rho_2 c_{p_2}} t^{k+1}} \sin(\mu_2 x_3) + \beta + \beta_1 x_3 = f\left(c_{p_2}\right), \\ T_3(t^{k+2}) - \sum_{n=1}^{\infty} D_n e^{-\mu_2 \frac{k_2}{\rho_2 c_{p_2}} t^{k+2}} \sin(\mu_2 x_3) + \beta + \beta_1 x_3 = f(h_{out}), \\ T_3(t^{k+3}) - \sum_{n=1}^{\infty} D_n e^{-\mu_2 \frac{k_2}{\rho_2 c_{p_2}} t^{k+3}} \sin(\mu_2 x_3) + \beta + \beta_1 x_3 = f(k_2). \end{cases} \rightarrow min \tag{123}$$

Which we also clarify by the measurements received from the fourth, last, device by:

$$\begin{cases} T_4(t^k) - \sum_{n=1}^{\infty} D_n e^{-\mu_2 \frac{k_2}{\rho_2 c_{p_2}} t^k} \sin(\mu_2 x_4) + \beta + \beta_1 x_4 = f(\rho_2), \\ T_4(t^{k+1}) - \sum_{n=1}^{\infty} D_n e^{-\mu_2 \frac{k_2}{\rho_2 c_{p_2}} t^{k+1}} \sin(\mu_2 x_4) + \beta + \beta_1 x_4 = f\left(c_{p_2}\right), \\ T_4(t^{k+2}) - \sum_{n=1}^{\infty} D_n e^{-\mu_2 \frac{k_2}{\rho_2 c_{p_2}} t^{k+2}} \sin(\mu_2 x_4) + \beta + \beta_1 x_4 = f(h_{out}), \\ T_4(t^{k+3}) - \sum_{n=1}^{\infty} D_n e^{-\mu_2 \frac{k_2}{\rho_2 c_{p_2}} t^{k+3}} \sin(\mu_2 x_4) + \beta + \beta_1 x_4 = f(k_2). \end{cases} \rightarrow min \tag{124}$$

We perform the evaluation of all system parameters through the algorithm 1, and observe the pattern variations through each iteration, however, in order to determine the geometrical characteristic of the proposed system, we do the implementation of the contact condition, by obtaining additional convex function:

$$\sum_{n=1}^{\infty} D_n e^{-\lambda_n \frac{k_2}{\rho_2 c_{p_2}} t^{k+5}} \sin[\mu_2 \xi] + \beta + \beta_1 \xi - \sum_{n=1}^{\infty} B_n e^{-\lambda_n \frac{k_1}{\rho_1 c_{p_1}} t^{k+5}} X_n(\xi) + \gamma + \\ + \gamma_1 \xi = f(\xi) \rightarrow min \tag{125}$$

Sequentially measuring the data over suitably selected positions, we are keen to avoid high level of fluctuations by computing the norms of the eigenfunctions at each iteration that we will present in the validation part of the thesis.

2.4 Analytical expressions for inverse analysis methodology derivation procedure for elasticity parameters in thermoelastic stress model.

The received model (16) – (23) along with the expressions (52) – (53) are now suitable for determination of the physical parameters via the functional construction methodological approach due, since we have already demonstrated the reduction of dimensionality for the proposed thermoelastic process and its analytical solutions by (54) – (57). For that reason, we present (20) – (23) by analogy to (34) – (38) and construct the thermoelastic model together with mentioned above system of equations and expressions and set the additional information, measuring the temperatures at the inlet and outlet of our domain $T|_{x=0} = Tg_1(t)$ and $T|_{x=L} = Tg_2(t)$. Afterwards we take initial approximation of observed coefficient at initialize zero iteration, i.e., k_0. It will allow to construct the auxiliary problem by observing fluctuation at neighbor iterations, i.e., $\Delta T = T_{n+1} - T_n$, which will take the form:

$$\rho c \frac{\partial \Delta T}{\partial t} = \frac{\partial}{\partial x}(\Delta \delta). \tag{126}$$

$$\Delta \delta|_{x=0} = h_{out}(\Delta T)|_{x=0}. \tag{127}$$

$$\Delta \delta|_{x=L} = -h_{ins}(\Delta T)|_{x=L}. \tag{128}$$

$$\Delta T|_{t=0} = 0. \tag{129}$$

Here, we have introduced the heat flux $\delta = k \frac{\partial T}{\partial x}$. Afterwards we proceed to the key part of suggested methodology, construction of the Pre-Hilbert space via the following inner product:

$$< f, g > = \int_0^L \int_0^{t_*} (f \times g)\, dt\, dx. \tag{130}$$

By using the inner product above, we apply it towards (126) – (129) via scalarly multiplying the governing equation of the auxiliary problem (126) by arbitrary continuously differentiable function $\psi(x, t)$ and integrate the received product along the whole region $Q = [0, t_*] \times [0, L]$:

$$< \rho c \frac{\partial \Delta T}{\partial t}, \psi > = < \frac{\partial \Delta \delta}{\partial x}, \psi >. \tag{131}$$

We observe an expression (131) as the definite iterated integral relation, that could be opened by applying the integration by parts formulas:

$$< \rho c \frac{\partial \Delta T}{\partial t}, \psi > = < \Delta T, \rho c \psi > |_0^{t_*} - < \Delta T, \rho c \frac{\partial \psi}{\partial t} >. \tag{132}$$

Here we are posing the hypothesis that will be used later in derivation of the conjugate problem, that is: $\psi|_{t=T_m} = \psi(x, T_m) = 0$. Now, by taking into account the condition (129), our integral relation (132) will take the form:

$$< \rho c \frac{\partial \Delta T}{\partial t}, \psi > = - < \Delta T, \rho c \frac{\partial \psi}{\partial t} >. \tag{133}$$

Analogically to above procedure, we evaluate the right side of the expression (131):

$$< \frac{\partial \Delta \delta}{\partial x}, \psi > = < \Delta \delta, \psi > |_0^L - < \Delta \delta, \frac{\partial \psi}{\partial x} >. \tag{134}$$

Afterwards, we use the auxiliary problem conditions (127) – (128) and obtain:

$$< \Delta \delta, \psi > |_0^L = < \Delta \delta, \psi > |_{x=L} - < \Delta \delta, \psi > |_{x=0} =$$

$$= - < h_{ins}(\Delta T), \psi > |_{x=L} - < h_{out}(\Delta T), \psi > |_{x=0}. \tag{135}$$

At this point, we shall imply the following algebraic identity in order to investigate the heat flux at neighbor iterations:

$$\Delta \delta = \lambda_{n+1} \frac{\partial T_{n+1}}{\partial x} - \lambda_n \frac{\partial T_n}{\partial x} + \lambda_n \frac{\partial T_{n+1}}{\partial x} - \lambda_n \frac{\partial T_{n+1}}{\partial x} = \Delta \lambda \frac{\partial T_{n+1}}{\partial x} + \lambda_n \frac{\partial \Delta T}{\partial x}. \tag{136}$$

Applying above identity towards the integral relation (134), we may alter it and obtain the following expression:

$$- < \Delta \delta, \frac{\partial \psi}{\partial t} > = - < \Delta \lambda \frac{\partial T_{n+1}}{\partial x} + \lambda_n \frac{\partial \Delta T}{\partial x}, \frac{\partial \psi}{\partial x} > = - < \Delta \lambda \frac{\partial T_{n+1}}{\partial x}, \frac{\partial \psi}{\partial x} > -$$

$$- < \lambda_n \frac{\partial \Delta T}{\partial x}, \frac{\partial \psi}{\partial x} > = - < \Delta \lambda \frac{\partial T_{n+1}}{\partial x}, \frac{\partial \psi}{\partial x} > -$$

$$- < \Delta T, \lambda_n \frac{\partial \psi}{\partial x} > |_{x=L} + < \Delta T, \lambda_n \frac{\partial \psi}{\partial x} > |_{x=0} + + < \Delta T, \frac{\partial}{\partial x}\left(\lambda_n \frac{\partial \psi}{\partial x}\right) >. \tag{137}$$

From this point we combine together above relations and plug them back in (133):

$$- < \Delta T, \rho c \frac{\partial \psi}{\partial t} > = < \Delta T, \frac{\partial}{\partial x}\left(\lambda_n \frac{\partial \psi}{\partial x}\right) > - < \Delta T, \lambda_n \frac{\partial \psi}{\partial x} > |_{x=L} +$$

$$+ < \Delta T, \lambda_n \frac{\partial \psi}{\partial x} > |_{x=0} - < \Delta \lambda \frac{\partial T_{n+1}}{\partial x}, \frac{\partial \psi}{\partial x} > -$$

$$-< h_{ins}(\Delta T), \psi > |_{x=L} - < h_{out}(\Delta T), \psi > |_{x=0}. \qquad (138)$$

Simultaneously, the derived expression (132) has another equivalent form:

$$-\int_0^L \int_0^{T_m} \left(\Delta T, \rho c \frac{\partial \psi}{\partial t}\right) dt\, dx = \int_0^L \int_0^{T_m} \left(\Delta T, \frac{\partial}{\partial x}\left(\lambda_n \frac{\partial \psi}{\partial x}\right)\right) dt\, dx -$$

$$-\int_0^{T_m} \left(\Delta T, \lambda_n \frac{\partial \psi}{\partial x}\right)|_{x=L}\, dt + \int_0^{T_m} \left(\Delta T, \lambda_n \frac{\partial \psi}{\partial x}\right)|_{x=0}\, dt - \int_0^L \int_0^{T_m} \left(\Delta\lambda \frac{\partial T_{n+1}}{\partial x}, \frac{\partial \psi}{\partial x}\right) dt\, dx$$

$$- \int_0^{T_m} (h_{ins}(\Delta T), \psi)|_{x=L}\, dt - \int_0^{T_m} (h_{out}(\Delta T), \psi)|_{x=0}\, dt. \qquad (139)$$

Further step is to collect all similar terms of the received integral relation and to set another working hypothesis $\psi|_{t=T_m} = \psi(x, T_m) = 0$, after that it will follow that:

$$-\int_0^L \int_0^{T_m} \left(\Delta T, \rho c \frac{\partial \psi}{\partial t} + \frac{\partial}{\partial x}\left(\lambda_n \frac{\partial \psi}{\partial x}\right)\right) dt\, dx + \int_0^L \int_0^{T_m} \left(\Delta\lambda \frac{\partial T_{n+1}}{\partial x}, \frac{\partial \psi}{\partial x}\right) dt\, dx +$$

$$+ \int_0^{T_m} \left(\Delta T, \lambda_n \frac{\partial \psi}{\partial x} + h_{ins}\psi\right)|_{x=L}\, dt +$$

$$+ \int_0^{T_m} \left(\Delta T, h_{out}\psi - \lambda_n \frac{\partial \psi}{\partial x}\right)|_{x=0}\, dt = 0. \qquad (140)$$

From above equation we see that the left part will be equal to zero only under the following circumstances:

$$\rho c \frac{\partial \psi}{\partial t} + \frac{\partial}{\partial x}\left(\lambda_n \frac{\partial \psi}{\partial x}\right) = 0 \ . \qquad (141)$$

$$\left(h_{out}\psi - \lambda_n \frac{\partial \psi}{\partial x}\right)|_{x=0} = 2\left(T - Tg_1(t)\right)|_{x=0}. \qquad (142)$$

$$\left(h_{ins}\psi + \lambda_n \frac{\partial \psi}{\partial x}\right)|_{x=L} = 2\left(T - Tg_2(t)\right)|_{x=L}. \qquad (143)$$

$$\psi|_{t=T_m} = \psi(x, T_m) = 0. \qquad (144)$$

The built conjugate model above may be solved numerically or analytically further by analogy to other models discussed in this thesis. We will present major notes on analytical investigations of the discussed model in the Appendix A. Even by satisfying above system (141) – (142), the left part may not be nulled if one more condition would not be achieved, that is the following hypothesis:

$$\int_0^L \int_0^{T_m} \left(-\Delta\lambda \frac{\partial T_{n+1}}{\partial x}, \frac{\partial \psi}{\partial x}\right) dt\, dx = < -\Delta\lambda \frac{\partial T_{n+1}}{\partial x}, \frac{\partial \psi}{\partial x} > =$$

$$= 2(< \Delta T, T - Tg_2 > |_{x=L} - < \Delta T, T - Tg_1 > |_{x=0}). \qquad (145)$$

By observing the above assumption, we may set up the following functional mappings, that are depicting the minimization of the error between computed and measured values:

$$\begin{cases} J_1(\lambda) = \int_0^{T_m} (T(0,t) - Tg_1)^2 dt\,, \\ J_2(\lambda) = \int_0^{T_m} (T(L,t) - Tg_2)^2 dt\,. \end{cases} \qquad (146)$$

The set mappings describe the potential energy surface for considered dynamical system in terms of the thermal conductivity coefficient through the temperature field, however, by analogical procedure, we may derive such mapping in other coefficients terms. By finding the absolute minimum of the functional, we will evaluate the state of equilibrium of considered dynamical system, which is reflecting the proper allocation of determined coefficients. The minimization could be performed by posing the monotonous decreasing condition over the functionals, such that they will satisfy to the following inequalities: $J_{1,2}(\lambda_{n+1}) - J_{1,2}(\lambda_n) \leq 0 \rightarrow J_{1,2}(\lambda_{n+1}) \leq J_{1,2}(\lambda_n)$. For that reason, in order to achieve such conditions, we consider the increment of the functionals over neighbor iterations for the first functional:

$$\Delta J_1 = J_1(\lambda_{n+1}) - J_1(\lambda_n) = J_1^{n+1} - J_1^n =$$

$$= \int_0^{T_m} (T_{n+1}(0,t) - Tg_1)^2 dt - \int_0^{T_m} (T_n(0,t) - Tg_1)^2 dt =$$

$$= |a^2 - b^2 = 2b(a-b) + (a-b)^2| =$$

$$= 2\int_0^{T_m} (T_n(0,t) - Tg_1)\Delta T(0,t) dt + \int_0^{T_m} [\Delta T(0,t)]^2 dt. \qquad (147)$$

Analogically, we consider the same difference for the second functional, obtaining:

$$\Delta J_2 = J_2(\lambda_{n+1}) - J_2(\lambda_n) = J_2^{n+1} - J_2^n =$$

$$= \int_0^{T_m} (T_{n+1}(L,t) - Tg_2)^2 dt - \int_0^{T_m} (T_n(L,t) - Tg_2)^2 dt =$$

$$= |a^2 - b^2 = 2b(a-b) + (a-b)^2| =$$

$$= 2\int_0^{T_m} (T_n(L,t) - Tg_2)\Delta T(L,t)dt + \int_0^{T_m} [\Delta T(L,t)]^2 dt. \qquad (148)$$

Comparing together expressions (147) and (148) along with the working hypothesis (39) we may notice that:

$$\int_0^L \int_0^{T_m} \left(-\Delta\lambda \frac{\partial T_{n+1}}{\partial x}, \frac{\partial \psi}{\partial x}\right) dt\, dx = < -\Delta\lambda \frac{\partial T_{n+1}}{\partial x}, \frac{\partial \psi}{\partial x} > =$$

$$= J_2(\lambda_{n+1}) - J_2(\lambda_n) - J_1(\lambda_{n+1}) + J_1(\lambda_n) -$$

$$- < \Delta T, \Delta T > |_{x=L} + < \Delta T, \Delta T > |_{x=0}. \qquad (149)$$

In the equation (149) we open the term: $\Delta T = T_{n+1} - T_n \rightarrow T_{n+1} = \Delta T + T_n$ in this way, the expression will be altered to:

$$\Delta\lambda < \frac{\partial T_{n+1}}{\partial x}, \frac{\partial \psi}{\partial x} > = \Delta\lambda < -\frac{\partial T_n}{\partial x}, \frac{\partial \psi}{\partial x} > -\Delta\lambda < \frac{\partial \Delta T}{\partial x}, \frac{\partial \psi}{\partial x} > +$$

$$+ < \Delta T, \Delta T > |_{x=L} - < \Delta T, \Delta T > |_{x=0} = J_2(\lambda_{n+1}) -$$

$$- J_2(\lambda_n) - J_1(\lambda_{n+1}) + J_1(\lambda_n). \qquad (150)$$

By observing the above equation, we will note that to reach the minimum value of the posed functional, the left part of the above expression should be less than zero, for that reason we pose the inequality:

$$-\Delta\lambda < \frac{\partial T_n}{\partial x}, \frac{\partial \psi}{\partial x} > -\Delta\lambda < \frac{\partial \Delta T}{\partial x}, \frac{\partial \psi}{\partial x} > +$$

$$+ < \Delta T, \Delta T > |_{x=L} - < \Delta T, \Delta T > |_{x=0} \leq 0. \qquad (151)$$

From above inequality, we may separately investigate the small quantities of higher orders:

$$\begin{cases} \Delta\lambda < \frac{\partial T_n}{\partial x}, \frac{\partial \psi}{\partial x} >= k_1, \\ \Delta\lambda < \frac{\partial \Delta T}{\partial x}, \frac{\partial \psi}{\partial x} >= k_2, \\ < \Delta T, \Delta T > |_{x=L} = k_3, \\ < \Delta T, \Delta T > |_{x=0} = k_4. \end{cases} \quad (152)$$

Here, the value of k_1 is a small quantity of the first order, and all other quantities $k_{2,3,4}$ are the small quantities of the second order, thus the values of k_1 will prevail over the sign convention, so that is the value $\Delta\lambda = \lambda(x)_{n+1} - \lambda(x)_n$ should be positive. Thus, we are deriving the following estimator:

$$\lambda(x)_{n+1} = \lambda(x)_n + \gamma(x)_n \int_0^L \int_0^{T_m} \frac{\partial T_n}{\partial x} \frac{\partial \psi}{\partial x} dt\, dx. \quad (153)$$

Here by the expression $\gamma(x)_n$ we have additionally introduced small quantity, which is at the same time represents the governing parameter in analogy to the gradient descent method, that should be appropriately sampled in order to satisfy the criteria of termination in iterative process, - it will allow us to determine the absolute value of the functional and satisfy the inequality (151). At the same time, in a case of non-homogeneous structure of the considered medium, we may apply the additivity property of integral, and decompose our expression (153), such that it will be applied towards the multilayered structure, i.e., $Q = \bigcup_{i=1}^{N} Q_i$:

$$\lambda(x)_{n+1} = \lambda(x)_n + +\gamma(x)_n \int_0^L \int_0^{T_m} \frac{\partial T_n}{\partial x} \frac{\partial \psi}{\partial x} dt\, dx \lambda(x)_n =$$

$$= \lambda(x)_n + \gamma(x)_n \int_0^{l_1} \int_0^{T_m} \frac{\partial T_n}{\partial x} \frac{\partial \psi}{\partial x} dt\, dx +$$

$$+\gamma(x)_n \int_{l_1}^{l_2} \int_0^{T_m} \frac{\partial T_n}{\partial x} \frac{\partial \psi}{\partial x} dt\, dx + \cdots + \gamma(x)_n \int_{l_{i-1}}^{L} \int_0^{T_m} \frac{\partial T_n}{\partial x} \frac{\partial \psi}{\partial x} dt\, dx. \quad (154)$$

By setting up the appropriate initial approximation, we may use the above recurrent relations and determine the conductivity coefficient iteratively. In a case of piece-wise constant function that represents the coefficient, we may separate above relation due to homogeneity of constructed functional by obtaining the below system of expressions:

$$\begin{cases} \lambda(x)_{n+1} = \lambda(x)_n + \gamma(x)_n \int_0^{l_1} \int_0^{T_m} \frac{\partial T_n}{\partial x} \frac{\partial \psi}{\partial x} dt\, dx, x \in [0, l_1], \\ \lambda(x)_{n+1} = \lambda(x)_n + \gamma(x)_n \int_{l_1}^{l_2} \int_0^{T_m} \frac{\partial T_n}{\partial x} \frac{\partial \psi}{\partial x} dt\, dx, x \in [l_1, l_2], \\ \vdots \\ \lambda(x)_{n+1} = \lambda(x)_n + \gamma(x)_n \int_{l_{N-1}}^{l_N} \int_0^{T_m} \frac{\partial T_n}{\partial x} \frac{\partial \psi}{\partial x} dt\, dx,\ x \in [l_{N-1}, l_N]. \end{cases} \quad (155)$$

In a case of the well-posedness of the proposed problem statement, we would apply the fundamental theorem of variational calculus and the condition of the existence of unique solution by investigation of the functional integrands in a form of the below system of differentiable functions with respect to the functional arguments:

$$\begin{cases} S_1 = 2[T(0,t) - Tg_1(t)]^2, \\ S_2 = 2[T(L,t) - Tg_2(t)]^2, \\ \frac{\partial S_1}{\partial T} - \frac{d}{dt}\frac{\partial S_1}{\partial T'} = 0 \to \frac{\partial S_1}{\partial T} = 0 \to 4[T(0,t) - Tg_1(t)] = 0, \\ \frac{\partial S_2}{\partial T} - \frac{d}{dt}\frac{\partial S_2}{\partial T'} = 0 \to \frac{\partial S_2}{\partial T} = 0 \to 4[T(L,t) - Tg_2(t)] = 0. \end{cases} \quad (156)$$

However, by observing the above Lagrange-Euler equation we will see that the computed and measured temperature fields over the boundary points of domain should be equal, which is never true due to ill-posedness of the inverse problem, for instance because of the error introduced by the measurement device and so on. Further we are presenting the algorithm – 2, which will allow us to determine all necessary terms of the thermal elasticity model.

Algorithm 2.

Step 0. Initially, we have to introduce the material parameters in terms of thermal and elasticity properties, assuming the initial approximations as the assumptions, - here we shall pose the knowledge of the Poisson and linear expansion coefficients values.

Step 1. Empirically, we introduce the small fluctuations by knowing the principal moments of the considered solid and measuring the appeared differences of the temperature field over the boundary points of investigated domain.

Step 2. Applying the recurrent relations, we may compute the thermal conductivity parameters along with the temperature field values using analytical expressions.

Step 3. Using the expression (18) we evaluate the Lame's coefficient and further by the expression (19) we determine the Young's modulus along with the cylindrical stiffness from the relation (17).

Step 4. Applying the Sophie-Germain equation we are adjusting the obtained results of coefficients via juxtaposing the bending moment for moderated fluctuation with measured and computed principal displacement values.

Step 5. Furthermore, we may proceed analyzing the thermal and elasticity parameters and validate the state of deterioration of structural material strength by comparing the evaluated data with the normative values.

3 TECHNICAL EXPERIMENTAL DESIGNS FOR VALIDATION OF DERIVED ANALYTICAL EXPRESSIONS FOR THE PROPOSED INVERSE ANALYSIS METHODOLOGY

Current chapter of the thesis intends to describe the major posed experimental designs to validate the received analytical expressions for the proposed inverse analysis methodology. We will separately present models and computational algorithms for each posed case study, like the heat and moisture transfer computer model, or the thermoelastic bending design, outlining the received results analysis.

3.1 Experimental design for multilayered heat transfer in medium terrain for both homogenized and non-homogeneous measurements

In order to validate the algorithm – 1, we are proposing the following experimental design scheme for epy (34) – (38) model domain presented in the one-dimensional form, two-layered medium terrain, introduced by $\Omega: (0,\xi) \cup (\xi, L) \times (0, t_{max})$ by the figure below:

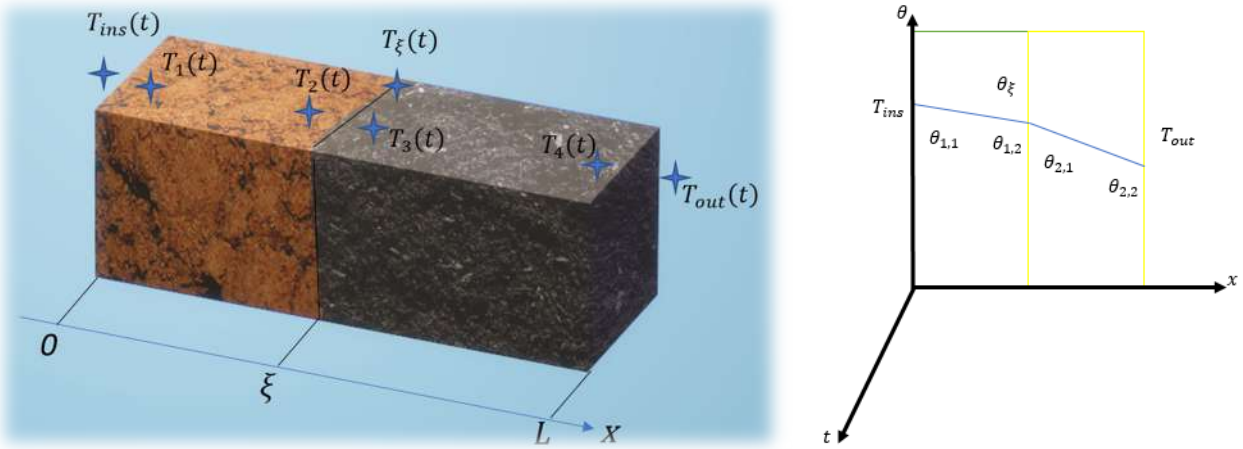

Figure 1 - Experimental design scheme

On the figure 1 we denote the measurement devices that sample data over investigated domain for two sets of parameters, where the geometrical characteristic ξ will be evaluated simultaneously by both sub-domain problems via the contact conditions:

$$\begin{cases} \pi_1 = \left\{\rho_1, c_{p_1}, h_{ins}, k_1, \xi\right\}, \\ \pi_2 = \left\{\rho_2, c_{p_2}, h_{out}, k_2, \xi\right\}. \end{cases} \tag{157}$$

In order to perform the homogenization sufficiently, we shall specify the time partition for the ambient temperature being constant, where we may omit the fluctuations by observing that they are negligible. This partition scheme is illustrated below:

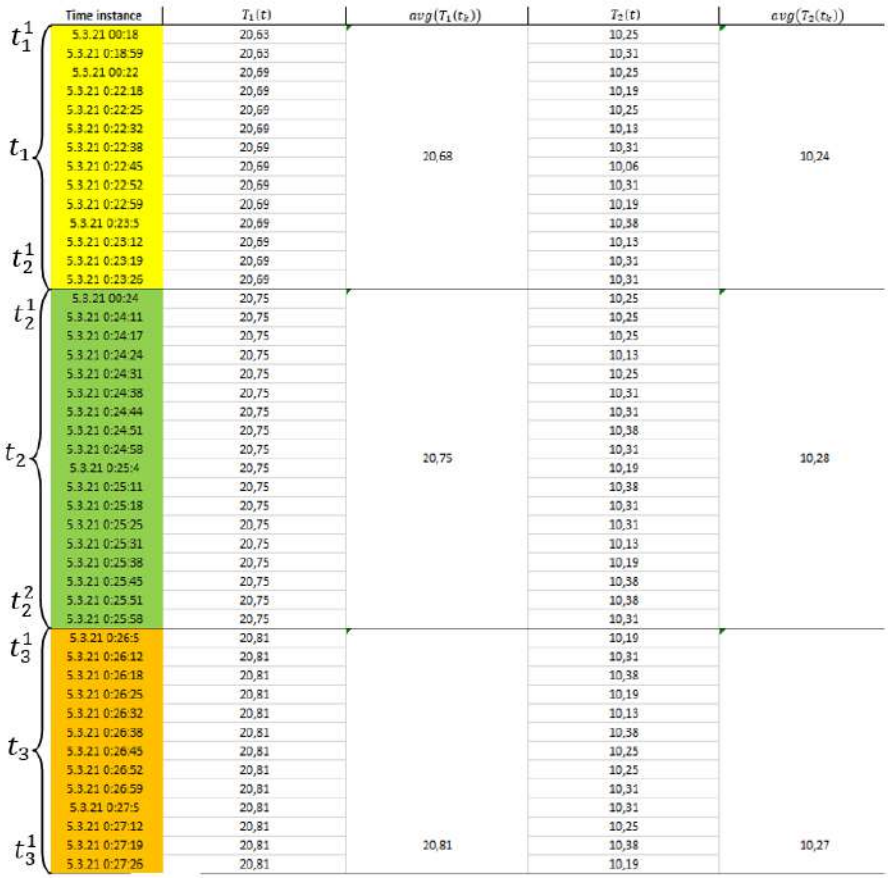

Figure 2 - Time domain decomposition scheme

Afterwards we may perform the algorithm 1 on each sub-division $t^k \in (t_i, t_{i+1})$ in order to iteratively compute parameters from the sets π_1 and π_2 one by one. To solve the system of nonlinear equations that we receive upon determination of unknown parameters, until we reach the following stop criteria:

$$\left|u(x_m, t) - T_{g_m}(t)\right| \leq \varepsilon. \tag{158}$$

Here ε is the predefined accuracy, and x_m – is the measurement device coordinate, meanwhile the term $T_{g_m}(t)$ – is the measured temperature. Right after perform of the algorithm – 1 by minimizing the expressions (120) – (124), we may verify the following eigenfunctions' roots behavior to clarify their orthonormal tendency along with the Cauchy sequence behavior for the Fourier coefficients $\mathrm{B_n}(\mu_n)$ for different roots of transcendental equation solutions:

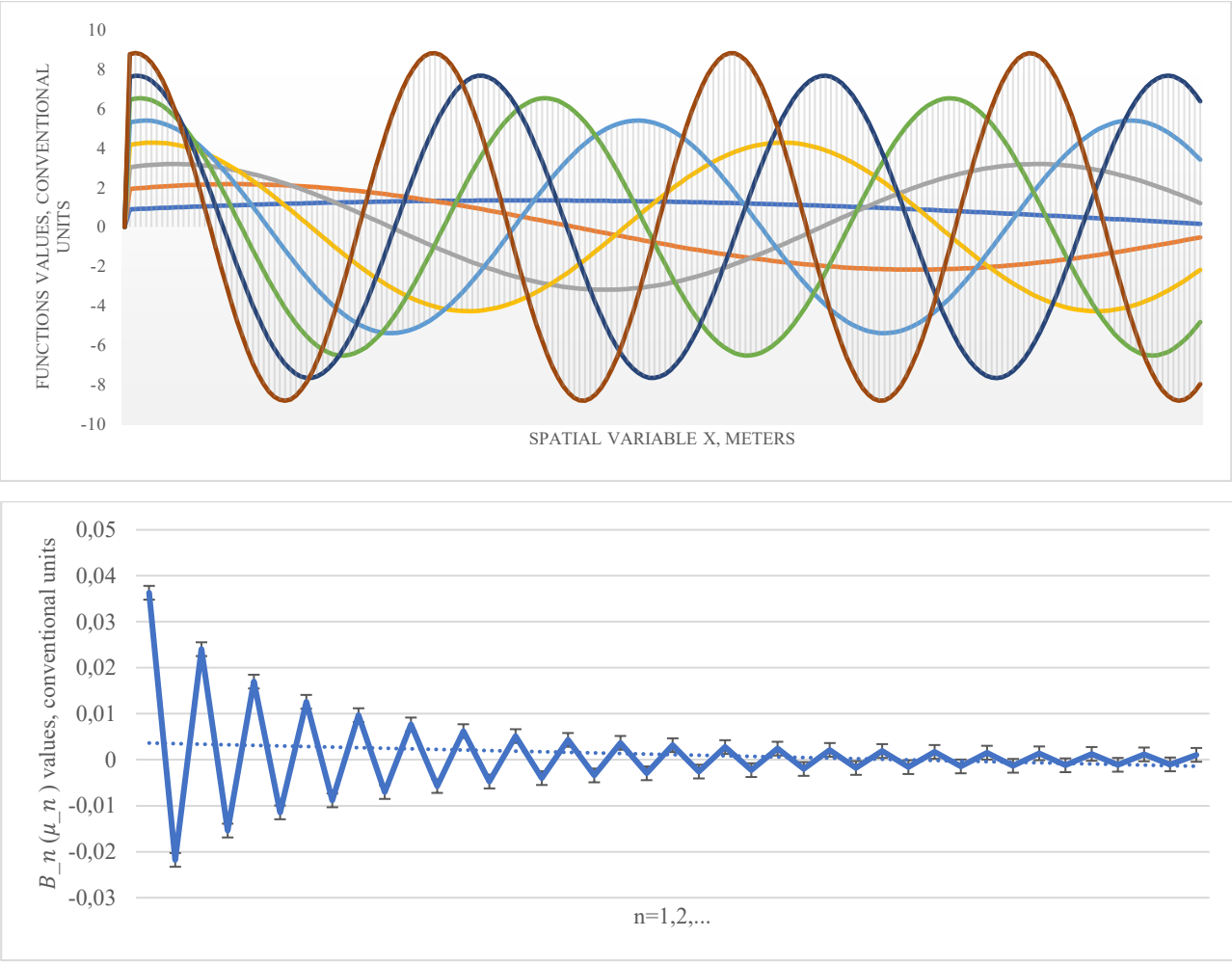

Figure 3 - Eigenfunctions values distribution for posed direct problem (above), Fourier coefficient $B_n(\mu_n)$ (below)

The next step is to derive the analytical expressions, which are going to include the non-homogeneous sampling over the boundary regions, and for that reason we transfer the time domain into the frequency domain via the Laplace transform. For non-homogenized samples we are decomposing the problem presented in the scheme on the figure 1 intro two sub-problems:

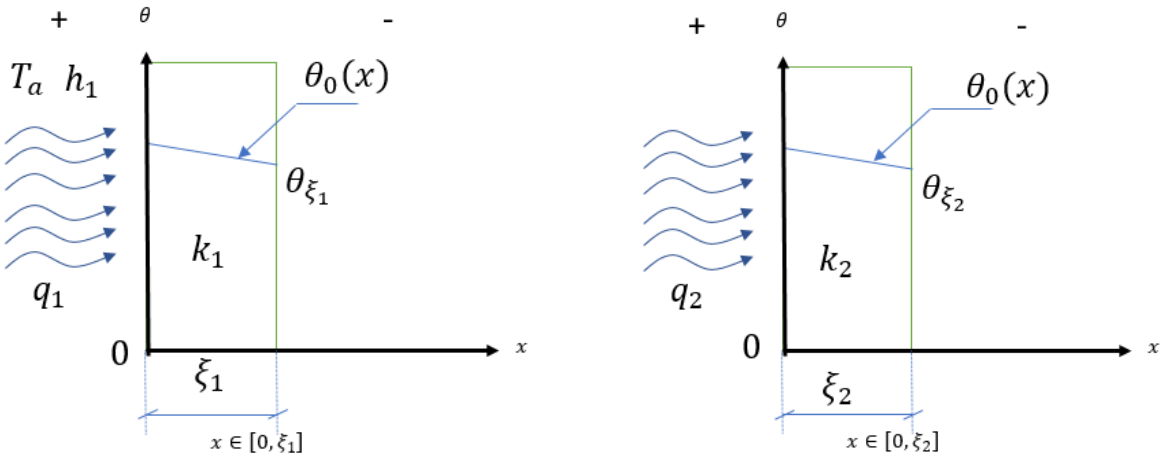

Figure 4 - Schemes of non-homogeneous problem decomposition

In the above formulation, we obtain two connected model:

$$\begin{cases} \frac{\partial \theta_1}{\partial t} = a_1 \frac{\partial^2 \theta_1}{\partial x^2}, \\ \frac{\partial \theta_2}{\partial t} = a_2 \frac{\partial^2 \theta_2}{\partial x^2}. \end{cases} \tag{159}$$

$$\begin{cases} \theta_1(x,0) = \theta_0(x), x \in (0, \xi_1), \\ \theta_2(x,0) = \theta_0(x), x \in (\xi_1, \xi_2). \end{cases} \tag{160}$$

$$\begin{cases} \theta_1(\xi_1, t) = \theta_{\xi_1}(t), \\ \theta_2(\xi_2, t) = \theta_{\xi_2}(t). \end{cases} \tag{161}$$

$$\begin{cases} -k_1 \frac{\partial \theta_1(0,t)}{\partial x} = h_1\left(T_a - \theta_1(0,t)\right), \\ -k_2 \frac{\partial \theta_2(0,t)}{\partial x} = q_2. \end{cases} \tag{162}$$

Here we introduce the dimensionless units:

$$\begin{cases} \bar{x}_1 = \frac{x}{\xi_1} - dimensionless\ coordinate,\ \bar{x}_1 \in [0,1], \\ \bar{x}_2 = \frac{x}{\xi_2} - dimensionless\ coordinate,\ \bar{x}_2 \in [0,1], \\ Fo_1 = \frac{a_1 t}{\xi_1^2}, Fo_2 = \frac{k_2 t}{\rho_2 c_{p_2} \xi_2^2} - Fourier\ number, \\ Bi_1 = \frac{h_1 \xi_1}{\lambda_1}, Bi_2 = \frac{h_2 \xi_2}{\lambda_2} - Bio\ number, \\ \bar{\theta}_1(\bar{x}_1, Fo_1) = \frac{\theta_1(x_1,t) - \theta_{\xi_1}}{\theta_{\xi_1}}, \bar{\theta}_2(\bar{x}_2, Fo_2) = \frac{\theta_2(x_2,t) - \theta_{\xi_2}}{\theta_{\xi_2}}, \\ Ki = \frac{q_2 \xi_2}{\lambda_2 \theta_{\xi_2}} - Kirpichev's\ number. \end{cases} \tag{163}$$

Using the above substitutions, we may transfer the model (159) – (162) to the following form:

$$\begin{cases} \frac{\partial \bar{\theta}_1}{\partial Fo_1} = \frac{\partial^2 \bar{\theta}_1}{\partial \bar{x}_1^2}, \\ \frac{\partial \bar{\theta}_2}{\partial Fo_2} = \frac{\partial^2 \bar{\theta}_2}{\partial \bar{x}_2^2}. \end{cases} \tag{164}$$

$$\begin{cases} \bar{\theta}_1(\bar{x}_1, 0) = \bar{\theta}_0(\bar{x}_1), \\ \bar{\theta}_2(\bar{x}_2, 0) = \bar{\theta}_0(\bar{x}_2). \end{cases} \tag{165}$$

$$\begin{cases} \bar{\theta}_1(1, Fo_1) = \bar{\theta}_{\xi_1}(Fo_1), \\ \bar{\theta}_2(1, Fo_2) = 0. \end{cases} \tag{166}$$

$$\begin{cases} \frac{\partial \bar{\theta}_1(0, Fo_1)}{\partial \bar{x}_1} = Bi\bar{\theta}_1(0, Fo_1), \\ -\frac{\partial \bar{\theta}_2(0, Fo)}{\partial \bar{x}_2} = Ki. \end{cases} \tag{167}$$

This approach allows us to use the solution of the first layer as the boundary measurement for the condition in the second problem, while the general solutions for both will take the following form in the frequency domain:

$$\begin{cases} \bar{\theta}_1(\bar{x}_1, Fo_1) = \bar{\theta}_{\xi_1}\left[\frac{Bi\bar{x}_1 + 1}{Bi + 1}\right] - 2\sum_{n=1}^{\infty} \frac{Bisin(\mu_n)(\bar{x}_1 - 1)}{Bi + \cos^2(\mu_n)} e^{-\mu_n Fo_1} \times \\ \times \left[\int_0^1 \bar{\theta}_0(\xi_1)\sin\big(\mu_n(1 - \xi_1)\big)d\xi_1 - \frac{\bar{\theta}_{\xi_1}}{\mu_n}\right], here\ \mu_n = tan(\mu_n'), \mu_n' = i\sqrt{s_n}, \\ \widetilde{\theta_2}(\overline{x_2}, s) = Ach\left[\overline{x_2}\sqrt{s}\right] + Bsh\left[\overline{x_2}\sqrt{s}\right] - \frac{1}{\sqrt{s}}\int_0^{\overline{x_2}} \bar{\theta}_0(\xi)sh\left[\sqrt{s}(\overline{x_2} - \xi)\right]d\xi\,. \end{cases} \tag{168}$$

In order to find the unknown coefficients for the second equation, we will use received boundary conditions, for that reason we will differentiate the second equation of the (168) and obtain:

$$\frac{\partial \widetilde{\theta_2}(\overline{x_2}, s)}{\partial \overline{x_2}} = A\sqrt{s}sh\left[\overline{x_2}\sqrt{s}\right] + B\sqrt{s}ch\left[\overline{x_2}\sqrt{s}\right] - \int_0^{\overline{x_2}} \bar{\theta}_0(\xi)ch\left[\sqrt{s}(\overline{x_2} - \xi)\right]d\xi. \tag{169}$$

Now, by applying the second expression of (167), we will receive the explicit value of the coefficient B:

$$\frac{\partial\widetilde{\theta_2}(0,s)}{\partial\overline{x_2}} = A\sqrt{s}sh\left[0\sqrt{s}\right] + B\sqrt{s}ch\left[0\sqrt{s}\right] - \int_0^0 \bar{\theta}_0(\xi)ch\left[\sqrt{s}(0-\xi)\right]d\xi \rightarrow$$

$$\rightarrow B\sqrt{s} = -\frac{Ki}{s}. \tag{170}$$

At the same time from the second expression of the (166), we will determine the coefficient A as:

$$\begin{cases} \widetilde{\theta_2}(1,s) = Ach\left[\sqrt{s}\right] - \frac{Ki}{s\sqrt{s}}sh\left[\sqrt{s}\right] - \frac{1}{\sqrt{s}}\int_0^1 \bar{\theta}_0(\xi)sh\left[\sqrt{s}(1-\xi)\right]d\xi = 0, \\ A = \frac{Ki\ sh\left[\sqrt{s}\right]}{s\sqrt{s}\ ch\left[\sqrt{s}\right]} + \frac{1}{\sqrt{s}ch\left[\sqrt{s}\right]}\int_0^1 \bar{\theta}_0(\xi)sh\left[\sqrt{s}(1-\xi)\right]d\xi\,. \end{cases} \tag{171}$$

By plugging the obtained coefficients to our general solution in the frequency domain, we will obtain the following expression:

$$\widetilde{\theta_2}(\overline{x_2},s) = \frac{Ki\ \left[sh\left[\sqrt{s}\right]ch\left[\overline{x_2}\sqrt{s}\right] - sh\left[\overline{x_2}\sqrt{s}\right]ch\left[\sqrt{s}\right]\right]}{s\sqrt{s}\ ch\left[\sqrt{s}\right]} +$$

$$+\frac{ch\left[\overline{x_2}\sqrt{s}\right]}{\sqrt{s}ch\left[\sqrt{s}\right]}\int_0^1 \bar{\theta}_0(\xi)sh\left[\sqrt{s}(1-\xi)\right]d\xi -$$

$$-\frac{1}{\sqrt{s}}\int_0^{\overline{x_2}} \bar{\theta}_0(\xi)sh\left[\sqrt{s}(\overline{x_2}-\xi)\right]d\xi. \tag{172}$$

We will simplify the above equation by using the following trigonometrical identities $sh(x)ch(y) - sh(y)ch(x) = sh(x-y)$ and reducing the integral expressions to a similar form, we obtain:

$$\widetilde{\theta_2}(\overline{x_2},s) = \frac{Ki\ sh\left[\sqrt{s}(1-\overline{x_2})\right]}{s\sqrt{s}\ ch\left[\sqrt{s}\right]} +$$

$$+\frac{1}{\sqrt{s}ch\left[\sqrt{s}\right]}\int_0^{\overline{x_2}} \bar{\theta}_0(\xi)sh\left[\sqrt{s}(1-\overline{x_2})\right]ch\left[\sqrt{s}\xi\right]d\xi +$$

$$+\frac{1}{\sqrt{s}ch\left[\sqrt{s}\right]}\int_0^1 \bar{\theta}_0(\xi)sh\left[\sqrt{s}(1-\xi)\right]ch\left[\overline{x_2}\sqrt{s}\right]d\xi. \tag{173}$$

The key part of the further work in derivation procedure for considered case is to obtain the inverse transform of the received expressions in order to derive real time domain solution. The inverse Laplace transform is applied term by term to (173) in accordance with the second decomposition theorem. The numerator and denominator of the first term in (173) are expanded as follows, knowing the expansion formulas for hyperbolic functions:

$$\begin{cases} sh(x) = x + \frac{x^3}{3!} + \frac{x^5}{5!} + \cdots, \\ sh\left[\sqrt{s}(1-\overline{x_2})\right] = \sqrt{s}(1-\overline{x_2}) + \frac{\sqrt{s}^3(1-\overline{x_2})^3}{3!} + \cdots = \\ = \sqrt{s}\left[(1-\overline{x_2}) + \frac{s^3(1-\overline{x_2})^3}{3!} + \cdots\right], \\ ch(x) = 1 + \frac{x^2}{2!} + \frac{x^4}{4!} + \cdots, \\ s\sqrt{s}\ ch\left[\sqrt{s}\right] = s\sqrt{s}\left[1 + \frac{s}{2!} + \frac{s^2}{4!} + \cdots\right]. \end{cases} \tag{174}$$

Taking into account above notations, our first term will be transformed into:

$$\frac{Ki\ sh\left[\sqrt{s}(1-\overline{x_2})\right]}{s\sqrt{s}\ ch\left[\sqrt{s}\right]} = Ki\frac{\left[(1-\overline{x_2}) + \frac{s(1-\overline{x_2})^3}{3!} + \cdots\right]}{s\left(1+\frac{s}{2!}+\cdots\right)}. \tag{175}$$

Taking into account the fact that the numerator and denominator of expression (175) are the polynomials with respect to the frequency variable, applying the inverse transformation, we can use the second expansion theorem. The second decomposition theorem allows us to determine the original from the image and says that if $F(s) = \frac{A(s)}{B(s)}$ is a rational proper and irreducible fraction, where $\mathrm{s}_1, \mathrm{s}_2, \mathrm{s}_3, \ldots, \mathrm{s}_\mathrm{k}$ are zeros of the denominator, then the original of this image function has the form:

$$f(t) = \sum_{s_k} res[F(s_k)e^{s_k t}] = \sum_{s_k} \frac{A(s_k)}{B'(s_k)} e^{s_k t}. \tag{176}$$

It should be noted that equality (176) is satisfied only if all poles of $F(s)$ are of the first order, that is, they are simple. Note that a point a is a pole if $\lim_{z\to a}|f(z)| = +\infty$, and also, if in the decomposition $f(z)$ in a Laurent series in the ring $0 < |z-a| < R$ the principal part has a finite number of terms. If the first term of the main part of the series contains $(z-a)^{-n}$, then we can consider the pole to be simple. In order to determine the zeros of the denominator (175), we will consider zero roots separately

from other roots. For that reason, according to the second decomposition theorem, we will write the original of the first term of the solution (173) in the form:

$$L^{-1}\left[Ki\frac{\Phi(s)}{\varphi(s)}\right]=\frac{\Phi(0)}{\varphi\prime(0)}+\sum_{n=1}^{\infty}\frac{\Phi(s_n)}{\varphi\prime(s_n)}e^{s_nFo}. \tag{177}$$

By considering the first term of (177), we will observe the following fact:

$$\begin{cases}\Phi(0)=\left[(1-\bar{x})+\frac{s(1-\bar{x})^3}{3!}+\cdots\right]_{s=0}=(1-\bar{x}),\\ \varphi'(0)=\left[s\left(1+\frac{s}{2!}+\cdots\right)'+s'\left(1+\frac{s}{2!}+\cdots\right)\right]_{s=0}=1.\end{cases} \tag{178}$$

It will give us the null root $Ki(1-\bar{x})$. By considering other roots when $n\geq 1$, we will use:

$$\begin{cases}sh(ix)=isin(x),\ sh[x]=\frac{1}{i}sin(ix),\\ ch(ix)=\cos(x),\ ch(x)=cos(ix).\end{cases} \tag{179}$$

Using above identities, we will receive:

$$\begin{cases}\Phi(s_n)=\frac{1}{i}\sin\left(i\sqrt{s}[1-\bar{x}]\right),\\ \varphi'(s_n)=\left(s\sqrt{s}ch\sqrt{s}\right)'=\frac{\sqrt{s}}{2}\left(3ch\sqrt{s}+\sqrt{s}sh\sqrt{s}\right)=\\ \quad=\frac{\sqrt{s}}{2}\left(3\cos\left(i\sqrt{s_n}\right)+\frac{\sqrt{s_n}}{i}\sin\left(i\sqrt{s_n}\right)\right).\end{cases} \tag{180}$$

We will consider the series (177) by applying the (180) identities and obtain another convenient form:

$$\sum_{n=1}^{\infty}\frac{2\sin\left(i\sqrt{s_n}[1-\bar{x}]\right)e^{s_nFo}}{i\sqrt{s}\left(3\cos\left(i\sqrt{s_n}\right)+\frac{\sqrt{s_n}}{i}\sin\left(i\sqrt{s_n}\right)\right)}. \tag{181}$$

The obtained expression above we will multiply and divide over i^2, then we will denote by $\mu_n=i\sqrt{s_n}$, the above expression will take the form:

$$\begin{cases}\sum_{n=1}^{\infty}\frac{2\sin\left(i\sqrt{s_n}[1-\bar{x}]\right)e^{s_nFo}}{i\sqrt{s}\left(3\cos\left(i\sqrt{s_n}\right)+\frac{\sqrt{s_n}}{i}\sin\left(i\sqrt{s_n}\right)\right)}=-\sum_{n=1}^{\infty}\frac{2\sin(\mu_n[1-\bar{x}])e^{-\mu_n^2Fo}}{\mu_n(\mu_n\sin(\mu_n)-3\cos(\mu_n))},\\ \frac{Ki\ sh[\sqrt{s}(1-\overline{x_2})]}{s\sqrt{s}\ ch[\sqrt{s}]}=Ki\left[(1-\overline{x_2})-\sum_{n=1}^{\infty}\frac{2\sin(\mu_n[1-\bar{x}])e^{-\mu_n^2Fo}}{\mu_n(\mu_n\sin(\mu_n)-3\cos(\mu_n))}\right].\end{cases} \tag{182}$$

By analogy we apply the second decomposition theorem of operational calculus towards second and third terms of our general solution (173):

$$\begin{cases} \Phi(s) = \left[\sqrt{s}(1-\bar{x}) + \frac{\sqrt{s}^3(1-\bar{x})^3}{3!} + \cdots\right]\left[1 + \frac{s\xi^2}{2!} + \cdots\right], \\ \varphi'^{(s)} = \left[\sqrt{s}ch\sqrt{s}\right]' = \frac{1}{2\sqrt{s}}\left(ch\sqrt{s} + \sqrt{s}sh\sqrt{s}\right). \end{cases} \quad (183)$$

Which results in the following quotient*:*

$$\frac{\Phi(s)}{\varphi\prime(s)} = \frac{2\sqrt{s}sh\left[\sqrt{s}(1-\bar{x})ch\left(\sqrt{s}\xi\right)\right]}{ch\sqrt{s}+\sqrt{s}sh\sqrt{s}}. \quad (184)$$

Taking into account that we have the frequency variable s, our null root will be equal to zero, i.e., $\frac{\Phi(0)}{\varphi\prime(0)} = 0$. By taking into account the trigonometrical identities (179), we will find the inverse transform as the following series:

$$L^{-1}\left[\frac{\Phi(s)}{\varphi'(s)}\right] = \sum_{n=1}^{\infty} \frac{2\sqrt{s_n}(1/i)sin\left[i\sqrt{s_n}(1-\bar{x})\right]cos\left(i\sqrt{s_n}\xi\right)}{\cos\left(i\sqrt{s_n}\right)+\sqrt{s_n}(1/i)\sin\left(i\sqrt{s_n}\right)} e^{s_n Fo}. \quad (185)$$

Similarly, like in the previous term, we will take the resulting expression to multiply and divide it by i^2, after that we will denote by $\mu_n = i\sqrt{s_n}$, then the above series will take the form:

$$L^{-1}\left[\frac{\Phi(s)}{\varphi'(s)}\right] = \sum_{n=1}^{\infty} \frac{2\mu_n sin[\mu_n(1-\bar{x})]cos(\mu_n\xi)}{\mu_n \sin(\mu_n)-\cos(\mu_n)} e^{-\mu_n^2 Fo}. \quad (186)$$

Thus, the original of the second term of the general solution takes the form:

$$L^{-1}\left[\frac{\Phi(s)}{\varphi'(s)}\right] = \sum_{n=1}^{\infty} \frac{2\mu_n sin[\mu_n(1-\bar{x})]}{\mu_n \sin(\mu_n)-\cos(\mu_n)} e^{-\mu_n^2 Fo} \int_0^{\bar{x}} \bar{\theta}_0(\xi)cos(\mu_n\xi)d\xi. \quad (187)$$

By analogy we will write the third term of the general solution (173) and determine the zeros of the denominator by determining the values μ_n:

$$\frac{\Phi(s)}{\varphi(s)} = \frac{sh\left[\sqrt{s}(1-\xi)\right]ch\left[\overline{x_2}\sqrt{s}\right]}{\sqrt{s}ch\left[\sqrt{s}\right]} = \frac{\left(sh\sqrt{s}ch\left(\sqrt{s}\xi\right)-sh\left(\sqrt{s}\xi\right)ch\sqrt{s}\right)ch\left[\overline{x_2}\sqrt{s}\right]}{\sqrt{s}ch\left[\sqrt{s}\right]}. \quad (188)$$

Considering the denominator, we will extract the characteristic equation $ch\sqrt{s} = 0$*, which is equivalent to* $\cos\left(i\sqrt{s}\right) = 0$*,* then, we will get $i\sqrt{s_n} = \frac{\pi n}{2}$*, that is* $s_n = -\frac{\pi^2 n^2}{4}$ or which is the same as $\mu_n = \frac{\pi n}{2}$, which is the set of roots of the characteristic equations of the considered system. By applying these characteristic equation roots towards (188), we will derive:

$$\begin{cases} \frac{\Phi(s)}{\varphi(s)} = \frac{sh\sqrt{s}ch(\sqrt{s}\xi)ch[\overline{x_2}\sqrt{s}]}{\sqrt{s}ch[\sqrt{s}]} \\ \frac{\Phi(s)}{\varphi\prime(s)} = \frac{2\sqrt{s}sh\sqrt{s}ch(\sqrt{s}\xi)ch[\overline{x_2}\sqrt{s}]}{\sqrt{s}sh[\sqrt{s}]-ch[\sqrt{s}]} \end{cases} \quad (189)$$

Applying now the trigonometrical identities (179) towards above equation and denoting by $i\sqrt{s_n} = \mu_n$, we will receive the original of the third term:

$$\begin{cases} L^{-1}\left[\frac{\Phi(s)}{\varphi'(s)}\right] = \sum_{n=1}^{\infty} \frac{2\mu_n \sin(\mu_n)cos(\mu_n\xi)cos[\overline{x_2}\mu_n]}{\mu_n sin[\mu_n]-cos[\mu_n]} e^{-\mu_n^2 Fo}, \\ L^{-1}\left[\frac{\Phi(s)}{\varphi'(s)}\right] = \sum_{n=1}^{\infty} \frac{2\mu_n \sin(\mu_n)cos[\overline{x_2}\mu_n]}{\mu_n sin[\mu_n]-cos[\mu_n]} e^{-\mu_n^2 Fo} \int_0^1 \bar{\theta}_0(\xi)cos(\mu_n\xi)d\xi\,. \end{cases} \quad (190)$$

Now by collecting together the identities (185), (187) and (190), we will receive the original of particular solution for the second decomposed model in dimensionless units:

$$\theta_2(\overline{x_2}, Fo) = Ki\left[(1-\overline{x_2}) - \sum_{n=1}^{\infty} \frac{2\sin(\mu_n[1-\bar{x}])\, e^{-\mu_n^2 Fo}}{\mu_n(\mu_n \sin(\mu_n) - 3\cos(\mu_n))}\right] +$$

$$+ \sum_{n=1}^{\infty} \frac{2\mu_n sin[\mu_n(1-\bar{x})]}{\mu_n \sin(\mu_n) - \cos(\mu_n)} e^{-\mu_n^2 Fo} \int_0^{\bar{x}} \bar{\theta}_0(\xi)cos(\mu_n\xi)d\xi +$$

$$+ \sum_{n=1}^{\infty} \frac{2\mu_n \sin(\mu_n)\, cos[\overline{x_2}\mu_n]}{\mu_n sin[\mu_n] - cos[\mu_n]} e^{-\mu_n^2 Fo} \int_0^1 \bar{\theta}_0(\xi)cos(\mu_n\xi)d\xi \quad (191)$$

Further by using the trigonometrical identities of the form: $sin[\mu_n(1-\bar{x})] = sin\mu_n\, cos(\mu_n\bar{x}) - sin(\mu_n\bar{x})\, cos\ \mu_n$, and taking into account the characteristic equation of the system, $cos\,\mu_n = 0$, we will get $sin\mu_n = (-1)^{n+1}$, that means that $sin\big(\mu_n(1-\bar{x})\big) = (-1)^{n+1}\, cos(\mu_n\bar{x})$. The final analytical solution will take the following form:

$$\theta_2(\overline{x_2}, Fo) = Ki\left[(1-\overline{x_2}) - \sum_{n=1}^{\infty} \frac{8\cos\left(\frac{\pi n\bar{x}}{2}\right) e^{-\frac{\pi^2 n^2}{2} Fo}}{\pi^2 n^2}\right] +$$

$$+ \sum_{n=1}^{\infty} 2cos\left[\frac{\pi n\bar{x}}{2}\right] e^{-\frac{\pi^2 n^2}{2} Fo} \int_0^1 \bar{\theta}_0(\xi)cos\left(\frac{\pi n}{2}\xi\right) d\xi \quad (192)$$

Since in the first problem solution we have only unknown heat flux over the inlet boundary, we use the computational model of the bulb lamp in order to simulate the process of heating flux from the environment and deduce the values of the heat flux, and to measure such values of the heat flux at x = 0, we model numerically by the finite element method the conductive, convective and radiative heat exchanges in an incandescent lamp filled with argon with a technical voltage of 220V in order to determine the point values of the heat flux. For the referent date we refer to SN RK 4.04-04-2013, which state that in outdoor electric lighting networks the voltage 380/220 V AC with grounded neutral is used. For the power supply of lighting devices, a voltage of not more than 220 V AC or DC should be utilized, we present below the average field distribution for the heat flux to derive the data over the boundary points of the considered lamp, first the corresponding figure for structured mesh and streamlines:

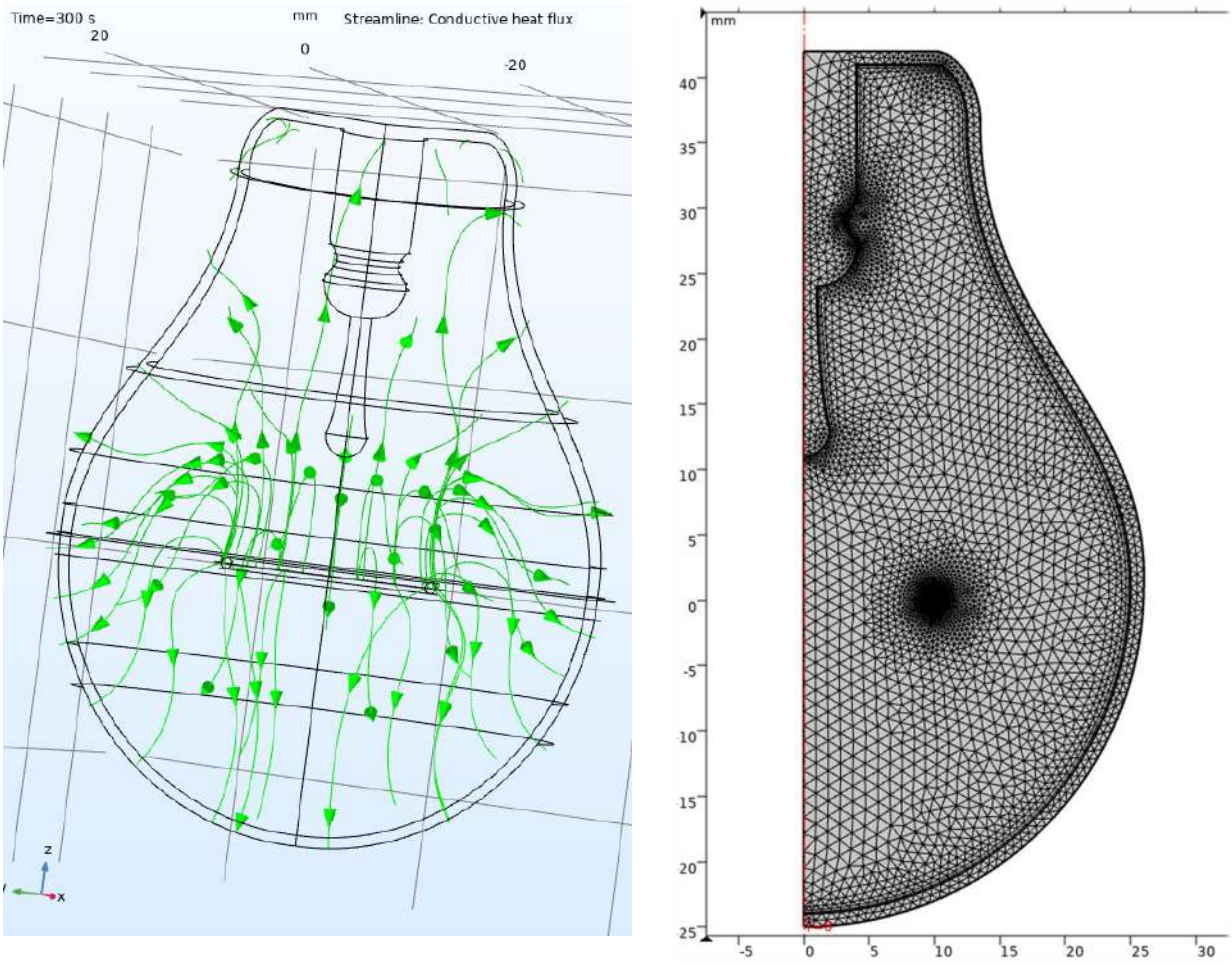

Figure 5 - Conductive streamline heat flux (left), structured mesh over axisymmetric region

The above computational mesh, based on the finite element method with the help of sampling of the test and basis functions, was performed for the considered multi-physical additional problem, which results further utilized for the model input boundary parameters as the heat flux. The method performed via construction of the

scalar product of the general equation and the arbitrary functions with further integration over the domain, which results in further construction of the infinite-dimensional function space, that is the Hilbert space with specific properties induced by Euclidian norm. This problem formulation is referred to as the pointwise-formulation, so-called the Galerking method, may be treated further by the Green's first identity results in weak formulation that relaxes the posed conditions over arbitrary basis functions. With the proposed weak formulation, it is possible to discretize the posed mathematical model equations an obtain the numerical model equations which correspond approximately to continuous model. Following these assumptions, the conductive heat flux $Q(x)$ is presented as a linear combination of a set of basis functions ψ_i that belong to the subspace of the constructed Hilbert space, i.e., $Q(x) \approx \sum_i Q_i \psi_i$, where $i = 1,2, \dots N$. That approximation results in construction of the system of N linear equations. Once the proposed system is discretized the system of linear equations presented by the matrix form, which is also referred as the stiffness matrix. Two neighboring basis functions afterwards share two triangular elements in common. These functions do not share the elements itself, but they have one element vertex in common. The obtained solution of the system of algebraic equations via iterative numerical algorithm gives an approximation of the solution to the system of partial differential equations that describe the physical process. The denser the constructed mesh, the closer the approximate solution gives results to the actual solution of continuous model. For instance, the one-dimensional dynamical system modelled by domain $\mho: [x_1, x_2] \cup [t_1, t_2]$ is meshed by integra-interpolation approximations and formulas:

$$\begin{cases} \Delta x = \frac{x_2 - x_1}{N}, \ \Delta t = \frac{t_2 - t_1}{M}, \\ x_i = x_1 + i\Delta x, t_j = t_1 + j\Delta t, \\ \frac{\partial Q}{\partial t} \approx \frac{Q_i^{j+1} - Q_i^j}{\Delta t}, \ \frac{\partial^2 Q}{\partial x^2} \approx \frac{Q_{i+1}^j - 2Q_i^j + Q_{i-1}^j}{(\Delta x)^2}. \end{cases} \tag{193}$$

Although the above assumptions could be sampled in accordance with the chose numerical accuracy resulting in selection of one of the suitable numerical scheme, this still illustrates the general idea of the constructed mesh and the finite element method utilized for discretization. For instance, the following approximations of the time marching scheme of the thermal components of the flux with the heat source g, using the Galerkin method could be written as the following explicit and implicit forms correspondingly:

$$\begin{cases} \rho c_p \frac{\partial Q}{\partial t} \sum_i \int_{\mho} \psi_i \psi_j dV + \sum_i Q_i \int_{\mho} k \nabla \psi_i \cdot \nabla \psi_j dV + \\ + \sum_i Q_i \int_{\partial \mho} (-k Q_i \nabla \psi_i \cdot \mathrm{n}) \psi_j dS = \int_{\mho} g(\sum_i Q_i \psi_i) \psi_j dV, \\ \rho c_p \frac{Q_i^{j+1} - Q_i^j}{\Delta t} \sum_i \int_{\mho} \psi_i \psi_j dV + \sum_i Q_i^{j+1} \int_{\mho} k \nabla \psi_i \cdot \nabla \psi_j dV + \\ + \sum_i Q_i^{j+1} \int_{\partial \mho} (-k Q_i^{j+1} \nabla \psi_i \cdot \mathrm{n}) \psi_j dS = \int_{\mho} g(\sum_i Q_i^{j+1} \psi_i) \psi_j dV, \\ \rho c_p \frac{Q_i^{j+1} - Q_i^j}{\Delta t} \sum_i \int_{\mho} \psi_i \psi_j dV + \sum_i Q_i^j \int_{\mho} k \nabla \psi_i \cdot \nabla \psi_j dV + \\ + \sum_i Q_i^j \int_{\partial \mho} (-k Q_i^j \nabla \psi_i \cdot \mathrm{n}) \psi_j dS = \int_{\mho} g(\sum_i Q_i^j \psi_i) \psi_j dV. \end{cases} \quad (194)$$

In practice, most of the modern time-stepping algorithms usually automatically switched between explicit and implicit steps depending on the problem posed. The difference equation (194) is further replaced with a polynomial expression that may vary in sampled order or the step length depending on the evolution of the solution in time. Most modern time-marching schemes are automatically controlled by the time evolution of the numerical solution. It is non-representative to depict the basis of the quadratic basis functions in 3-D by using the second-order elements, like tetrahedral, pyramidal, hexahedral etc., but color fields mapped on the domain may be used to plot the function values on the element surfaces giving us the illustration of the obtained solution. Regarding the distribution of the principal fields inside of the bulb, the average values during the first 5 minutes are represented by the figure below:

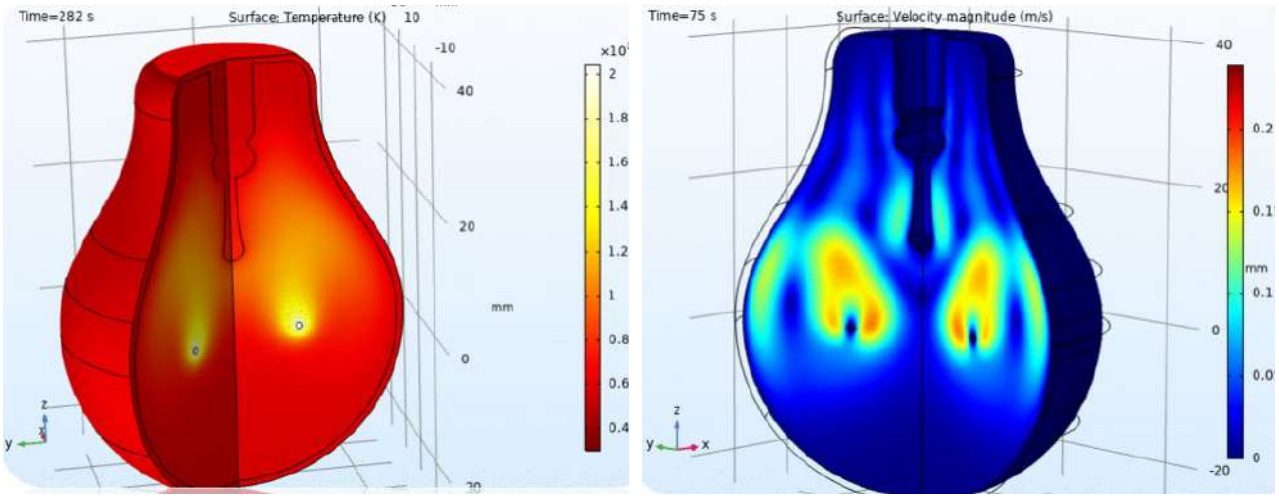

Figure 6 - Temperature field (left), velocity magnitude (right)

As for the heat flux along the lamp surface, we may take an average value from the below output:

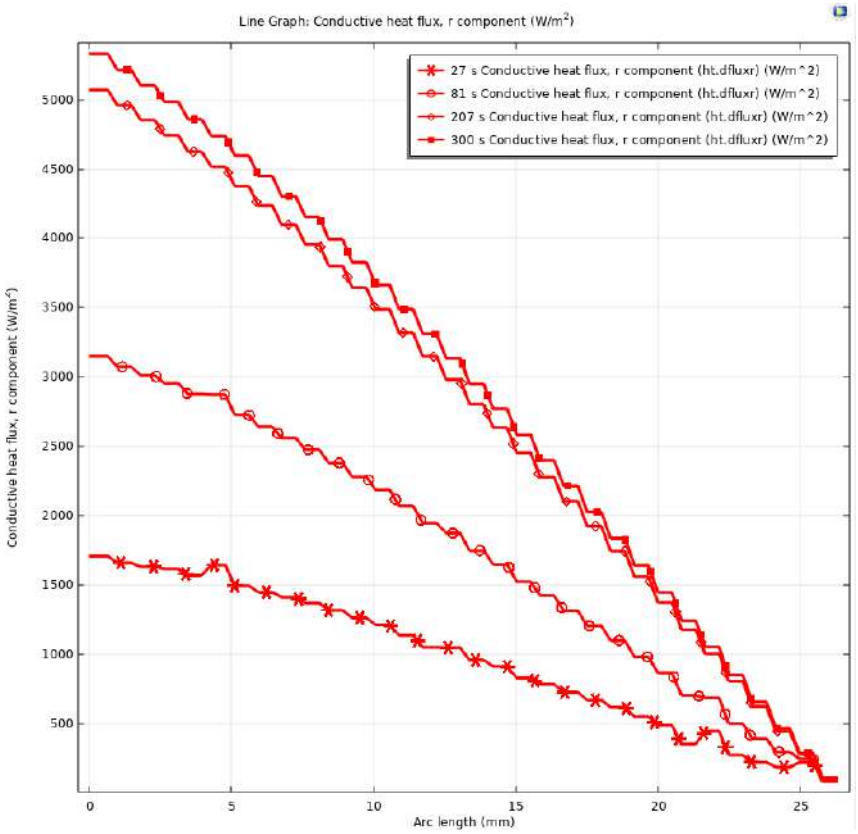

Figure 7 - Conductive heat flux during 5 minutes in cross-section over the boundary arc-length

Afterwards we present the computational results for the difference values between the measured and computational values of the sampled devices along time-domain:

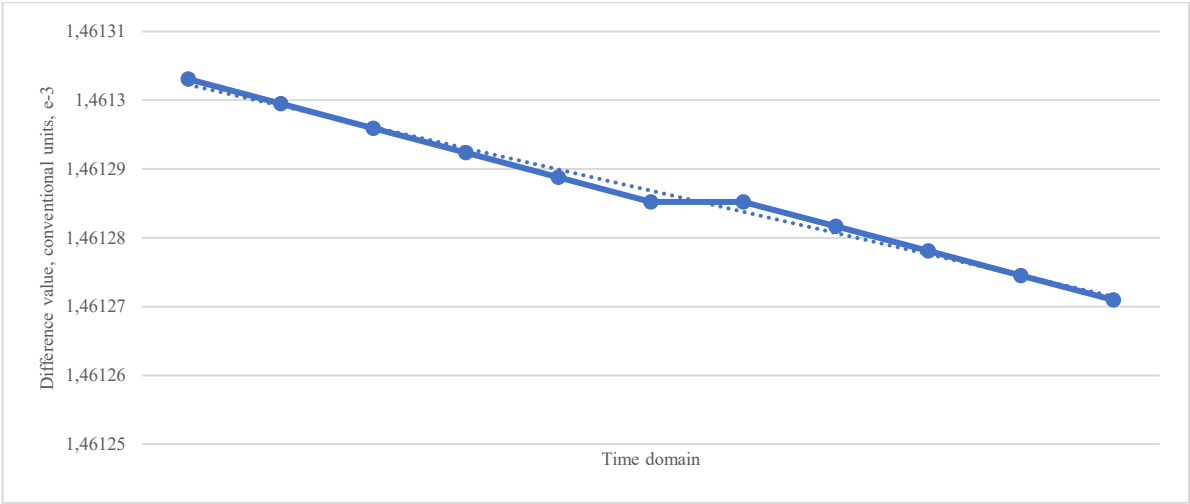

Figure 8 - Difference values at selected measuring device and evaluated temperatures through iterations

Concerning the estimated parameters π_1, we may observe the gradual approach towards the stationary values by performance of the algorithm – 1, when we determining the minimized values of the objective functions (121) and (122):

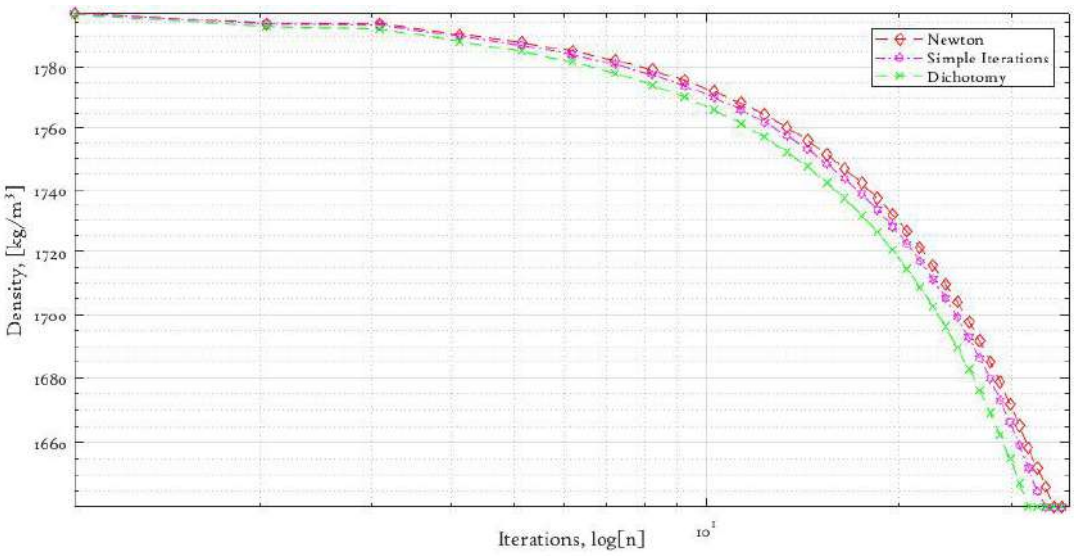

Figure 9 - The density estimation of the first sub-domain

By the gradual decrease of the estimated parameters, we observe by the above figures that our initial approximations were overestimated, since the same behavior we have for the volumetric heat capacity:

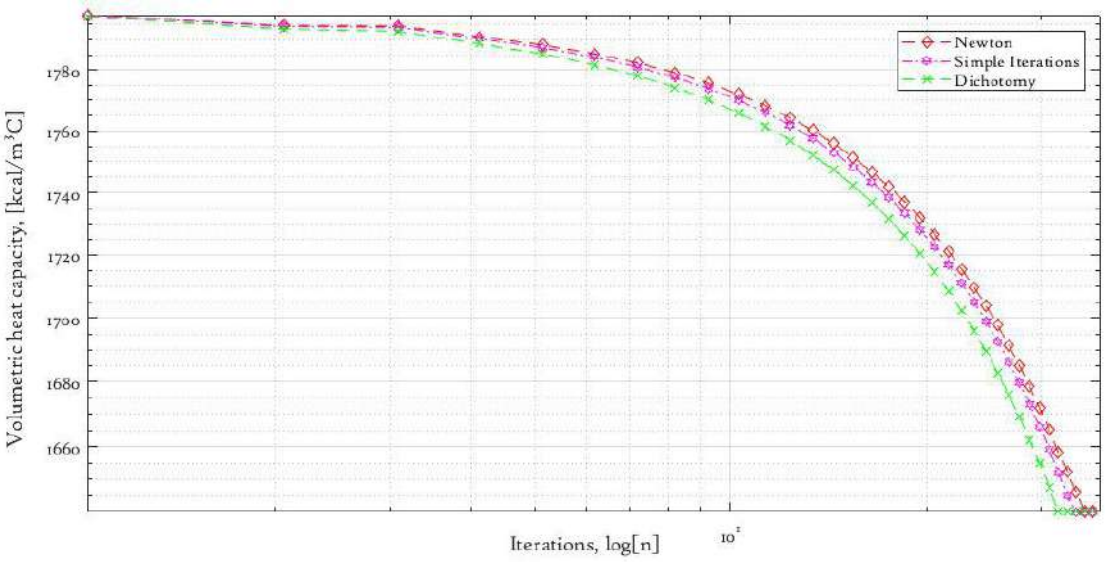

Figure 10 - Volumetric heat capacity estimation

The same tendency we receive by computing the heat transfer and thermal conductivity coefficients estimators via the proposed algorithm:

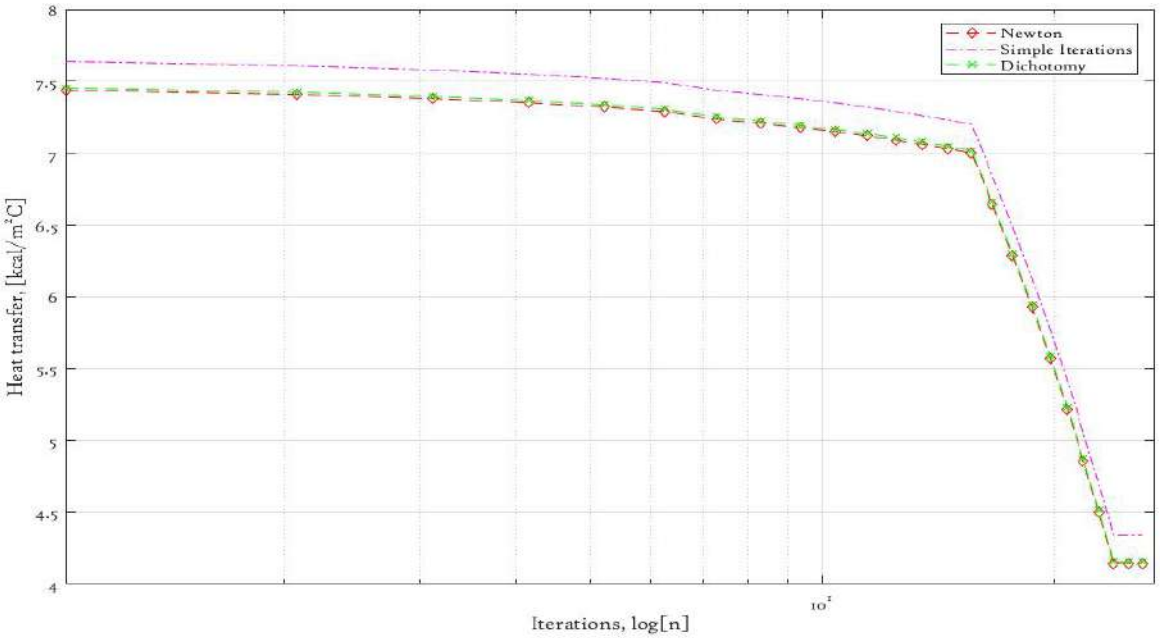

Figure 11 - Heat transfer determination over the first sub-domain

Since the conductivity parameter perceive the same overestimated initial guess, we also obtain the same gradual decrease towards stationary value:

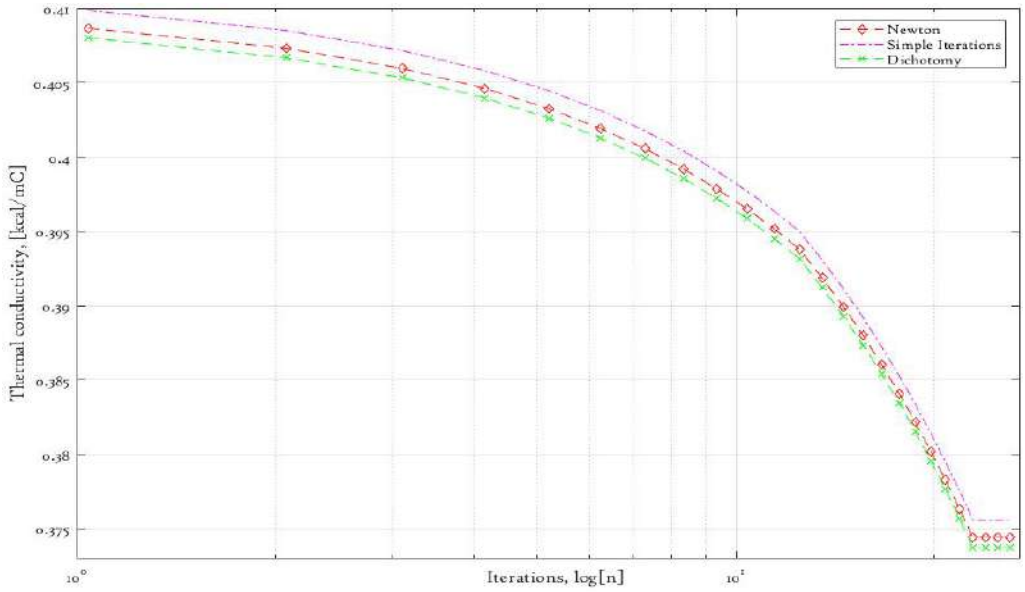

Figure 12 - Heat conductivity parameter estimation

For the second sub-domain problem we intentionally select the underestimated approximations for initial iteration in order to verify if the algorithm will demonstrate same smoothness in approaching the stationary values:

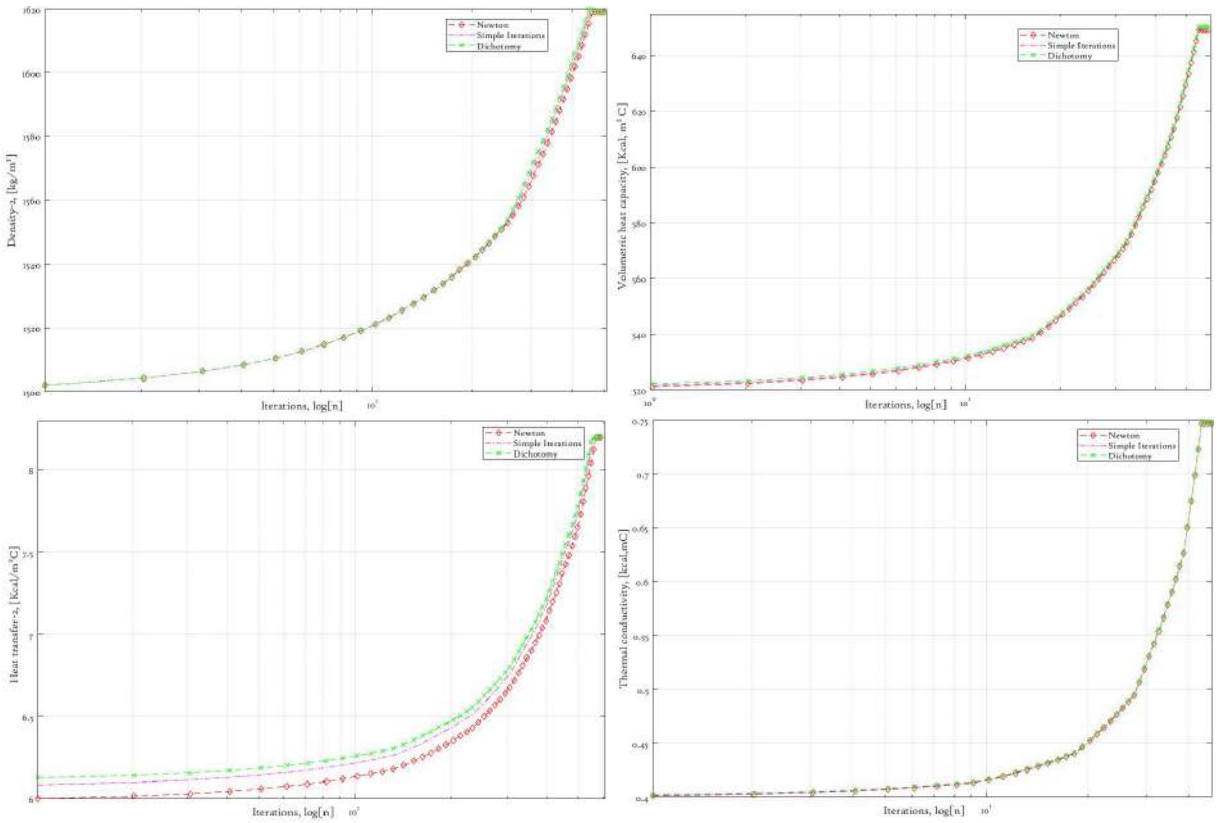

Figure 13 - Second layer parameters estimation

However, for the geometrical characteristic, we perform estimations for both under and overestimated initial sampling, in order to compare their convergency rates:

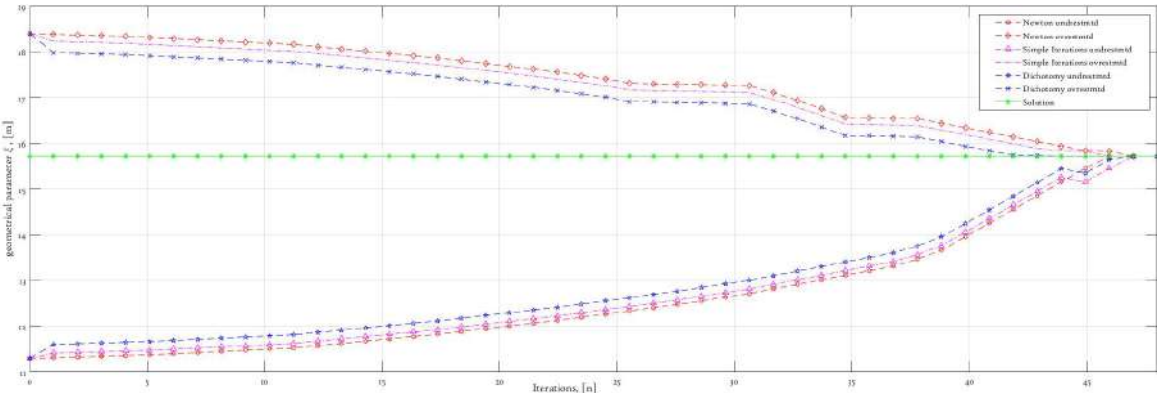

Figure 14 - Geometrical characteristic estimation

As could be clearly observable from above figures, we have a stable approach towards the stationary values by appropriate selection of the initial samplings. However, if we would determine the parameters sequentially as presented in our algorithm – 1, the tunning of parameters is not necessary as discussed in regularization issues in [80]. This fact is critical, as could be observed in various experimental works [81 – 83], where the regularization of the inverse problem affects the results and optimal convergency order. At the same time, the convergency issues could be

considered to be improved by appropriate sample of the iterative approach if certain stability condition constrains would be utilized for the posed model [84 – 88]. Since the measurement devices are also subjects that introduce the measurement error, we perform the test for noise simulation over the suggested algorithm. While the stable approach for exact value determination from both under and overestimated cases could be achieved by the meaningful samplings of some physical constraints represented by the governing coefficient in the recurrent computational formulas. Thus, in such case the sequential selection of the mentioned constrains, parameters tunning will be not necessary [89]. However, it was discussed by different investigations [90-92], that the parameter value utilized for the regularized inverse problems critically affects the obtained results and optimal selected order of convergency. The noise simulation is considered as the divergency free vector field via the noise error introduction:

$$\widetilde{T_{\xi}} = T_{\xi}\left(1 + \breve{\xi}_{n}\right). \tag{195}$$

Here the introduced $\breve{\xi}_{n}$ is prescribed error of the measuring device considered at selected point, that we assume as the smooth-step sigmoid-like interpolation and clamping function as depicted on below figure where we depict the normalized frequency for selected samples:

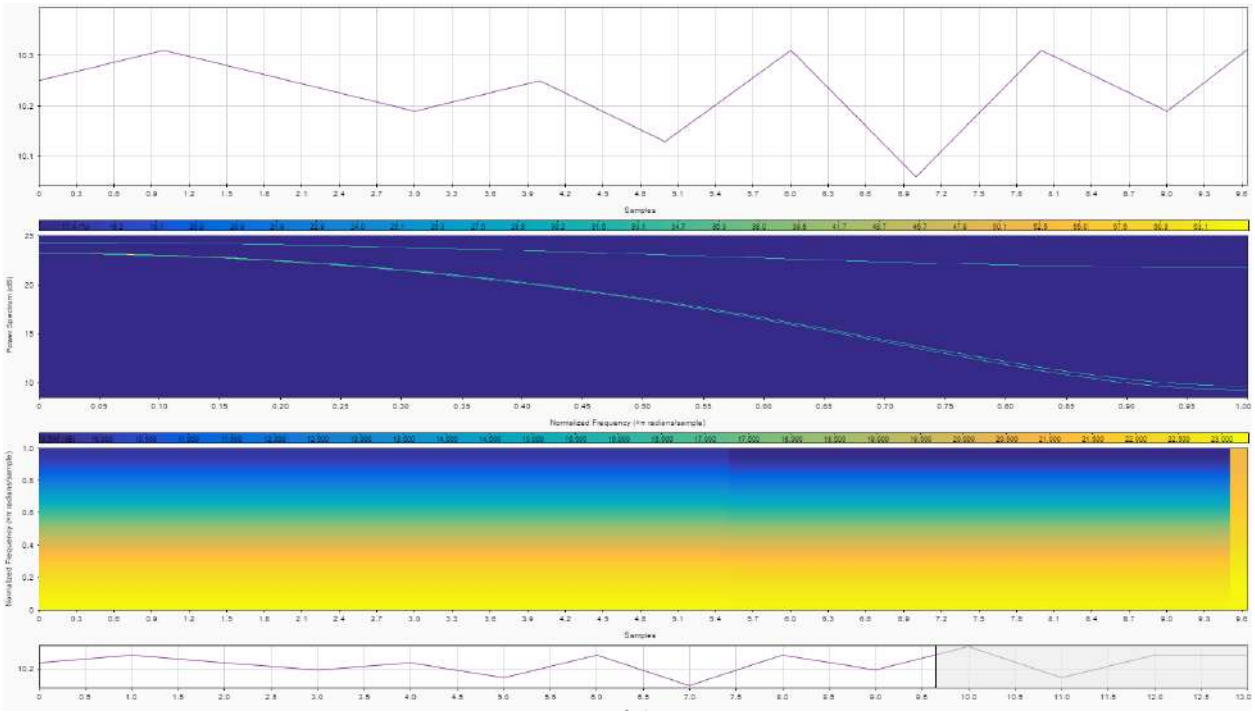

Figure 15 - Noise analysis for selected sampled measurements

The smoothness in the above profile reflects that the prescribed error is analogue of the simplex noise scaling procedure, and that the algorithm has high tendency to stability perseverance towards introduced measurements fluctuations.

3.2 Experimental design for inverse problem of the thermoelastic stress analysis model

For the second multiphysical model results validation, we perform the following numerical experiment. We consider a thin plate with fixed boundary edges constrain with homogeneous isotropic domain subjected to gravity load and thermal expansion due to introduced heat inward and outward fluxes in parallel directions. We consider a case with structural steel in order to perceive small fluctuations and the referent parameters are derived from typical normative documentation. The key formulation of the posed design is to evaluate the field distributions with normative referent parameters and afterwards perform the algorithm – 2 to adjust the key physical parameters according to set measurement data over the boundary edges. Following this approach iteratively we will seek computations with evaluated coefficients and continue simultaneously observing the functional behavior. The referent parameters are presented in the table below.

Table 1 - Reference physical parameters derived from typical normative

Name	Value	Unit
Heat capacity at constant pressure	475[J/(kg*K)]	J/(kg·K)
Thermal conductivity	44.5[W/(m*K)]	W/(m·K)
Coefficient of thermal expansion	12.3e-6[1/K]	1/K
Density	7850[kg/m^3]	kg/m³
Young's modulus	200e9[Pa]	Pa
Poisson's ratio	0.30	1
Lamé parameter λ	1.15e11[Pa]	Pa

Afterwards we introduce the physically controlled mesh over the domain which satisfies statistics presented in the below table – 2. The initial choice of the reference parameters is a key point in algorithm – 2, since the general convergency of the iterative mentioned algorithm will depend on the closeness level of the initial approximations towards the exact real values.

Table 2 - Mesh statistics

Description	Value
Minimum element quality	0.2609
Average element quality	0.6278
Tetrahedron	16157
Triangle	10700
Edge element	380
Vertex element	8

Continuation of the table 2

Maximum element size	0.055
Minimum element size	0.004
Curvature factor	0.4
Resolution of narrow regions	0.7
Maximum element growth rate	1.4

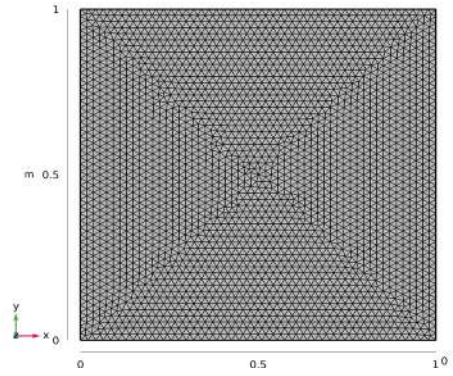

Since we are aimed to compare the functional values at each iteration, we evaluate the comparison of the key physical quantities, that are the gradient magnitude of the temperature field, the principal stress major component, and the domain displacement field. We will observe the gradual decrease of the potential energy surface profile which is presented by the posed functionals. Introducing the sampled physically controlled mesh towards our continuous domain with the above statistics presented in table 2, we perform the direct numerical simulation by simple numerical approach such as the discretized finite difference method for the posed model keeping the stability condition in accordance with the physically controlled mesh, in accordance with the described approximation finite element method via the system (193) – (194). Firstly, the discretization procedure may be illustrated via the formulas presented in system (196) through the covering of considered domain by the mesh elements $x_i = i\Delta x$, where $\Delta x = \frac{L}{N}, i = \overline{0,N}$. We will demonstrate the discretized analogue of the posed continuous model for the system (34) – (37) as follows:

$$\rho(x_i)c_p(x_i)\frac{Y_i^{j+1}-Y_i^j}{\Delta x} = \lambda\left(x_{i+\frac{1}{2}}\right)\frac{Y_{i+1}^j-Y_i^j}{(\Delta x)^2} - \lambda\left(x_{i-\frac{1}{2}}\right)\frac{Y_i^j+Y_{i-1}^j}{(\Delta x)^2}. \quad (196)$$

$$\lambda(x_0)\frac{Y_1^j-Y_0^j}{\Delta x} = h_{out}\left(Y_0^j - T_{out}(x_0)\right). \quad (197)$$

$$\lambda(x_N)\frac{Y_N^j-Y_{N-1}^j}{\Delta x} = -h_{ins}\left(Y_N^j - T_{out}(x_0)\right). \quad (198)$$

$$Y_i^0 = T_0(x). \quad (199)$$

The introduced discrete system (196) – (197) may be calculated for values of $Y(x_i)$, $i = \overline{0,N}$ via any iterative method that gives the best convergency rate depending on the preferred computational time, available memory available to sustain the high accuracy level by increasing the meshing points with respect to the length of considered medium.

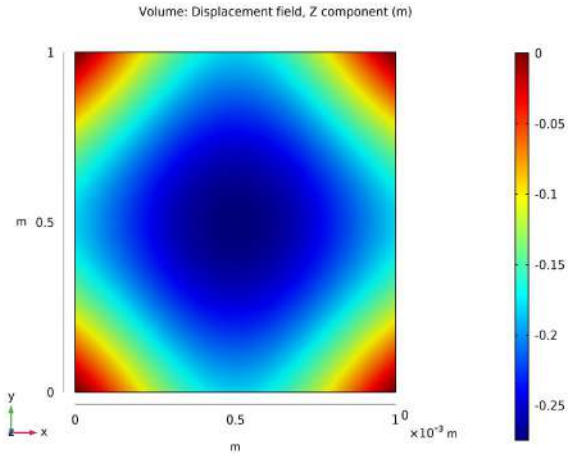

Figure 16 - Displacement field with reference parameters

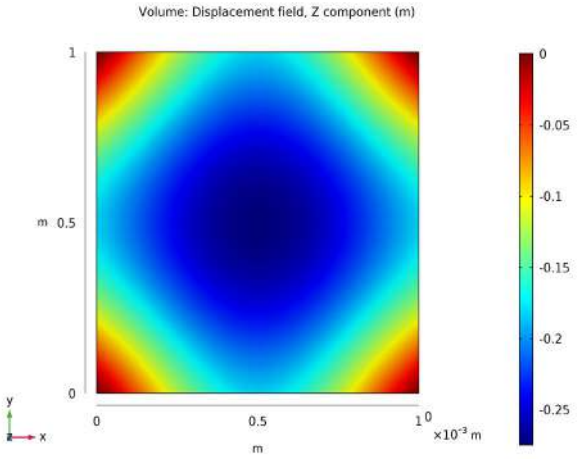

Figure 17 - Displacement field with analytically evaluated parameters

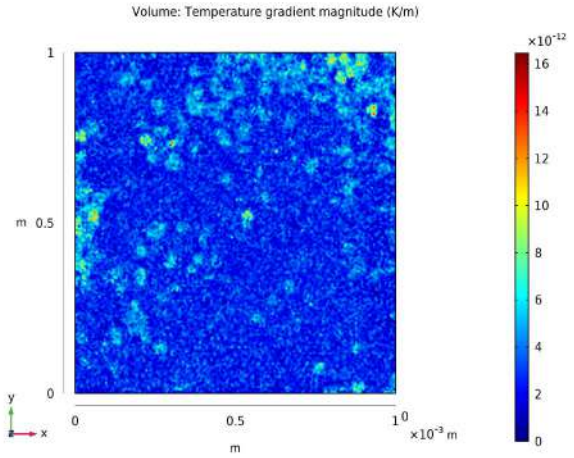

Figure 18 - Temperature gradient magnitude with reference parameters

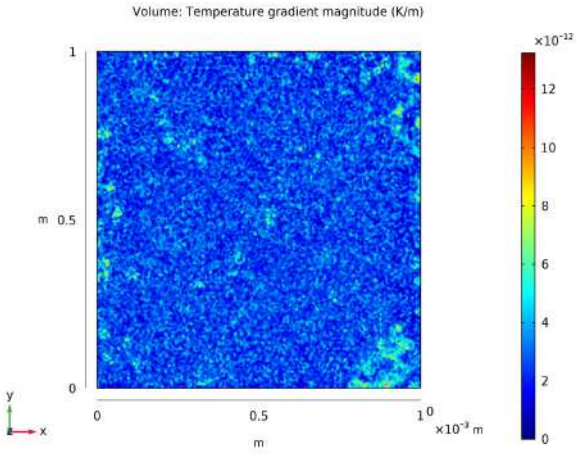

Figure 19 - Temperature gradient magnitude with analytically evaluated parameters

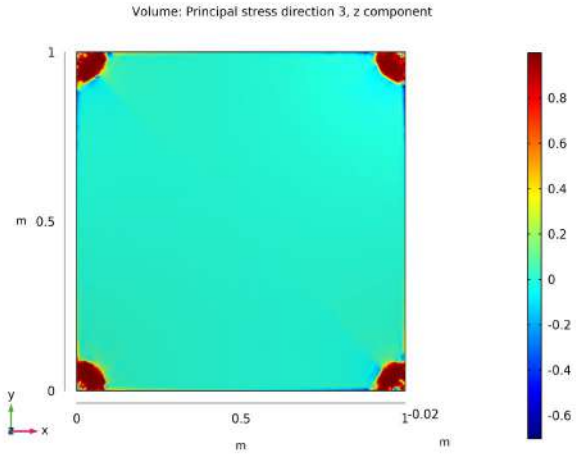

Figure 20 - Stress distribution with reference parameters

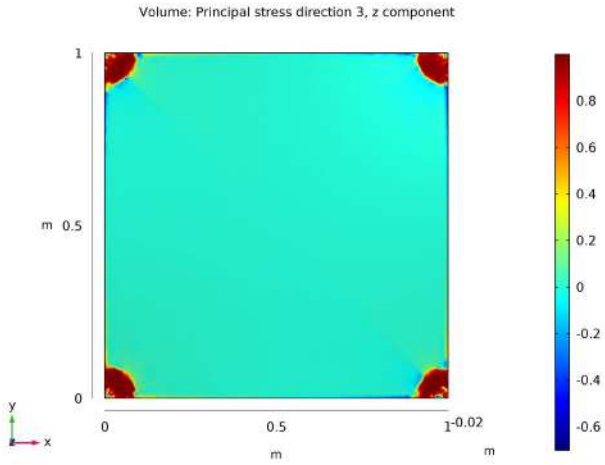

Figure 21 - Stress distribution with analytically evaluated parameters

The temperature gradient magnitude presents small fluctuations due to the linear thermal expansion as a response to the uniformly distributed loads introduced along with the principal stresses over the nodes of fixed constraints. We also may note the maximum displacement at the center where the dissipation of energy demonstrates its maximum value so that the stress inside solid is minimum over discussed region. Above figures (16) – (21) are demonstrating the typical profiles for the posed mathematical model (16) – (23). The scenario is altered after re-evaluated key physical parameters which are the domains of objective functions from the algorithms – 2. However, this alternation is only applicable towards the temperature gradient magnitude, since the introduce fluctuations are sufficiently small to introduce the high level of oscillations towards the energy dissipation of the structural steel plate. The figures below illustrate the evaluation of the key physical parameters of discussed thermoelastic stress analysis model.

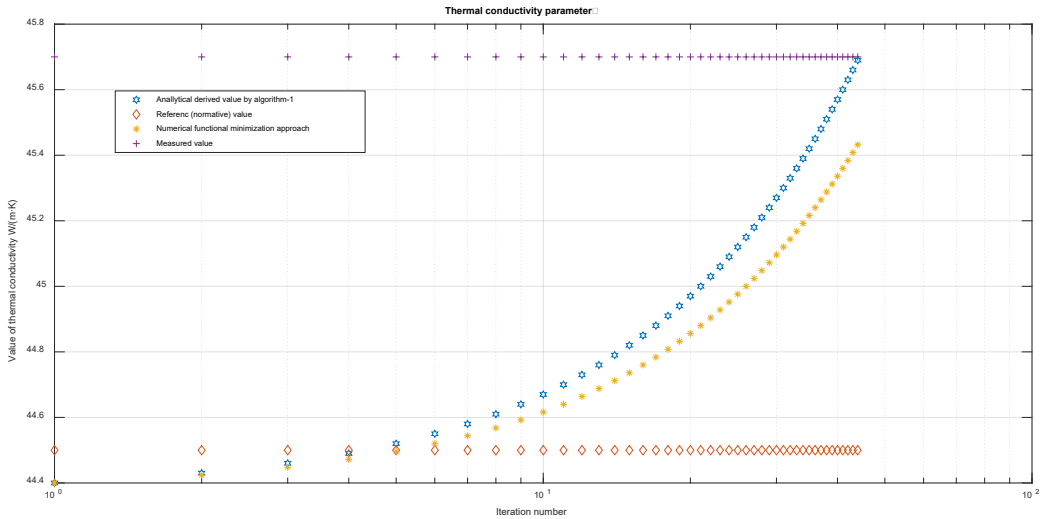

Figure 22 - Thermal conductivity parameter evaluation through each iteration

On the figure 22 we may note that the determination of parameters with the analytical approach is performed faster in comparison to the numerical functional minimization and it illustrates the gradual decrease, since the initial guess had underestimated value.

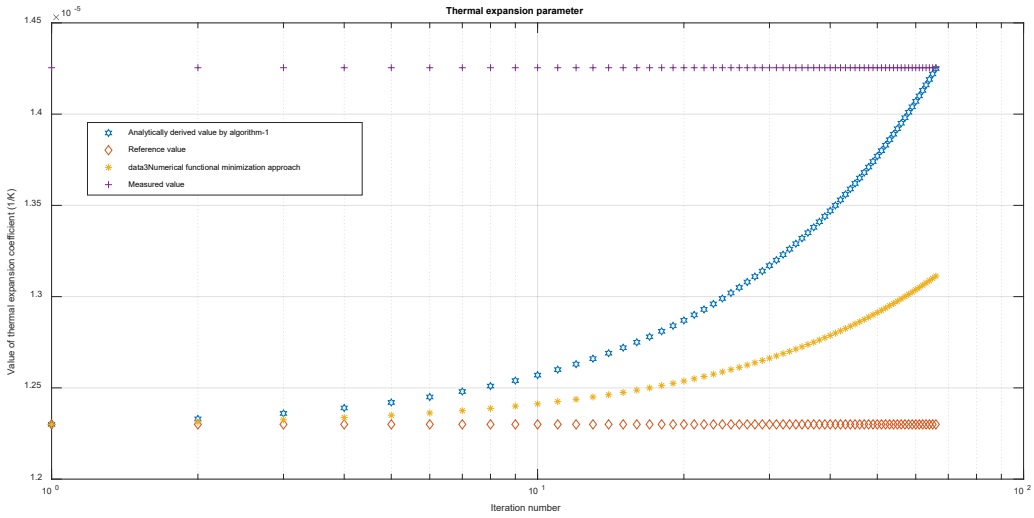

Figure 23 - Thermal expansion parameter evaluation over each iteration

The above figure 23 has the same patterns as the thermal conductivity evaluation profile, even though the referent value had such small order, we still perceive approximately the same number of iterations in the algorithm – 2.

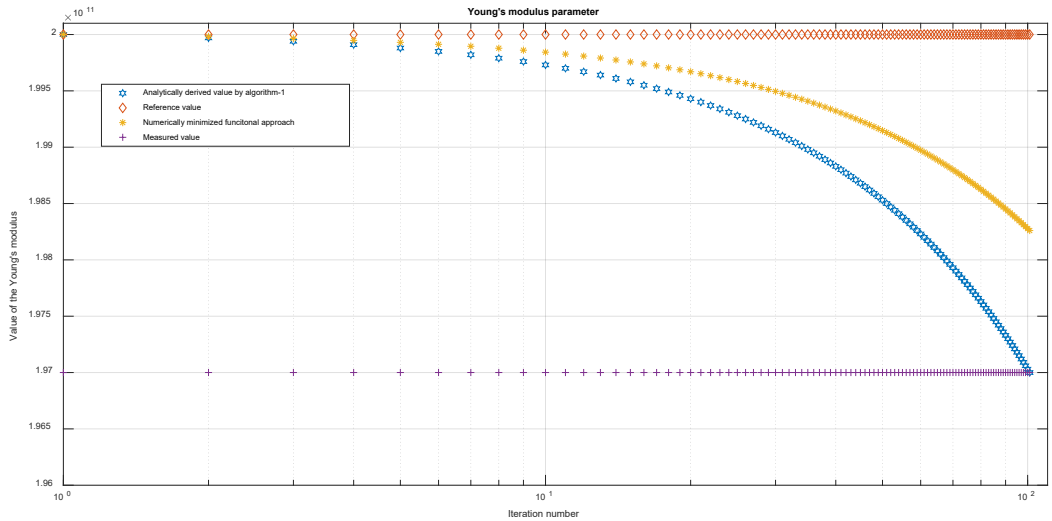

Figure 24 - The Young's modulus parameter determination through each iteration

As could be observed on the above scatters, we choose the values for initial approximations to be overestimated and obtained the gradual increase of corrected

value in this case, that contrasts with the overestimated initial samples. However, the algorithm provides a smooth convergency rate to the exact values in both cases.

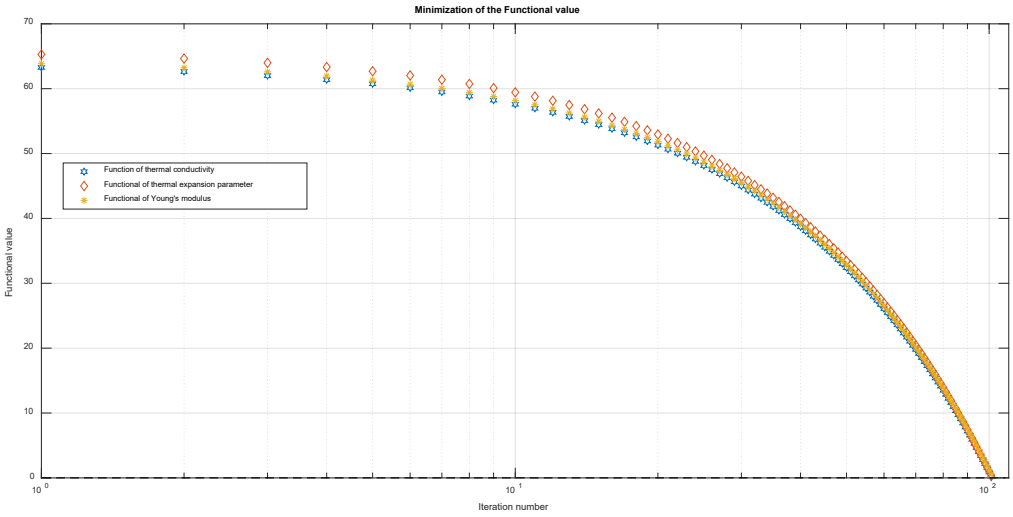

Figure 25 - Functional minimization over parameters on each iteration

The monotonous decrease of the functional value could be observed on the above scatter plot, that is figure 25. The decrement rate strictly depends on the proper choice of the governing coefficient and initial sample, as could be deduced by observing different parameters' functionals. For example, the Young's modulus parameter has a lower rate of convergency for the proposed algorithm – 2 in comparison to the thermal conductivity parameter evaluation manner. The appropriate error tolerance may be introduced for the functional minimization by:

$$|J_{n+1}(\pi^{\circ}) - J_n(\pi^{\circ})| \leq \varepsilon \qquad (200)$$

Where the parameter ε is a prescribed error tolerance that we may introduce in order to control the iterations number for determination parameter π°.

3.3 Experimental design for quasi-linearized problem with non-homogenized boundary conditions

In the current subchapter we will illustrate the approach towards analytical solution derivation with the case when instead of homogenization of the posed model (34) – (38) we perform the linearization via the decomposition of the general problem into several sub-problems connected via the continuity conditions:

$$\begin{cases} \rho(x)c_p(x)\dfrac{\partial\theta}{\partial t} = \dfrac{\partial}{\partial x}\left(k(x)\dfrac{\partial\theta}{\partial x}\right), x \in \Omega \\ -k(x)\dfrac{\partial\theta}{\partial x}_{x=0} = h_{ins}(\theta - T_{ins})_{x=0}, \\ k(x)\dfrac{\partial\theta}{\partial x}_{x=L} = h_{ins}(\theta - T_{out})_{x=L}, \\ \theta_{t=0} = T_0. \end{cases} \rightarrow \begin{cases} \rho_1 c_{p_1}\dfrac{\partial\theta}{\partial t} = k_1\dfrac{\partial\theta}{\partial x}, x \in [0, \xi_1] \\ -k_1\dfrac{\partial\theta}{\partial x}_{x=0} = h_{ins}(\theta - T_{ins})_{x=0}, \rightarrow \\ \theta_{x=\xi_1} = T_\xi, \\ \theta_{t=0} = T_0. \end{cases}$$

$$\rightarrow \begin{cases} \rho_2 c_{p_2}\dfrac{\partial\theta}{\partial t} = k_2\dfrac{\partial\theta}{\partial x}, x \in [\xi_1, L] \\ k_2\dfrac{\partial\theta}{\partial x}_{x=L} = h_{out}(\theta - T_{out})_{x=L}, \\ \theta_{x=\xi_1} = T_\xi, \\ \theta_{t=0} = T_0. \end{cases} \quad (201)$$

The sequence of systems (201) presents the decomposition scheme towards initially formulated direct problem. Afterwards we separately consider both obtained system and investigate their Laplace transforms.

$$\mathcal{L}\left[\rho_1 c_{p_1}\frac{\partial\theta}{\partial t} - k_1\frac{\partial^2\theta}{\partial x^2}\right] = \mathcal{L}\left[\rho_1 c_{p_1}\frac{\partial\theta}{\partial t}\right] - \mathcal{L}\left[k_1\frac{\partial^2\theta}{\partial x^2}\right] =$$

$$= \begin{vmatrix} \mathcal{L}[\theta(x,t)] = \int_0^{+\infty} e^{-pt}\theta(x,t)dt = \tilde{\theta}(x,p), \\ \mathcal{L}\left[\rho_1 c_{p_1}\frac{\partial\theta(x,t)}{\partial t}\right] = \rho_1 c_{p_1}\int_0^{+\infty}\frac{e^{-pt}\partial\theta(x,t)}{\partial t}dt = \rho_1 c_{p_1}[p\tilde{\theta}(x,p) - \theta(x,0)]. \end{vmatrix} =$$

$$= \begin{cases} \rho_1 c_{p_1}[p\tilde{\theta}(x,p) - \theta_0] - k_1\frac{\partial^2\tilde{\theta}}{\partial x^2} = 0, \\ k_1\tilde{\theta}'' - \rho_1 c_{p_1} p\tilde{\theta} = -\rho_1 c_{p_1} T_0. \end{cases} \quad (202)$$

The last received equation in (196) is a non-homogeneous second-order differential equation with respect to the spatial variable. By analogy we transform the boundary conditions and receive:

$$\begin{cases} -k_1\frac{\partial\tilde{\theta}}{\partial x}_{x=0} = h_{ins}\left(\tilde{\theta} - \tilde{T}_{ins}\right)_{x=0}, \\ \tilde{\theta}_{x=\xi_1} = \tilde{T}_\xi. \end{cases} \quad (203)$$

The general solution of obtained governing equation (202) has the following form through undetermined coefficients:

$$\tilde{\theta}(x,p) = Ae^{\sqrt{\frac{\rho_1 c_{p_1} p}{k_1}}x} + Be^{-\sqrt{\frac{\rho_1 c_{p_1} p}{k_1}}x} + \tilde{\theta}_{n.h}(x,p). \qquad (204)$$

Where the term $\tilde{\theta}_{n.h}(x,p)$ is the solution of non-homogeneous equation in the frequency domain, that depend on the heat source and type of ambient conditions. Using the conditions (203), we will construct the following system to determine the unknown coefficients in (204):

$$\begin{cases} Ae^{\sqrt{\frac{\rho_1 c_{p_1} p}{k_1}}\xi} + Be^{-\sqrt{\frac{\rho_1 c_{p_1} p}{k_1}}\xi} = \tilde{T}_\xi - \tilde{\theta}_{\text{н.р.}}(\xi,p), \\ B\left(k_1\sqrt{\frac{\rho_1 c_{p_1} p}{k_1}} - h_{ins}\right) - A\left(k_1\sqrt{\frac{\rho_1 c_{p_1} p}{k_1}} + h_{ins}\right) = \\ \quad = \tilde{\theta}_{\text{н.р.}}(0,p)h_{ins} - h_{ins}\tilde{T}_{ins} + k_1\frac{\partial\tilde{\theta}_{\text{н.р.}}(0,p)}{\partial x}. \end{cases} \qquad (205)$$

The expression (205) will have the following equivalent matrix form $Ax = B$, where:

$$\begin{cases} A = \begin{pmatrix} e^{\sqrt{\frac{\rho_1 c_{p_1} p}{k_1}}\xi} & e^{-\sqrt{\frac{\rho_1 c_{p_1} p}{k_1}}\xi} \\ -k_1\sqrt{\frac{\rho_1 c_{p_1} p}{k_1}} - h_{ins} & k_1\sqrt{\frac{\rho_1 c_{p_1} p}{k_1}} - h_{ins} \end{pmatrix}, \\ B = \begin{pmatrix} \tilde{T}_\xi - \tilde{\theta}_{\text{н.р.}}(\xi,p) \\ \tilde{\theta}_{\text{н.р.}}(0,p)h_{ins} - h_{ins}\tilde{T}_{ins} + k_1\frac{\partial\tilde{\theta}_{\text{н.р.}}(0,p)}{\partial x} \end{pmatrix}, \\ x = \begin{pmatrix} A \\ B \end{pmatrix}, unknown\ coefficients\ from\ (204). \end{cases} \qquad (206)$$

We will directly determine unknown coefficients x by the expression $A^{-1}B$, if the matrix A is invertible, for that reason we verify:

$$\begin{cases} \Delta A = k_1\sqrt{\frac{\rho_1 c_{p_1} p}{k_1}}\left[e^{\sqrt{\frac{\rho_1 c_{p_1} p}{k_1}}\xi} + e^{-\sqrt{\frac{\rho_1 c_{p_1} p}{k_1}}\xi}\right] - h_{ins}\left[e^{-\sqrt{\frac{\rho_1 c_{p_1} p}{k_1}}\xi} - e^{\sqrt{\frac{\rho_1 c_{p_1} p}{k_1}}\xi}\right], \\ A^{-1} = \frac{1}{\Delta A}\begin{pmatrix} k_1\sqrt{\frac{\rho_1 c_{p_1} p}{k_1}} - h_{ins} & -e^{-\sqrt{\frac{\rho_1 c_{p_1} p}{k_1}}\xi} \\ k_1\sqrt{\frac{\rho_1 c_{p_1} p}{k_1}} - h_{ins} & e^{\sqrt{\frac{\rho_1 c_{p_1} p}{k_1}}\xi} \end{pmatrix}. \end{cases} \quad (207)$$

Observing the above trivial expressions, we will determine the unknown vector by:

$$\begin{pmatrix} A \\ B \end{pmatrix} =$$

$$= \begin{pmatrix} \left[\frac{\left(k_1\sqrt{\frac{\rho_1 c_{p_1} p}{k_1}} - h_{ins}\right)\left[\tilde{T}_\xi - \tilde{\theta}_{\text{н.р.}}(\xi,p)\right] - e^{-\sqrt{\frac{\rho_1 c_{p_1} p}{k_1}}\xi}\left[\tilde{\theta}_{\text{н.р.}}(0,p)h_{ins} - h_{ins}\tilde{T}_{ins} + k_1\frac{\partial\tilde{\theta}_{\text{н.р.}}(0,p)}{\partial x}\right]}{\Delta A}\right] \\ \left[\frac{\left(k_1\sqrt{\frac{\rho_1 c_{p_1} p}{k_1}} - h_{ins}\right)\left[\tilde{T}_\xi - \tilde{\theta}_{\text{н.р.}}(\xi,p)\right] + e^{\sqrt{\frac{\rho_1 c_{p_1} p}{k_1}}\xi}\left[\tilde{\theta}_{\text{н.р.}}(0,p)h_{ins} - h_{ins}\tilde{T}_{ins} + k_1\frac{\partial\tilde{\theta}_{\text{н.р.}}(0,p)}{\partial x}\right]}{\Delta A}\right] \end{pmatrix}. \quad (208)$$

So that the particular solution for the first sub-problem will take the following form:

$$\tilde{\theta}(x,p) =$$

$$= \left[\begin{array}{c} \frac{\left[k_1\sqrt{\frac{\rho_1 c_{p_1} p}{k_1}} - h_{ins}\right]\left[\tilde{T}_\xi - \tilde{\theta}_{\text{н.р.}}(\xi,p)\right]ch\left(\sqrt{\frac{\rho_1 c_{p_1} p}{k_1}}x\right)}{\Delta A} + \\ + \frac{\left[\tilde{\theta}_{\text{н.р.}}(0,p)h_{ins} - h_{ins}\tilde{T}_{ins} + k_1\frac{\partial\tilde{\theta}_{\text{н.р.}}(0,p)}{\partial x}\right]\left(sh\left(\sqrt{\frac{\rho_1 c_{p_1} p}{k_1}}\xi - \sqrt{\frac{\rho_1 c_{p_1} p}{k_1}}x\right)\right)}{\Delta A} \end{array}\right] +$$

$$+\tilde{\theta}_{\text{н.р.}}(x,p). \quad (209)$$

The inverse Laplace transform is applied term by term to (209) in accordance with the second expansion theorem. The numerator and denominator of the first term in (209) are expanded separately, by knowing the expansion formulas for hyperbolic functions:

$$\begin{cases} \mathrm{sh}(\mathrm{x}) = \mathrm{x} + \frac{\mathrm{x}^3}{3!} + \frac{\mathrm{x}^5}{5!} + \cdots, \\ \mathrm{ch}(\mathrm{x}) = 1 + \frac{\mathrm{x}^2}{2!} + \frac{\mathrm{x}^4}{4!} + \cdots, \\ sh\left(\sqrt{\frac{\rho_1 c_{p_1} p}{k_1}}\xi - \sqrt{\frac{\rho_1 c_{p_1} p}{k_1}}x\right) = \left(\sqrt{\frac{\rho_1 c_{p_1} p}{k_1}}\xi - \sqrt{\frac{\rho_1 c_{p_1} p}{k_1}}x\right) + \\ + \frac{\left(\sqrt{\frac{\rho_1 c_{p_1} p}{k_1}}\xi - \sqrt{\frac{\rho_1 c_{p_1} p}{k_1}}x\right)^3}{3!} + \frac{\left(\sqrt{\frac{\rho_1 c_{p_1} p}{k_1}}\xi - \sqrt{\frac{\rho_1 c_{p_1} p}{k_1}}x\right)^5}{5!} + \cdots \\ k_1\sqrt{\frac{\rho_1 c_{p_1} p}{k_1}}\, ch\left(\sqrt{\frac{\rho_1 c_{p_1} p}{k_1}}\xi\right) = k_1\sqrt{\frac{\rho_1 c_{p_1} p}{k_1}} + \frac{k_1\sqrt{\frac{\rho_1 c_{p_1} p}{k_1}}\left(\sqrt{\frac{\rho_1 c_{p_1} p}{k_1}}\xi\right)^2}{2!} + \\ + \frac{k_1\sqrt{\frac{\rho_1 c_{p_1} p}{k_1}}\left(\sqrt{\frac{\rho_1 c_{p_1} p}{k_1}}\xi\right)^4}{4!} + \cdots, \\ h_{ins} sh\left(\sqrt{\frac{\rho_1 c_{p_1} p}{k_1}}\xi\right) = h_{ins}\sqrt{\frac{\rho_1 c_{p_1} p}{k_1}}\xi + \frac{h_{ins}\left(\sqrt{\frac{\rho_1 c_{p_1} p}{k_1}}\xi\right)^3}{3!} + \\ + \frac{h_{ins}\left(\sqrt{\frac{\rho_1 c_{p_1} p}{k_1}}\xi\right)^5}{5!} + \cdots. \end{cases} \quad (210)$$

By the second decomposition theorem that was applied in the part 3.1 we will analogically look for the nulls of denominators in order to deduce the inverse transform of the received expressions. However, in this quasi-linearized case, we will perform it numerically by constructing the following objective function.

$$\frac{k_1\rho_1 c_{p_1} p_n}{h_{ins}^2} - th^2\left(\sqrt{\frac{\rho_1 c_{p_1} p_n}{k_1}}\xi\right) = f(p_n) \to min. \quad (211)$$

Where we present the frequency variable in a polar form $p_n = x_n + iy_n = r_n(cos\varphi_n + isin\varphi_n)$. Numerically evaluating the first several roots, enough to consider the fluctuations of the signal to decease for (211), we may construct the analytical solution of the direct first sub-problem by the following series:

$$\theta(x,t)=\sum_{n=0}^{15}\frac{\left[k_1\sqrt{\frac{\rho_1 c_{p_1} p_n}{k_1}}-h_{ins}\right]\left[\tilde{T}_\xi-\tilde{\theta}_{\text{н.р.}}(\xi,p_n)\right]ch\left(\sqrt{\frac{\rho_1 c_{p_1} p_n}{k_1}}x\right)}{\frac{k_1\rho_1 c_{p_1}}{h_{ins}^2}-\text{sech}^2\sqrt{\frac{\rho_1 c_{p_1} p_n}{k_1}}\xi\, th\left(\sqrt{\frac{\rho_1 c_{p_1} p_n}{k_1}}\xi\right)\left(\sqrt{\frac{\rho_1 c_{p_1}}{k_1 p_n}}\xi\right)}\text{e}^{-p_n\text{t}}+$$

$$+\sum_{n=0}^{15}\left[\begin{matrix}\tilde{\theta}_{\text{н.р.}}(0,p_n)h_{ins}-h_{ins}\tilde{T}_{ins}+\\+k_1\frac{\partial\tilde{\theta}_{\text{н.р.}}(0,p_n)}{\partial x}\end{matrix}\right]\left(sh\left(\begin{matrix}\sqrt{\frac{\rho_1 c_{p_1} p_n}{k_1}}\xi-\\-\sqrt{\frac{\rho_1 c_{p_1} p_n}{k_1}}x\end{matrix}\right)\right)\text{e}^{-p_n\text{t}}+\theta_{\text{н.р.}}(x,t) \tag{212}$$

Analogically we perform the same manipulations over the second sub-domain problem and obtain the following system with undetermined coefficients:

$$\begin{cases}A\left(k_2\sqrt{\frac{\rho_2 c_{p_2} p}{k_2}}e^{\sqrt{\frac{\rho_2 c_{p_2} p}{k_2}}L}-h_{out}e^{\sqrt{\frac{\rho_2 c_{p_2} p}{k_2}}L}\right)-\\ -B\left(k_2\sqrt{\frac{\rho_2 c_{p_2} p}{k_2}}e^{-\sqrt{\frac{\rho_2 c_{p_2} p}{k_2}}L}+h_{out}e^{-\sqrt{\frac{\rho_2 c_{p_2} p}{k_2}}L}\right)=\\ =h_{out}\tilde{\theta}_{\text{н.р.}}(L,p)-h_{out}\tilde{T}_{out}-k_2\frac{\partial\tilde{\theta}_{\text{н.р.}}(L,p)}{\partial x},\\ Ae^{\sqrt{\frac{\rho_2 c_{p_2} p}{k_2}}\xi_1}+Be^{-\sqrt{\frac{\rho_2 c_{p_2} p}{k_2}}\xi_1}=\tilde{T}_\xi-\tilde{\theta}_{\text{н.р.}}(\xi,p).\end{cases} \tag{213}$$

Again, by rewriting the posed system in the matrix form $Ax=B$, where x is the vector of unknown coefficients, we obtain:

$$\begin{cases}A=\begin{pmatrix}k_2\gamma e^{\gamma L}-h_{out}e^{\gamma L} & -k_2\gamma e^{-\gamma L}-h_{out}e^{-\gamma L}\\ e^{\gamma\xi_1} & e^{-\gamma\xi_1}\end{pmatrix},\\ B=\begin{pmatrix}h_{out}\tilde{\theta}_{\text{н.р.}}(L,p)-h_{out}\tilde{T}_{out}-k_2\frac{\partial\tilde{\theta}_{\text{н.р.}}(L,p)}{\partial x}\\ \tilde{T}_\xi-\tilde{\theta}_{\text{н.р.}}(\xi,p)\end{pmatrix}.\end{cases} \tag{214}$$

Where $\gamma=\sqrt{\frac{\rho_2 c_{p_2} p}{k_2}}$ for simplicity. We will verify if the matrix A is invertible:

$$\Delta A = k_2\sqrt{\frac{\rho_2 c_{p_2} p}{k_2}}\left(e^{\sqrt{\frac{\rho_2 c_{p_2} p}{k_2}}L-\sqrt{\frac{\rho_2 c_{p_2} p}{k_2}}\xi_1} + e^{\sqrt{\frac{\rho_2 c_{p_2} p}{k_2}}\xi_1-\sqrt{\frac{\rho_2 c_{p_2} p}{k_2}}L}\right)+$$

$$+h_{out}\left(e^{\sqrt{\frac{\rho_2 c_{p_2} p}{k_2}}\xi_1-\sqrt{\frac{\rho_2 c_{p_2} p}{k_2}}L} - e^{\sqrt{\frac{\rho_2 c_{p_2} p}{k_2}}L-\sqrt{\frac{\rho_2 c_{p_2} p}{k_2}}\xi_1}\right) \neq 0. \quad (215)$$

In that case the system coefficients will take the following form:

$$\begin{pmatrix} A \\ B \end{pmatrix} = \begin{pmatrix} \frac{e^{-\gamma\xi_1}\left(h_{out}\tilde{\theta}_{\text{н.р.}}(L,p)-h_{out}\tilde{T}_{out}-k_2\frac{\partial\tilde{\theta}_{\text{н.р.}}(L,p)}{\partial x}\right)+}{+\left(k_2\gamma e^{-\gamma L}+h_{out}e^{-\gamma L}\right)\left(k_2\gamma e^{-\gamma L}+h_{out}e^{-\gamma L}\right)}}{\Delta A} \\ \frac{-e^{\gamma\xi_1}\left(h_{out}\tilde{\theta}_{\text{н.р.}}(L,p)-h_{out}\tilde{T}_{out}-k_2\frac{\partial\tilde{\theta}_{\text{н.р.}}(L,p)}{\partial x}\right)+}{+\left(k_2\gamma e^{\gamma L}-h_{out}e^{\gamma L}\right)\left(\tilde{T}_{\xi}-\tilde{\theta}_{\text{н.р.}}(\xi,p)\right)}}{\Delta A} \end{pmatrix}. \quad (216)$$

Determining the analytical solution in the frequency domain and applying further the second decomposition theorem we will derive the analytical solution for the second sub-problem in the real time domain. However, the key reason for that experimental design is to discuss the general peculiarities of such methodology, which is the necessity of determining the nulls of the received polynomials in the frequency domain around attenuation parameter p_n, that could be also considered as the inverse problem itself, that is we are keen to determine the characteristic roots in order to evaluate the decomposition, while the roots are the part of transcendental equations posed in the frequency domain. Meanwhile, there is a strong dependency on whether we implement the numerical or analytical investigations to solve the posed problem and the obtained results over the determined physical coefficients. For instance, if we will consider separately the first sub-problem of the discussed experimental design and rewrite its solution in the frequency domain by:

$$T(x,p) = \frac{\sqrt{\frac{\rho c_p p}{k}}\xi-\sqrt{\frac{\rho c_p p}{k}}x+\begin{pmatrix}\frac{1}{6}\left(\sqrt{\frac{\rho c_p p}{k}}\right)^3\xi^3-\frac{\rho c_p p}{2k}\xi^2\sqrt{\frac{\rho c_p p}{k}}x+\\ +\sqrt{\frac{\rho c_p p}{k}}\xi\frac{\rho c_p p}{2k}x^2-\frac{1}{6}\left(\sqrt{\frac{\rho c_p p}{k}}\right)^3 x^3\end{pmatrix}\left(\begin{matrix}h_{ins}T_{ins}-\\ -\frac{\partial T_{nh.s.}(0)}{\partial x}\end{matrix}\right)}{-\sqrt{\frac{\rho c_p p}{k}}-\sqrt{\frac{\rho c_p p}{k}}\frac{\rho c_p p\xi^2}{2k}-h_{ins}-h_{ins}\frac{\rho c_p p\xi^2}{2k}} - \frac{T_{nh.s.}}{2}. \quad (217)$$

We will note that in such formulation the roots could be investigated by the solution of the following problem:

$$\begin{cases} \sqrt{\frac{\rho c_p p}{k}}\left(1-\frac{\rho c_p p\xi^2}{2k}\right)=h_{ins}\left(\frac{\rho c_p p\xi^2}{2k}+1\right)\rightarrow \\ \frac{\rho c_p p}{kh_{ins}^2}=\left[\frac{\left(\frac{\rho c_p p\xi^2}{2k}+1\right)}{\left(1-\frac{\rho c_p p\xi^2}{2k}\right)}\right]^2=\frac{\frac{\rho^2 c_p^2 p\xi^4}{4k^2}+\frac{\rho c_p p\xi^2}{k}+1}{1-\frac{\rho c_p p\xi^2}{k}+\frac{\rho^2 c_p^2 p\xi^4}{4k^2}}\rightarrow \\ p^2\left[\frac{\rho^4 c_p^3\xi^4}{4k^3h_{ins}^2}-\frac{\rho^2 c_p^2\xi^2}{k^2h_{ins}^2}\right]+p\left[\frac{\rho c_p}{kh_{ins}^2}-\frac{\rho^2 c_p^2\xi^4}{4k^2}-\frac{\rho c_p\xi^2}{k}\right]=1\rightarrow \\ p_{1,2}=\frac{k\rho c_p\left[k\rho c_p h_{ins}^2\xi^4+4k^2\left(h_{ins}^2\xi^2-1\right)\right]\pm 4k^3h_{ins}^2\sqrt{\left[\frac{\rho c_p}{kh_{ins}^2}-\frac{\rho^2 c_p^2\xi^4}{4k^2}-\frac{\rho c_p\xi^2}{k}\right]^2+4\left[\frac{\rho^4 c_p^3\xi^4}{4k^3h_{ins}^2}-\frac{\rho^2 c_p^2\xi^2}{k^2h_{ins}^2}\right]}}{2\rho^2 c_p^2\left[\rho^2 c_p\xi^4-4k\xi^2\right]}. \end{cases} \tag{218}$$

These are the first two roots. However, from another side the solution (217) could be taken via the trigonometrical functions as:

$$\begin{cases} T(x,p)=\frac{isin\left(i\sqrt{\frac{\rho c_p p}{k}}\xi-i\sqrt{\frac{\rho c_p p}{k}}x\right)\left(h_{ins}T_{ins}-\frac{\partial T_{nh.s.}(0)}{\partial x}\right)}{cos\left(i\sqrt{\frac{\rho c_p p}{k}}\xi\right)\left(\sqrt{\frac{\rho c_p p}{k}}+h_{ins}\right)}+\frac{T_{nh.s.}}{2}, \\ T(x,p)=\frac{sh\left(\sqrt{\frac{\rho c_p p}{k}}\xi-\sqrt{\frac{\rho c_p p}{k}}x\right)\left(h_{ins}T_{ins}-\frac{\partial T_{nh.s.}(0)}{\partial x}\right)}{ch\left(\sqrt{\frac{\rho c_p p}{k}}\xi\right)\left(-\sqrt{\frac{\rho c_p p}{k}}-h_{ins}\right)}-\frac{T_{nh.s.}}{2}. \end{cases} \tag{219}$$

By observing this form, we will deduce the root of denominator by:

$$\begin{cases} p_n=\frac{kh_{ins}^2}{\rho c_p}-\frac{\pi^2n^2k}{\rho c_p\xi^2}-\frac{\pi^2nk}{\rho c_p\xi^2}-\frac{\pi^2k}{4\rho c_p\xi^2}=\lambda h_{ins}^2-\frac{\lambda\pi^2}{\xi^2}\left[n^2+n+\frac{1}{4}\right], \\ p_n=-\frac{k\pi^2n^2}{\rho c_p\xi^2}-\frac{k\pi^2n}{\rho c_p\xi^2}-\frac{k\pi^2}{4\rho c_p\xi^2}=-\frac{\lambda\pi^2}{\xi^2}\left[n^2+n+\frac{1}{4}\right], \\ ch\left(\sqrt{\frac{\rho c_p p}{k}}\xi\right)=0, \\ -\sqrt{\frac{\rho c_p p}{k}}-h_{ins}\neq 0. \end{cases} \tag{220}$$

By investigations of the (220), we may note that:

$$h\left(\sqrt{\frac{\rho c_p p}{k}}\xi\right)=0\rightarrow\frac{e^{\sqrt{\frac{\rho c_p p}{k}}\xi}+e^{-\sqrt{\frac{\rho c_p p}{k}}\xi}}{2}=e^{-\sqrt{\frac{\rho c_p p}{k}}\xi}\left[1+e^{2\sqrt{\frac{\rho c_p p}{k}}\xi}\right]=0. \tag{221}$$

From which we may conclude two following facts:

$$\begin{cases} e^{2\sqrt{\frac{\rho c_p p}{k}}\xi}=-1, \\ e^{-\sqrt{\frac{\rho c_p p}{k}}\xi}\neq 0, \\ 2\sqrt{\frac{\rho c_p p_n}{k}}\xi=i\pi(2n+1), \\ p_n=-\frac{k\pi}{4\xi^2\rho c_p}(2n+1)=-\frac{\lambda\pi}{4\xi^2}(2n+1)=-\frac{\lambda\pi[2n+1]}{4\xi^2}. \end{cases} \tag{222}$$

Where $\lambda=k/\rho c_p$ and the polynomials and its derivatives of the parameter p will take the form:

$$\begin{cases} \varphi(p)=ch\left(\sqrt{\frac{\rho c_p p}{k}}\xi\right)\left(-\sqrt{\frac{\rho c_p p}{k}}-h_{ins}\right) \\ \frac{\partial\varphi}{\partial p}=\frac{\sqrt{\frac{\rho c_p}{k}}\xi sh\left(\sqrt{\frac{\rho c_p p}{k}}\xi\right)\left(-\sqrt{\frac{\rho c_p p}{k}}-h_{ins}\right)-ch\left(\sqrt{\frac{\rho c_p p}{k}}\xi\right)\sqrt{\frac{\rho c_p p}{k}}}{2\sqrt{p}} \end{cases} \tag{223}$$

While the general solution in the time domain may be rewritten as the following series:

$$\theta(x,t)=\sum_{n\geq 0}\frac{\frac{\sqrt{\lambda\pi(2n+1)}}{2\xi^2}sin\left(\begin{matrix}\frac{x}{2\xi}\sqrt{\pi[2n+1]}- \\ -\frac{1}{2}\sqrt{\pi[2n+1]}\end{matrix}\right)\left(\begin{matrix}h_{ins}T_{ins}- \\ -\frac{\partial\theta_{nh.s.}(0)}{\partial x}\end{matrix}\right)}{\xi sin\left(\frac{\sqrt{\pi(2n+1)}}{2}\right)\sqrt{\frac{\pi}{\lambda}(2n+1)}-i\left(\begin{matrix}\frac{2h_{ins}}{\sqrt{\lambda}}sin\left(\frac{\sqrt{\pi(2n+1)}}{2}\right)- \\ -\sqrt{\pi(2n+1)}cos\left(\sqrt{\pi(2n+1)}\right)\end{matrix}\right)}e^{-\frac{k\pi[2n+1]}{4\rho c_p\xi^2}t}-\frac{\theta_{nh.s.}}{2}. \tag{224}$$

Obviously, the analytical form will provide more exact values for the evaluation of the key parameters' values, since we may increase the number of terms for preferable convergency rate, while the deduced expression (212) has limitations in terms of accuracy for each computed null of the parameter p_n via some numerical method and we are restricted by choosing of the number of roots, whereas in (224) the accuracy matter is not considered at all due to analyticity of the derived expression.

3.4 Derivation of the exact expressions for the coefficient's determination in selected case studies

The expressions that we received in the previous part play the key role in derivations of the exact analytical expressions. Here we will demonstrate the further steps by considering the whole problem as the unite domain, thus without decomposing it to sub-problems, afterwards we will utilize the information obtained in the previous part to receive analytical expressions for the governing coefficients. The non-decomposed problem in the frequency domain will have the following form:

$$\begin{cases} k\frac{\partial^2\tilde{\theta}}{\partial x^2} - \rho cp\tilde{\theta} = -\rho cT_{init} \rightarrow k\tilde{\theta}'' - \rho cp\tilde{\theta} + \rho cT_{init} = 0, \\ k(x)\frac{\partial\tilde{\theta}}{\partial x}|_{x=0} = h_{out}\tilde{\theta}|_{x=0} - h_{out}\widetilde{T_{ins}}, \\ k(x)\frac{\partial\tilde{\theta}}{\partial x}|_{x=L} = h_{out}\widetilde{T_{out}} - h_{out}\tilde{\theta}|_{x=L}, \\ [\tilde{\theta}]|_{x=\xi} = 0, \ \left[k(x)\frac{\partial\tilde{\theta}}{\partial x}\right]|_{x=0} = 0. \end{cases} \tag{225}$$

Whereas its general solution in the frequency domain will have:

$$\tilde{\theta}_{h.s.}(x,p) = \begin{cases} Ae^{\sqrt{\frac{\rho cp}{k_1}}(x)} + Be^{-\sqrt{\frac{\rho cp}{k_1}}(x)} + \tilde{\theta}_{non-h.s.}(x), \ x \in (0,\xi), \\ Ce^{\sqrt{\frac{\rho cp}{k_2}}(x)} + De^{-\sqrt{\frac{\rho cp}{k_2}}(x)} + \tilde{\theta}_{non-h.s.}(x), \ x \in (\xi,L). \end{cases} \tag{226}$$

Where non-homogeneous solution could be derived through the sampled measurements by the following methodology. Using the measured temperatures, to obtain a smoothly differentiable and continuous functions suitable for the Laplace transform, we apply the interpolation polynomials of the discrete Fourier series, that is:

$$\begin{cases} T_{out}(t) = a_0 + a_1 cos(\omega t) + b_1 sin(\omega t) + a_2 cos(2\omega t) + b_2 sin(2\omega t), \\ T_{init} = a_0 + d cos(\omega x). \end{cases} \quad (227)$$

While the coefficients of interpolation are determined with 95% tolerance trust interval and presented in the below table with the following statistics:

Table 3 - Statistics for the adequacy of the interpolation model

Parameter	$T_{out}(t)$	T_{init}
Residual sum of squares	6.19e-06	1.115e-19;
Coefficient of determination (percentage of variance of dependent variable)	0.9965	1
Adjusted determination coefficient	0.9922	-
Standard deviation:	0.001244	-

While the coefficients itself are presented by the table below and determined via the curve fitting by parametrical and non-parametrical interpolation:

Table 4 - Interpolation coefficients determination

Value	$T_{out}(t)$	T_{init}
a_0	$288.5\ (288.5, 288.5)$	289
a_1	$-0.01198\ (-0.01393, -0.01002)$	6.005
b_1	$0.006643\ (0.004826, 0.008459)$	-
a_2	$0.006566\ (0.004053, 0.00908)$	-
b_2	$-0.01052\ (-0.01283, -0.008217)$	-
ω	$0.1863\ (0.183, 0.1897)$	22.49

The profiles fittings will have the following interpolations:

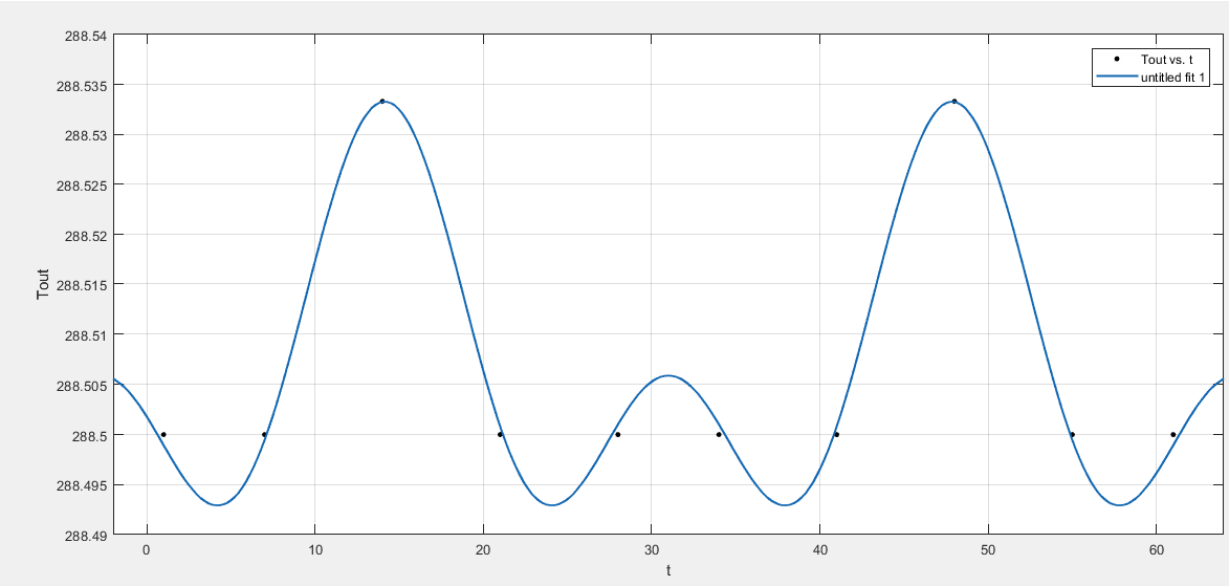

Figure 26 - Interpolation profile of the samples around inwards flux boundary points

As for the initial time samples, we will have the following fit:

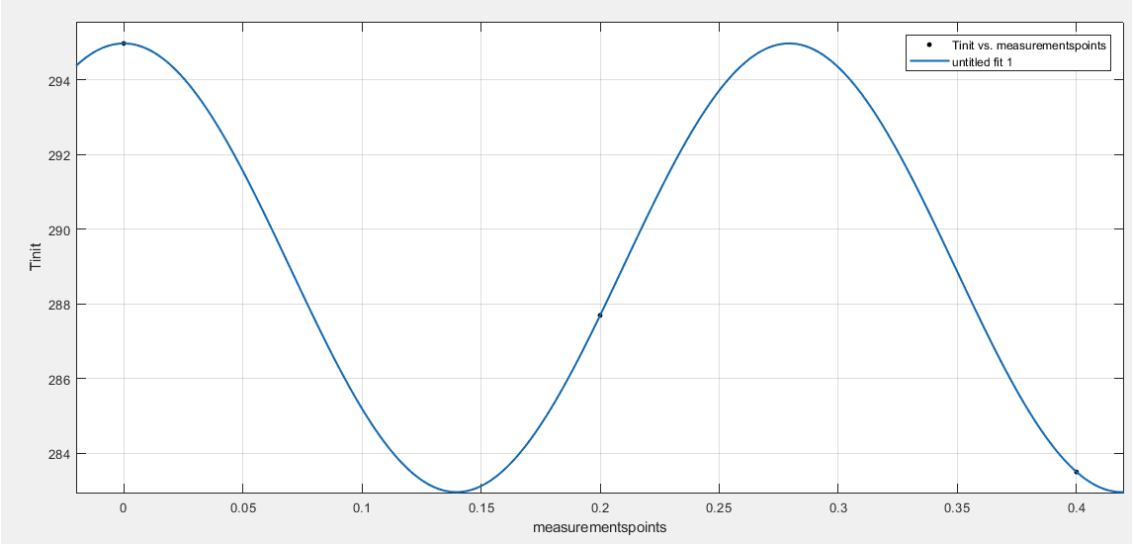

Figure 27 - Interpolation profile of the samples at initial time

Now we may perform the Laplace transform over the boundary condition as:

$$\mathcal{L}[T_{out}(t)] = \frac{1}{a_0} + \frac{a_1 p}{p^2+\omega^2} + \frac{b_1 \omega}{p^2+\omega^2} + \frac{a_2 p}{p^2+4\omega^2} + \frac{2\omega b_2}{p^2+\omega^2} = \widetilde{T_{out}}(p). \quad (228)$$

While due to the equivalence of the polynomials order initial time samples will be determined analogically. By using the (228), we may determine the non-homogeneous solution of the (226) by:

$$\tilde{\theta}_{non-h.s.}(x) = \frac{a}{p} + \frac{\rho cd}{k\omega^2+\rho cp} cos[\omega x]. \tag{229}$$

Therefore, the general solution (228) in the frequency domain will have the following form:

$$\tilde{\theta}_{g.s.}(x,p) = \begin{cases} Ae^{\sqrt{\frac{\rho cp}{k_1}}(x)} + Be^{-\sqrt{\frac{\rho cp}{k_1}}(x)} + \frac{a}{p} + \frac{\rho cd}{k_1\omega^2+\rho cp} cos[\omega x], \ x \in (0,\xi), \\ Ce^{\sqrt{\frac{\rho cp}{k_2}}(x)} + De^{-\sqrt{\frac{\rho cp}{k_2}}(x)} + \frac{a}{p} + \frac{\rho cd}{k_2\omega^2+\rho cp} cos[\omega x], \ x \in (\xi,L). \end{cases} \tag{230}$$

Now, we may apply the boundary conditions from (225) and deduce the matrix form for determination of unknown coefficients:

$$\begin{cases} Ak_1\gamma_1 + Bk_1\gamma_1 - \gamma_2 = -h_{ins}\widetilde{T_{ins}} + h_{ins}(A + B + \gamma_2), \\ Ck_2\gamma_2 e^{\gamma_2 L} - Dk_2\gamma_2 e^{-\gamma_2 L} - \gamma_3 = h_{out}\widetilde{T_{out}} - h_{out}(Ce^{\gamma_2 L} + De^{-\gamma_2 L} + \gamma_4), \\ Ae^{\gamma_1\xi} + Be^{-\gamma_1\xi} + \gamma_5 = Ce^{\gamma_2\xi} + De^{-\gamma_2\xi} + \gamma_6, \\ Ak_1\gamma_1 e^{\gamma_1\xi} - k_1\gamma_1 Be^{-\gamma_1\xi} - \gamma_7 = Ck_2\gamma_2 e^{\gamma_2\xi} - k_2\gamma_2 De^{-\gamma_2\xi} - \gamma_8. \end{cases} \tag{231}$$

Where for the readability reasons we have denoted by introduced constants:

$$\begin{cases} \sqrt{\frac{\rho cp}{k_1}} = \gamma_1, \sqrt{\frac{\rho cp}{k_2}} = \gamma_2, \\ \frac{k_2\omega\rho cd}{k_2\omega^2+\rho cp} sin[\omega L] = \gamma_3, \ \frac{a}{p} + \frac{\rho cd}{k_2\omega^2+\rho cp} cos[\omega L] = \gamma_4, \\ \frac{a}{p} + \frac{\rho cd}{k_1\omega^2+\rho cp} cos[\omega\xi] = \gamma_5, \ \frac{a}{p} + \frac{\rho cd}{k_2\omega^2+\rho cp} cos[\omega\xi] = \gamma_6, \\ \omega\frac{\rho cd}{k_1\omega^2+\rho cp} sin[\omega\xi] = \gamma_7, \ \omega\frac{\rho cd}{k_2\omega^2+\rho cp} sin[\omega\xi] = \gamma_8. \end{cases} \tag{232}$$

After elementary algebraic manipulations over the system (231), we will receive the matrix form equation:

$$\begin{pmatrix} 1 & -1 & 0 & 0 \\ 0 & 0 & (k_2\gamma_2 e^{\gamma_2 L} + h_{out}e^{\gamma_2 L}) & (h_{out}e^{-\gamma_2 L} - k_2\gamma_2 e^{-\gamma_2 L}) \\ e^{\gamma_1\xi} & e^{-\gamma_1\xi} & -e^{\gamma_2\xi} & -e^{-\gamma_2\xi} \\ k_1\gamma_1 e^{\gamma_1\xi} & -k_1\gamma_1 e^{-\gamma_1\xi} & -k_2\gamma_2 e^{\gamma_2\xi} & k_2\gamma_2 e^{-\gamma_2\xi} \end{pmatrix} * \\ * \begin{pmatrix} A \\ B \\ C \\ D \end{pmatrix} = \begin{pmatrix} \frac{q_0}{pk_1\gamma_1} \\ h_{out}\widetilde{T_{out}} - h_{out}\gamma_4 + \gamma_3 \\ \gamma_6 - \gamma_5 \\ -\gamma_8 + \gamma_7 \end{pmatrix}. \quad (233)$$

By setting up the following corresponding notations:

$$\begin{pmatrix} \zeta_1 & \zeta_2 & 0 & 0 \\ 0 & 0 & \zeta_3 & \zeta_4 \\ \zeta_5 & \zeta_6 & \zeta_7 & \zeta_8 \\ \zeta_9 & \zeta_{10} & \zeta_{11} & \zeta_{12} \end{pmatrix} \begin{pmatrix} A \\ B \\ C \\ D \end{pmatrix} = \begin{pmatrix} \zeta_{13} \\ \zeta_{14} \\ \zeta_{15} \\ \zeta_{16} \end{pmatrix}. \quad (234)$$

We will obtain the expressions for undetermined coefficients of the system (231):

$$\begin{cases} A = \frac{\zeta_{13}(\zeta_3\zeta_6\zeta_{12} - \zeta_3\zeta_8\zeta_{10} - \zeta_4\zeta_6\zeta_{11} + \zeta_4\zeta_7\zeta_{10}) + \\ +\zeta_{16}(\zeta_2\zeta_3\zeta_8 - \zeta_2\zeta_4\zeta_7) - \zeta_{15}(\zeta_2\zeta_3\zeta_{12} - \zeta_2\zeta_4\zeta_{11}) + \\ +\zeta_{14}(\zeta_2\zeta_7\zeta_{12} - \zeta_2\zeta_8\zeta_{11})}{\zeta_1\zeta_3(\zeta_6\zeta_{12} - \zeta_8\zeta_{10}) - \zeta_1\zeta_4(\zeta_6\zeta_{11} + \zeta_7\zeta_{10}) + \zeta_2\zeta_3(\zeta_8\zeta_9 - \zeta_5\zeta_{12}) + \\ + \zeta_2\zeta_4(\zeta_5\zeta_{11} - \zeta_7\zeta_9)}, \\ B = \frac{-\zeta_{13}(\zeta_3\zeta_5\zeta_{12} - \zeta_3\zeta_8\zeta_9 - \zeta_4\zeta_5\zeta_{11} + \zeta_4\zeta_7\zeta_9) - \zeta_{16}(\zeta_1\zeta_3\zeta_8 - \zeta_1\zeta_4\zeta_7) + \\ +\zeta_{15}(\zeta_1\zeta_3\zeta_{12} - \zeta_1\zeta_4\zeta_{11}) - \zeta_{14}(\zeta_1\zeta_7\zeta_{12} - \zeta_1\zeta_8\zeta_{11})}{\zeta_1\zeta_3(\zeta_6\zeta_{12} - \zeta_8\zeta_{10}) - \zeta_1\zeta_4(\zeta_6\zeta_{11} + \zeta_7\zeta_{10}) + \zeta_2\zeta_3(\zeta_8\zeta_9 - \zeta_5\zeta_{12}) + \\ + \zeta_2\zeta_4(\zeta_5\zeta_{11} - \zeta_7\zeta_9)}, \\ C = \frac{\zeta_{14}(\zeta_1\zeta_6\zeta_{12} - \zeta_1\zeta_8\zeta_{10} - \zeta_2\zeta_5\zeta_{12} + \zeta_2\zeta_8\zeta_9) - \zeta_4\zeta_{16}(\zeta_1\zeta_6 - \zeta_2\zeta_5) + \\ +\zeta_4\zeta_{15}(\zeta_1\zeta_{10} - \zeta_2\zeta_9) - \zeta_4\zeta_{13}(\zeta_2\zeta_{10} - \zeta_6\zeta_9)}{\zeta_1\zeta_3(\zeta_6\zeta_{12} - \zeta_8\zeta_{10}) - \zeta_1\zeta_4(\zeta_6\zeta_{11} + \zeta_7\zeta_{10}) + \zeta_2\zeta_3(\zeta_8\zeta_9 - \zeta_5\zeta_{12}) + \\ + \zeta_2\zeta_4(\zeta_5\zeta_{11} - \zeta_7\zeta_9)}, \\ D = \frac{-\zeta_{14}(\zeta_1\zeta_6\zeta_{11} - \zeta_1\zeta_7\zeta_{10} - \zeta_2\zeta_5\zeta_{11} + \zeta_2\zeta_7\zeta_9) + \zeta_3\zeta_{16}(\zeta_1\zeta_6 - \zeta_2\zeta_5) - \\ -\zeta_3\zeta_{15}(\zeta_1\zeta_{10} - \zeta_2\zeta_9) + \zeta_3\zeta_{13}(\zeta_5\zeta_{10} - \zeta_6\zeta_9)}{\zeta_1\zeta_3(\zeta_6\zeta_{12} - \zeta_8\zeta_{10}) - \zeta_1\zeta_4(\zeta_6\zeta_{11} + \zeta_7\zeta_{10}) + \zeta_2\zeta_3(\zeta_8\zeta_9 - \zeta_5\zeta_{12}) + \zeta_2\zeta_4(\zeta_5\zeta_{11} - \zeta_7\zeta_9)}. \end{cases} \quad (232)$$

Afterwards we may analogically apply the above coefficients towards the previous methodology and determine the real time domain solution. However, since further we are keen to present the analytical terms for the physical coefficients determination itself, we continue by implementing the computations of the constructed system of objective functions via the Newton iterative algorithm. First of all, in order to construct the mentioned system, we implement two fundamental theorems of the operational calculus, which are the shifting and similarity that could be presented by the following expression:

$$\begin{cases} \frac{1}{p}e^{-\frac{\sqrt{p}}{\lambda}x} \to Erf\left(\frac{x}{2\lambda\sqrt{t}}\right), \\ \frac{F(\sqrt{p})}{\sqrt{p}} = \frac{1}{\sqrt{p}}\frac{1}{\frac{\sqrt{p}}{a}+h_{ins}}e^{-\frac{\sqrt{p}}{a}x} = \\ = \frac{a}{\sqrt{\pi t}}\int_{\frac{x}{a}}^{\infty} e^{-h_{ins}(\lambda\tau-x)-\frac{\tau^2}{4t}}d\tau\,. \end{cases} \quad (233)$$

Here we substitute by $\xi = \frac{\tau+2\lambda ht}{2\sqrt{t}}$ and deduce the solution in real time domain for the initially pose problem with open boundaries:

$$u(x,t) = u_0\left[erf\left(\frac{x}{2\lambda\sqrt{t}}\right) + e^{hx+a^2h^2t}erfc\left(\frac{x}{2\lambda\sqrt{t}}+\lambda h\sqrt{t}\right)\right] =$$

$$= u_0\left[\frac{2}{\sqrt{\pi}}\int_0^{\frac{x}{2\lambda\sqrt{t}}} e^{-t^2}dt + e^{hx+\lambda^2h^2t}\frac{2}{\sqrt{\pi}}\int_{\frac{x}{2\lambda\sqrt{t}}+\lambda h\sqrt{t}}^{\infty} e^{-t^2}dt\right] =$$

$$= u_0\left[\frac{2}{\sqrt{\pi}}\int_0^{\frac{x}{2\lambda\sqrt{t}}} e^{-t^2}dt + e^{\frac{q}{\lambda u(0,t)}x+\left(\frac{q}{u(0,t)}\right)^2 t}\frac{2}{\sqrt{\pi}}\int_{\left(\frac{x}{2\lambda\sqrt{t}}+\frac{q}{u(0,t)}\sqrt{t}\right)}^{\infty} e^{-t^2}dt\right]. \quad (234)$$

Where u_0 is the initial temperature, q is the heat flux on the inward boundary and has the following form:

$$k_1u_0\left[\frac{2}{\sqrt{\pi}} + h_{ins}e^{\lambda^2h_{ins}^2t}erfc\left(\lambda h_{ins}\sqrt{t}\right) - \frac{2}{\sqrt{\pi}}e^{\lambda^2h_{ins}^2t}e^{-\left(\lambda h_{ins}\sqrt{t}\right)^2}\right] = q. \quad (235)$$

Using above deductions, now we may construct the system by introducing the distance w_i to i^{th} measurement device:

$$\begin{cases} u(w_1,t)-u_0\left[\begin{matrix} erf\left(\frac{\xi\,\rho_1c_1}{2k_1\sqrt{t}}\right)+ \\ +e^{h_{ins}\xi+(k_1\rho_1c_1)^2h_{ins}^2t}erfc\left(\frac{\rho_1c_1(\xi-w_i)}{2k_1\sqrt{t}}+\frac{k_1}{\rho_1c_1}h_{ins}\sqrt{t}\right)\end{matrix}\right]= \\ =f_1\left(k_1^0,\rho_1^0,c_1^0,h_{ins}^0,\right), \\ u(\xi-w_2,t)-u_0\left[\begin{matrix} erf\left(\frac{\xi\,\rho_1c_1}{2k_1\sqrt{t}}\right)+ \\ +e^{h_{ins}\xi+(k_1\rho_1c_1)^2h_{ins}^2t}erfc\left(\frac{\rho_1c_1(\xi-w_i)}{2k\sqrt{t}}+\frac{k_1}{\rho_1c_1}h_{ins}\sqrt{t}\right)\end{matrix}\right]= \\ =f_2\left(k_1^0,\rho_1^0,c_1^0,h_{ins}^0\right), \\ u(\xi+w_3,t)-u_0\left[\begin{matrix} erf\left(\frac{\xi\,\rho_2c_2}{2k_2\sqrt{t}}\right)+ \\ +e^{h_{out}x+(k_2\rho_2c_2)^2h_{out}^2t}erfc\left(\frac{\rho_2c_2(\xi+w_i)}{2k_2\sqrt{t}}+\frac{k_1}{\rho_1c_1}h_{out}\sqrt{t}\right)\end{matrix}\right]= \\ =f_3(k_2^0,\rho_2^0,c_2^0,h_{out}^0), \\ u(L-w_4,t)-u_0\left[\begin{matrix} erf\left(\frac{\xi\,\rho_2c_2}{2k_2\sqrt{t}}\right)+ \\ +e^{h_{out}x+(k_2\rho_2c_2)^2h_{out}^2t}erfc\left(\frac{\rho_2c_2(\xi+w_i)}{2k_2\sqrt{t}}+\frac{k_1}{\rho_1c_1}h_{out}\sqrt{t}\right)\end{matrix}\right]= \\ =f_4(k_2^0,\rho_2^0,c_2^0,h_{out}^0), \\ u(\xi,t)-(f_1)=f_5\left(k_1^0,\rho_1^0,c_1^0,h_{ins}^0,k_2^0,\rho_2^0,c_2^0,h_{out}^0\right) \\ T_{ins}-u_0\left[\begin{matrix} erf\left(\frac{\xi\,\rho_1c_1}{2k_1\sqrt{t}}\right)+ \\ +e^{h_{ins}\xi+(k_1\rho_1c_1)^2h_{ins}^2t}erfc\left(\frac{\rho_1c_1(\xi-w_i)}{2k\sqrt{t}}+\frac{k_1}{\rho_1c_1}h_{ins}\sqrt{t}\right)\end{matrix}\right]= \\ =f_6(k_1^0,\rho_1^0,c_1^0,h_{out}^0), \\ T_{out}-u_0\left[\begin{matrix} erf\left(\frac{\xi\,\rho_2c_2}{2k_2\sqrt{t}}\right)+ \\ +e^{h_{out}x+(k_2\rho_2c_2)^2h_{out}^2t}erfc\left(\frac{\rho_2c_2(\xi+w_i)}{2k_2\sqrt{t}}+\frac{k_1}{\rho_1c_1}h_{out}\sqrt{t}\right)\end{matrix}\right]= \\ =f_7(k_2^0,\rho_2^0,c_2^0,,h_{out}^0), \\ u(\xi,t)-(f_2)=f_6\left(k_1^0,\rho_1^0,c_1^0,h_{ins}^0,k_2^0,\rho_2^0,c_2^0,h_{out}^0\right). \end{cases} \tag{236}$$

Further, we may introduce the vector of unknowns:

$$x^0=\left(k_1^0,\rho_1^0,c_1^0,k_2^0,\rho_2^0,c_2^0,h_{ins}^0,h_{out}^0\right). \tag{237}$$

Also, we introduce the notation for the objective functions that should be minimized via the iterative approach:

$$F(x) = \begin{pmatrix} f_1\left(k_1^0, \rho_1^0, c_1^0, h_{ins}^0,\right) \\ f_2\left(k_1^0, \rho_1^0, c_1^0, h_{ins}^0\right) \\ f_3(k_2^0, \rho_2^0, c_2^0, h_{out}^0) \\ f_3(k_2^0, \rho_2^0, c_2^0, h_{out}^0) \\ f_4(k_2^0, \rho_2^0, c_2^0, h_{out}^0) \\ f_5\left(k_1^0, \rho_1^0, c_1^0, h_{ins}^0, k_2^0, \rho_2^0, c_2^0, h_{out}^0\right) \\ f_6(k_1^0, \rho_1^0, c_1^0, h_{out}^0) \\ f_7(k_2^0, \rho_2^0, c_2^0, h_{out}^0) \\ f_8\left(k_1^0, \rho_1^0, c_1^0, h_{ins}^0, k_2^0, \rho_2^0, c_2^0, h_{out}^0\right) \end{pmatrix}. \quad (238)$$

Afterwards we may write the algorithm in the form of the following recurrent formula:

$$x^{k+1} = x^k - W^{-1}(x^k)F(x^k). \quad (239)$$

Where we have introduced the Wronskian matrix:

$$W = \begin{pmatrix} \frac{\partial f_1}{\partial k_1} & \frac{\partial f_1}{\partial \rho_1} & \frac{\partial f_1}{\partial c_1} & \frac{\partial f_1}{\partial k_2} & \frac{\partial f_1}{\partial \rho_2} & \frac{\partial f_1}{\partial c_2} & \frac{\partial f_1}{\partial h_{ins}} & \frac{\partial f_1}{\partial h_{out}} \\ \frac{\partial f_2}{\partial k_1} & \frac{\partial f_2}{\partial \rho_1} & \frac{\partial f_2}{\partial c_1} & \frac{\partial f_2}{\partial k_2} & \frac{\partial f_2}{\partial \rho_2} & \frac{\partial f_2}{\partial c_2} & \frac{\partial f_2}{\partial h_{ins}} & \frac{\partial f_2}{\partial h_{out}} \\ \frac{\partial f_3}{\partial k_1} & \frac{\partial f_3}{\partial \rho_1} & \frac{\partial f_3}{\partial c_1} & \frac{\partial f_3}{\partial k_2} & \frac{\partial f_3}{\partial \rho_2} & \frac{\partial f_3}{\partial c_2} & \frac{\partial f_3}{\partial h_{ins}} & \frac{\partial f_3}{\partial h_{out}} \\ \frac{\partial f_4}{\partial k_1} & \frac{\partial f_4}{\partial \rho_1} & \frac{\partial f_4}{\partial c_1} & \frac{\partial f_4}{\partial k_2} & \frac{\partial f_4}{\partial \rho_2} & \frac{\partial f_4}{\partial c_2} & \frac{\partial f_4}{\partial h_{ins}} & \frac{\partial f_4}{\partial h_{out}} \\ \frac{\partial f_5}{\partial k_1} & \frac{\partial f_5}{\partial \rho_1} & \frac{\partial f_5}{\partial c_1} & \frac{\partial f_5}{\partial k_2} & \frac{\partial f_5}{\partial \rho_2} & \frac{\partial f_5}{\partial c_2} & \frac{\partial f_5}{\partial h_{ins}} & \frac{\partial f_5}{\partial h_{out}} \\ \frac{\partial f_6}{\partial k_1} & \frac{\partial f_6}{\partial \rho_1} & \frac{\partial f_6}{\partial c_1} & \frac{\partial f_6}{\partial k_2} & \frac{\partial f_6}{\partial \rho_2} & \frac{\partial f_6}{\partial c_2} & \frac{\partial f_6}{\partial h_{ins}} & \frac{\partial f_6}{\partial h_{out}} \\ \frac{\partial f_7}{\partial k_1} & \frac{\partial f_7}{\partial \rho_1} & \frac{\partial f_7}{\partial c_1} & \frac{\partial f_7}{\partial k_2} & \frac{\partial f_7}{\partial \rho_2} & \frac{\partial f_7}{\partial c_2} & \frac{\partial f_7}{\partial h_{ins}} & \frac{\partial f_7}{\partial h_{out}} \\ \frac{\partial f_8}{\partial k_1} & \frac{\partial f_8}{\partial \rho_1} & \frac{\partial f_8}{\partial c_1} & \frac{\partial f_8}{\partial k_2} & \frac{\partial f_8}{\partial \rho_2} & \frac{\partial f_8}{\partial c_2} & \frac{\partial f_8}{\partial h_{ins}} & \frac{\partial f_8}{\partial h_{out}} \end{pmatrix}. \quad (240)$$

For the readability matter, we will present the explicit formulas derivation only for three parameters. However, by using the above notations and below derivation procedure explanations, it could be easily expanded towards eight parameters as well. Further, we will denote by $a = \frac{k}{\rho c_p}$. For the three parameters evaluation we may consider only the left side of multilayered domain and look for the following parameters:

$$\begin{cases} u(\xi, t_1) - u_0 \left[erf\left(\frac{\xi}{2a\sqrt{t_1}}\right) + e^{h\xi + a^2h^2t_1} erfc\left(\frac{\xi}{2a\sqrt{t_1}} + ah\sqrt{t_1}\right)\right] = f_1(a, h, u_0), \\ u(\xi, t_2) - u_0 \left[erf\left(\frac{\xi}{2a\sqrt{t_2}}\right) + e^{hx + a^2h^2t_2} erfc\left(\frac{\xi}{2a\sqrt{t_2}} + ah\sqrt{t_2}\right)\right] = f_2(a, h, u_0), \\ u(\xi, t_3) - u_0 \left[erf\left(\frac{\xi}{2a\sqrt{t_3}}\right) + e^{hx + a^2h^2t_2} erfc\left(\frac{\xi}{2a\sqrt{t_3}} + ah\sqrt{t_3}\right)\right] = f_2(a, h, u_0). \end{cases} \tag{241}$$

The Wronskian in this case will be a 3×3 matrix with the minimization goal functions and unknown vectors:

$$\begin{cases} W = \begin{pmatrix} \frac{\partial f_1}{\partial a} & \frac{\partial f_1}{\partial h} & \frac{\partial f_1}{\partial u_0} \\ \frac{\partial f_2}{\partial a} & \frac{\partial f_2}{\partial h} & \frac{\partial f_2}{\partial u_0} \\ \frac{\partial f_3}{\partial a} & \frac{\partial f_3}{\partial h} & \frac{\partial f_3}{\partial u_0} \end{pmatrix}, \\ x^0 = (a^0, h^0, u_0^0), \\ F(x) = \begin{pmatrix} f_1(a, h, u_0) \\ f_2(a, h, u_0) \\ f_3(a, h, u_0) \end{pmatrix}. \end{cases} \tag{242}$$

In order to perform the (238) recurrent formula, we have to determine the inverse of Wronskian W^{-1} by the Transposed matrix of Wronskian algebraic complements $\mathrm{W}_*^{\mathrm{T}}$ as well as the Wronskian determinant $|W|$, such that $W^{-1} = \frac{\mathrm{W}_*^{\mathrm{T}}}{|\mathrm{W}|}$:

$$|W| = \left|\begin{pmatrix} \frac{\partial f_1}{\partial a} & \frac{\partial f_1}{\partial h} & \frac{\partial f_1}{\partial u_0} \\ \frac{\partial f_2}{\partial a} & \frac{\partial f_2}{\partial h} & \frac{\partial f_2}{\partial u_0} \\ \frac{\partial f_3}{\partial a} & \frac{\partial f_3}{\partial h} & \frac{\partial f_3}{\partial u_0} \end{pmatrix}\right| = \frac{\partial f_1}{\partial a}\begin{pmatrix} \frac{\partial f_2}{\partial h} & \frac{\partial f_2}{\partial u_0} \\ \frac{\partial f_3}{\partial h} & \frac{\partial f_3}{\partial u_0} \end{pmatrix} - \frac{\partial f_1}{\partial h}\begin{pmatrix} \frac{\partial f_2}{\partial a} & \frac{\partial f_2}{\partial u_0} \\ \frac{\partial f_3}{\partial a} & \frac{\partial f_3}{\partial u_0} \end{pmatrix} +$$

$$\frac{\partial f_1}{\partial u_0}\begin{pmatrix} \frac{\partial f_2}{\partial a} & \frac{\partial f_2}{\partial h} \\ \frac{\partial f_3}{\partial a} & \frac{\partial f_3}{\partial h} \end{pmatrix} =$$

$$= \frac{\partial f_1}{\partial a}\left(\frac{\partial f_2}{\partial h}\frac{\partial f_3}{\partial u_0} - \frac{\partial f_3}{\partial h}\frac{\partial f_2}{\partial u_0}\right) - \frac{\partial f_1}{\partial h}\left(\frac{\partial f_2}{\partial a}\frac{\partial f_3}{\partial u_0} - \frac{\partial f_3}{\partial a}\frac{\partial f_2}{\partial u_0}\right) +$$

$$+ \frac{\partial f_1}{\partial u_0}\left(\frac{\partial f_2}{\partial a}\frac{\partial f_3}{\partial h} - \frac{\partial f_3}{\partial a}\frac{\partial f_2}{\partial h}\right) =$$

$$= \frac{\partial f_1}{\partial a}\frac{\partial f_2}{\partial h}\frac{\partial f_3}{\partial u_0} - \frac{\partial f_1}{\partial a}\frac{\partial f_3}{\partial h}\frac{\partial f_2}{\partial u_0} - \frac{\partial f_1}{\partial h}\frac{\partial f_2}{\partial a}\frac{\partial f_3}{\partial u_0} + \frac{\partial f_1}{\partial h}\frac{\partial f_3}{\partial a}\frac{\partial f_2}{\partial u_0} + \frac{\partial f_1}{\partial u_0}\frac{\partial f_2}{\partial a}\frac{\partial f_3}{\partial h} -$$
$$- \frac{\partial f_1}{\partial u_0}\frac{\partial f_3}{\partial a}\frac{\partial f_2}{\partial h}.$$

(243)

At the same time the transposed matrix of Wronskian algebraic complements will take the following form:

$$W_*^T = \begin{pmatrix} \begin{pmatrix} \frac{\partial f_2}{\partial h} & \frac{\partial f_2}{\partial u_0} \\ \frac{\partial f_3}{\partial h} & \frac{\partial f_3}{\partial u_0} \end{pmatrix} & -\begin{pmatrix} \frac{\partial f_1}{\partial h} & \frac{\partial f_1}{\partial u_0} \\ \frac{\partial f_3}{\partial h} & \frac{\partial f_3}{\partial u_0} \end{pmatrix} & \begin{pmatrix} \frac{\partial f_1}{\partial h} & \frac{\partial f_1}{\partial u_0} \\ \frac{\partial f_2}{\partial h} & \frac{\partial f_2}{\partial u_0} \end{pmatrix} \\ -\begin{pmatrix} \frac{\partial f_2}{\partial a} & \frac{\partial f_2}{\partial u_0} \\ \frac{\partial f_3}{\partial a} & \frac{\partial f_3}{\partial u_0} \end{pmatrix} & \begin{pmatrix} \frac{\partial f_1}{\partial a} & \frac{\partial f_1}{\partial u_0} \\ \frac{\partial f_3}{\partial a} & \frac{\partial f_3}{\partial u_0} \end{pmatrix} & -\begin{pmatrix} \frac{\partial f_1}{\partial a} & \frac{\partial f_1}{\partial u_0} \\ \frac{\partial f_2}{\partial a} & \frac{\partial f_2}{\partial u_0} \end{pmatrix} \\ \begin{pmatrix} \frac{\partial f_2}{\partial a} & \frac{\partial f_2}{\partial h} \\ \frac{\partial f_3}{\partial a} & \frac{\partial f_3}{\partial h} \end{pmatrix} & -\begin{pmatrix} \frac{\partial f_1}{\partial a} & \frac{\partial f_1}{\partial h} \\ \frac{\partial f_3}{\partial a} & \frac{\partial f_3}{\partial h} \end{pmatrix} & \begin{pmatrix} \frac{\partial f_1}{\partial a} & \frac{\partial f_1}{\partial h} \\ \frac{\partial f_2}{\partial a} & \frac{\partial f_2}{\partial h} \end{pmatrix} \end{pmatrix}. \quad (244)$$

Further the inverse matrix will have the following expression:

$$W^{-1} = \frac{W_*^T}{|W|} =$$

$$= \frac{1}{|W|}\begin{pmatrix} \frac{\partial f_2}{\partial h}\frac{\partial f_3}{\partial u_0} - \frac{\partial f_3}{\partial h}\frac{\partial f_2}{\partial u_0} & -\left(\frac{\partial f_1}{\partial h}\frac{\partial f_3}{\partial u_0} - \frac{\partial f_3}{\partial h}\frac{\partial f_1}{\partial u_0}\right) & \frac{\partial f_1}{\partial h}\frac{\partial f_2}{\partial u_0} - \frac{\partial f_1}{\partial u_0}\frac{\partial f_2}{\partial h} \\ -\left(\frac{\partial f_2}{\partial a}\frac{\partial f_3}{\partial u_0} - \frac{\partial f_2}{\partial u_0}\frac{\partial f_3}{\partial a}\right) & \frac{\partial f_1}{\partial a}\frac{\partial f_3}{\partial u_0} - \frac{\partial f_1}{\partial u_0}\frac{\partial f_3}{\partial a} & -\left(\frac{\partial f_1}{\partial a}\frac{\partial f_2}{\partial u_0} - \frac{\partial f_1}{\partial u_0}\frac{\partial f_2}{\partial a}\right) \\ \frac{\partial f_2}{\partial a}\frac{\partial f_3}{\partial h} - \frac{\partial f_2}{\partial h}\frac{\partial f_3}{\partial a} & -\left(\frac{\partial f_1}{\partial a}\frac{\partial f_3}{\partial h} - \frac{\partial f_1}{\partial h}\frac{\partial f_3}{\partial a}\right) & \frac{\partial f_1}{\partial a}\frac{\partial f_2}{\partial h} - \frac{\partial f_1}{\partial h}\frac{\partial f_2}{\partial a} \end{pmatrix}. \quad (245)$$

By simplifying and opening some factors in the above expression, we may obtain:

$$W^{-1}(x^k)F(x^k) =$$

$$= \begin{pmatrix} \frac{\left(\frac{\partial f_2}{\partial h}\frac{\partial f_3}{\partial u_0} - \frac{\partial f_3}{\partial h}\frac{\partial f_2}{\partial u_0}\right)f_1 - \left(\frac{\partial f_1}{\partial h}\frac{\partial f_3}{\partial u_0} - \frac{\partial f_3}{\partial h}\frac{\partial f_1}{\partial u_0}\right)f_2 + \left(\frac{\partial f_1}{\partial h}\frac{\partial f_2}{\partial u_0} - \frac{\partial f_1}{\partial u_0}\frac{\partial f_2}{\partial h}\right)f_3}{\frac{\partial f_1}{\partial a}\frac{\partial f_2}{\partial h}\frac{\partial f_3}{\partial u_0} - \frac{\partial f_1}{\partial a}\frac{\partial f_3}{\partial h}\frac{\partial f_2}{\partial u_0} - \frac{\partial f_1}{\partial h}\frac{\partial f_2}{\partial a}\frac{\partial f_3}{\partial u_0} + \frac{\partial f_1}{\partial h}\frac{\partial f_3}{\partial a}\frac{\partial f_2}{\partial u_0} + \frac{\partial f_1}{\partial u_0}\frac{\partial f_2}{\partial a}\frac{\partial f_3}{\partial h} - \frac{\partial f_1}{\partial u_0}\frac{\partial f_3}{\partial a}\frac{\partial f_2}{\partial h}} \\ \frac{-\left(\frac{\partial f_2}{\partial a}\frac{\partial f_3}{\partial u_0} - \frac{\partial f_2}{\partial u_0}\frac{\partial f_3}{\partial a}\right)f_1 + \left(\frac{\partial f_1}{\partial a}\frac{\partial f_3}{\partial u_0} - \frac{\partial f_1}{\partial u_0}\frac{\partial f_3}{\partial a}\right)f_2 - \left(\frac{\partial f_1}{\partial a}\frac{\partial f_2}{\partial u_0} - \frac{\partial f_1}{\partial u_0}\frac{\partial f_2}{\partial a}\right)f_3}{\frac{\partial f_1}{\partial a}\frac{\partial f_2}{\partial h}\frac{\partial f_3}{\partial u_0} - \frac{\partial f_1}{\partial a}\frac{\partial f_3}{\partial h}\frac{\partial f_2}{\partial u_0} - \frac{\partial f_1}{\partial h}\frac{\partial f_2}{\partial a}\frac{\partial f_3}{\partial u_0} + \frac{\partial f_1}{\partial h}\frac{\partial f_3}{\partial a}\frac{\partial f_2}{\partial u_0} + \frac{\partial f_1}{\partial u_0}\frac{\partial f_2}{\partial a}\frac{\partial f_3}{\partial h} - \frac{\partial f_1}{\partial u_0}\frac{\partial f_3}{\partial a}\frac{\partial f_2}{\partial h}} \\ \frac{\left(\frac{\partial f_2}{\partial a}\frac{\partial f_3}{\partial h} - \frac{\partial f_2}{\partial h}\frac{\partial f_3}{\partial a}\right)f_1 - \left(\frac{\partial f_1}{\partial a}\frac{\partial f_3}{\partial h} - \frac{\partial f_1}{\partial h}\frac{\partial f_3}{\partial a}\right)f_2 + \left(\frac{\partial f_1}{\partial a}\frac{\partial f_2}{\partial h} - \frac{\partial f_1}{\partial h}\frac{\partial f_2}{\partial a}\right)f_3}{\frac{\partial f_1}{\partial a}\frac{\partial f_2}{\partial h}\frac{\partial f_3}{\partial u_0} - \frac{\partial f_1}{\partial a}\frac{\partial f_3}{\partial h}\frac{\partial f_2}{\partial u_0} - \frac{\partial f_1}{\partial h}\frac{\partial f_2}{\partial a}\frac{\partial f_3}{\partial u_0} + \frac{\partial f_1}{\partial h}\frac{\partial f_3}{\partial a}\frac{\partial f_2}{\partial u_0} + \frac{\partial f_1}{\partial u_0}\frac{\partial f_2}{\partial a}\frac{\partial f_3}{\partial h} - \frac{\partial f_1}{\partial u_0}\frac{\partial f_3}{\partial a}\frac{\partial f_2}{\partial h}} \end{pmatrix}. \quad (246)$$

From the above identity, we may explicitly deduce the unknown physical coefficients:

$$x^k - W^{-1}(x^k)F(x^k) =$$

$$= \begin{pmatrix} a^k - \frac{\left(\frac{\partial f_2}{\partial h}\frac{\partial f_3}{\partial u_0} - \frac{\partial f_3}{\partial h}\frac{\partial f_2}{\partial u_0}\right)f_1 - \left(\frac{\partial f_1}{\partial h}\frac{\partial f_3}{\partial u_0} - \frac{\partial f_3}{\partial h}\frac{\partial f_1}{\partial u_0}\right)f_2 + \left(\frac{\partial f_1}{\partial h}\frac{\partial f_2}{\partial u_0} - \frac{\partial f_1}{\partial u_0}\frac{\partial f_2}{\partial h}\right)f_3}{\frac{\partial f_1}{\partial a}\frac{\partial f_2}{\partial h}\frac{\partial f_3}{\partial u_0} - \frac{\partial f_1}{\partial a}\frac{\partial f_3}{\partial h}\frac{\partial f_2}{\partial u_0} - \frac{\partial f_1}{\partial h}\frac{\partial f_2}{\partial a}\frac{\partial f_3}{\partial u_0} + \frac{\partial f_1}{\partial h}\frac{\partial f_3}{\partial a}\frac{\partial f_2}{\partial u_0} + \frac{\partial f_1}{\partial u_0}\frac{\partial f_2}{\partial a}\frac{\partial f_3}{\partial h} - \frac{\partial f_1}{\partial u_0}\frac{\partial f_3}{\partial a}\frac{\partial f_2}{\partial h}} \\ h^k - \frac{-\left(\frac{\partial f_2}{\partial a}\frac{\partial f_3}{\partial u_0} - \frac{\partial f_2}{\partial u_0}\frac{\partial f_3}{\partial a}\right)f_1 + \left(\frac{\partial f_1}{\partial a}\frac{\partial f_3}{\partial u_0} - \frac{\partial f_1}{\partial u_0}\frac{\partial f_3}{\partial a}\right)f_2 - \left(\frac{\partial f_1}{\partial a}\frac{\partial f_2}{\partial u_0} - \frac{\partial f_1}{\partial u_0}\frac{\partial f_2}{\partial a}\right)f_3}{\frac{\partial f_1}{\partial a}\frac{\partial f_2}{\partial h}\frac{\partial f_3}{\partial u_0} - \frac{\partial f_1}{\partial a}\frac{\partial f_3}{\partial h}\frac{\partial f_2}{\partial u_0} - \frac{\partial f_1}{\partial h}\frac{\partial f_2}{\partial a}\frac{\partial f_3}{\partial u_0} + \frac{\partial f_1}{\partial h}\frac{\partial f_3}{\partial a}\frac{\partial f_2}{\partial u_0} + \frac{\partial f_1}{\partial u_0}\frac{\partial f_2}{\partial a}\frac{\partial f_3}{\partial h} - \frac{\partial f_1}{\partial u_0}\frac{\partial f_3}{\partial a}\frac{\partial f_2}{\partial h}} \\ u_0^k - \frac{\left(\frac{\partial f_2}{\partial a}\frac{\partial f_3}{\partial h} - \frac{\partial f_2}{\partial h}\frac{\partial f_3}{\partial a}\right)f_1 - \left(\frac{\partial f_1}{\partial a}\frac{\partial f_3}{\partial h} - \frac{\partial f_1}{\partial h}\frac{\partial f_3}{\partial a}\right)f_2 + \left(\frac{\partial f_1}{\partial a}\frac{\partial f_2}{\partial h} - \frac{\partial f_1}{\partial h}\frac{\partial f_2}{\partial a}\right)f_3}{\frac{\partial f_1}{\partial a}\frac{\partial f_2}{\partial h}\frac{\partial f_3}{\partial u_0} - \frac{\partial f_1}{\partial a}\frac{\partial f_3}{\partial h}\frac{\partial f_2}{\partial u_0} - \frac{\partial f_1}{\partial h}\frac{\partial f_2}{\partial a}\frac{\partial f_3}{\partial u_0} + \frac{\partial f_1}{\partial h}\frac{\partial f_3}{\partial a}\frac{\partial f_2}{\partial u_0} + \frac{\partial f_1}{\partial u_0}\frac{\partial f_2}{\partial a}\frac{\partial f_3}{\partial h} - \frac{\partial f_1}{\partial u_0}\frac{\partial f_3}{\partial a}\frac{\partial f_2}{\partial h}} \end{pmatrix}. \quad (247)$$

That gives us an opportunity to determine the following identities for recurrent evaluation of the physical parameters:

$$\begin{cases} a^{k+1} = a^k - \dfrac{\left(\frac{\partial f_2}{\partial h}\frac{\partial f_3}{\partial u_0} - \frac{\partial f_3}{\partial h}\frac{\partial f_2}{\partial u_0}\right)f_1 - \left(\frac{\partial f_1}{\partial h}\frac{\partial f_3}{\partial u_0} - \frac{\partial f_3}{\partial h}\frac{\partial f_1}{\partial u_0}\right)f_2 + \left(\frac{\partial f_1}{\partial h}\frac{\partial f_2}{\partial u_0} - \frac{\partial f_1}{\partial u_0}\frac{\partial f_2}{\partial h}\right)f_3}{\frac{\partial f_1}{\partial a}\frac{\partial f_2}{\partial h}\frac{\partial f_3}{\partial u_0} - \frac{\partial f_1}{\partial a}\frac{\partial f_3}{\partial h}\frac{\partial f_2}{\partial u_0} - \frac{\partial f_1}{\partial h}\frac{\partial f_2}{\partial a}\frac{\partial f_3}{\partial u_0} + \frac{\partial f_1}{\partial h}\frac{\partial f_3}{\partial a}\frac{\partial f_2}{\partial u_0} + \frac{\partial f_1}{\partial u_0}\frac{\partial f_2}{\partial a}\frac{\partial f_3}{\partial h} - \frac{\partial f_1}{\partial u_0}\frac{\partial f_3}{\partial a}\frac{\partial f_2}{\partial h}}, \\ h^{k+1} = h^k - \dfrac{-\left(\frac{\partial f_2}{\partial a}\frac{\partial f_3}{\partial u_0} - \frac{\partial f_2}{\partial u_0}\frac{\partial f_3}{\partial a}\right)f_1 + \left(\frac{\partial f_1}{\partial a}\frac{\partial f_3}{\partial u_0} - \frac{\partial f_1}{\partial u_0}\frac{\partial f_3}{\partial a}\right)f_2 - \left(\frac{\partial f_1}{\partial a}\frac{\partial f_2}{\partial u_0} - \frac{\partial f_1}{\partial u_0}\frac{\partial f_2}{\partial a}\right)f_3}{\frac{\partial f_1}{\partial a}\frac{\partial f_2}{\partial h}\frac{\partial f_3}{\partial u_0} - \frac{\partial f_1}{\partial a}\frac{\partial f_3}{\partial h}\frac{\partial f_2}{\partial u_0} - \frac{\partial f_1}{\partial h}\frac{\partial f_2}{\partial a}\frac{\partial f_3}{\partial u_0} + \frac{\partial f_1}{\partial h}\frac{\partial f_3}{\partial a}\frac{\partial f_2}{\partial u_0} + \frac{\partial f_1}{\partial u_0}\frac{\partial f_2}{\partial a}\frac{\partial f_3}{\partial h} - \frac{\partial f_1}{\partial u_0}\frac{\partial f_3}{\partial a}\frac{\partial f_2}{\partial h}}, \\ u_0^{k+1} = u_0^k - \dfrac{\left(\frac{\partial f_2}{\partial a}\frac{\partial f_3}{\partial h} - \frac{\partial f_2}{\partial h}\frac{\partial f_3}{\partial a}\right)f_1 - \left(\frac{\partial f_1}{\partial a}\frac{\partial f_3}{\partial h} - \frac{\partial f_1}{\partial h}\frac{\partial f_3}{\partial a}\right)f_2 + \left(\frac{\partial f_1}{\partial a}\frac{\partial f_2}{\partial h} - \frac{\partial f_1}{\partial h}\frac{\partial f_2}{\partial a}\right)f_3}{\frac{\partial f_1}{\partial a}\frac{\partial f_2}{\partial h}\frac{\partial f_3}{\partial u_0} - \frac{\partial f_1}{\partial a}\frac{\partial f_3}{\partial h}\frac{\partial f_2}{\partial u_0} - \frac{\partial f_1}{\partial h}\frac{\partial f_2}{\partial a}\frac{\partial f_3}{\partial u_0} + \frac{\partial f_1}{\partial h}\frac{\partial f_3}{\partial a}\frac{\partial f_2}{\partial u_0} + \frac{\partial f_1}{\partial u_0}\frac{\partial f_2}{\partial a}\frac{\partial f_3}{\partial h} - \frac{\partial f_1}{\partial u_0}\frac{\partial f_3}{\partial a}\frac{\partial f_2}{\partial h}}. \end{cases} \quad (248)$$

The only part that we have to demonstrate for the derived set of parameters is the construction of the system of partial derivatives expressions:

$$\begin{cases} -u_0\left[-\frac{\xi}{a^2}\frac{2}{\sqrt{\pi}}e^{-\frac{\xi^2}{4a^2t_1}} + 2ae^{h\xi}e^{a^2h^2t_1}erfc\left(\frac{\xi}{2a\sqrt{t_1}} + ah\sqrt{t_1}\right) - \frac{e^{h\xi}e^{a^2h^2t_1}2e^{\left(\frac{\xi}{2a\sqrt{t_1}}+ah\sqrt{t_1}\right)^2\left(-\frac{\xi}{2a^2\sqrt{t_1}}+h\sqrt{t_1}\right)}}{\sqrt{\pi}}\right] = \frac{\partial f_1}{\partial a}, \\ -u_0\left[-\frac{\xi}{a^2}\frac{2}{\sqrt{\pi}}e^{-\frac{\xi^2}{4a^2t_2}} + 2ae^{h\xi}e^{a^2h^2t_2}erfc\left(\frac{\xi}{2a\sqrt{t_2}} + ah\sqrt{t_2}\right) - \frac{e^{h\xi}e^{a^2h^2t_2}2e^{\left(\frac{\xi}{2a\sqrt{t_2}}+ah\sqrt{t_2}\right)^2\left(-\frac{\xi}{2a^2\sqrt{t_2}}+h\sqrt{t_2}\right)}}{\sqrt{\pi}}\right] = \frac{\partial f_2}{\partial a}, \\ -u_0\left[-\frac{\xi}{a^2}\frac{2}{\sqrt{\pi}}e^{-\frac{\xi^2}{4a^2t_3}} + 2ae^{h\xi}e^{a^2h^2t_3}erfc\left(\frac{\xi}{2a\sqrt{t_3}} + ah\sqrt{t_3}\right) - \frac{e^{h\xi}e^{a^2h^2t_3}2e^{\left(\frac{\xi}{2a\sqrt{t_3}}+ah\sqrt{t_3}\right)^2\left(-\frac{\xi}{2a^2\sqrt{t_3}}+h\sqrt{t_3}\right)}}{\sqrt{\pi}}\right] = \frac{\partial f_3}{\partial a}. \end{cases} \quad (249)$$

Which are the partial derivatives with respect to the first physical parameter. Then we have the similar system for the second parameter:

$$\begin{cases} -u_0\left[\begin{array}{c}(\xi+2a^2t_1)e^{h\xi+a^2h^2t_1}erfc\left(\frac{\xi}{2a\sqrt{t_1}}+ah\sqrt{t_1}\right)- \\ -2\frac{e^{\left(\frac{\xi}{2a\sqrt{t_1}}+ah\sqrt{t_1}\right)^2}e^{h\xi+a^2h^2t_1}a\sqrt{t_1}}{\sqrt{\pi}}\end{array}\right]=\frac{\partial f_1}{\partial h}, \\ -u_0\left[\begin{array}{c}(\xi+2a^2t_2)e^{h\xi+a^2h^2t_2}erfc\left(\frac{\xi}{2a\sqrt{t_2}}+ah\sqrt{t_2}\right)- \\ -2\frac{e^{\left(\frac{\xi}{2a\sqrt{t_2}}+ah\sqrt{t_2}\right)^2}e^{h\xi+a^2h^2t_2}a\sqrt{t_2}}{\sqrt{\pi}}\end{array}\right]=\frac{\partial f_2}{\partial h}, \\ -u_0\left[\begin{array}{c}(\xi+2a^2t_3)e^{h\xi+a^2h^2t_3}erfc\left(\frac{\xi}{2a\sqrt{t_3}}+ah\sqrt{t_3}\right)- \\ -2\frac{e^{\left(\frac{\xi}{2a\sqrt{t_3}}+ah\sqrt{t_3}\right)^2}e^{h\xi+a^2h^2t_3}a\sqrt{t_3}}{\sqrt{\pi}}\end{array}\right]=\frac{\partial f_3}{\partial h}. \end{cases} \quad (250)$$

For the third physical parameter, which is the initial temperature in this case, we construct the following system:

$$\begin{cases} -\left[erf\left(\frac{\xi}{2a\sqrt{t_1}}\right)+e^{h\xi+a^2h^2t_1}erfc\left(\frac{\xi}{2a\sqrt{t_1}}+ah\sqrt{t_1}\right)\right]=\frac{\partial f_1}{\partial u_0}, \\ -\left[erf\left(\frac{\xi}{2a\sqrt{t_2}}\right)+e^{h\xi+a^2h^2t_2}erfc\left(\frac{\xi}{2a\sqrt{t_2}}+ah\sqrt{t_2}\right)\right]=\frac{\partial f_2}{\partial u_0}, \\ -\left[erf\left(\frac{\xi}{2a\sqrt{t_3}}\right)+e^{h\xi+a^2h^2t_3}erfc\left(\frac{\xi}{2a\sqrt{t_3}}+ah\sqrt{t_3}\right)\right]=\frac{\partial f_3}{\partial u_0}. \end{cases} \quad (251)$$

After we have derived all necessary terms, we may conclude that (248) are the explicit analytical expressions for the physical parameter's determination together with the above depicted notations and observations.

CONCLUSION

The presented PhD thesis was completed in the accordance to all necessary provisions and legislation standards. During the implementation of the conducted work, there were performed international research and pedagogical practices. All derivations and deductions were performed in cooperative advisory contacts with the local and research supervisors. General results approbations were described and published in [93 – 94].

The posed problems in the current thesis were completed to the full extent and beyond, since we have demonstrated the general analytical inverse analysis methodology derived towards the multiphysical processes with layered structure and various formulations of the boundary conditions along with homogenized and non-homogenized measurement samples.

Beside the achieved goal, the presented thesis results are the fruitful subject for the further fundamental investigations, since it presents and discusses principal epistemology that could be enriched further to extend the general formulation of the inverse problems theory in terms of the regularization, stability, and solution derivation issues.

We may also conclude that the constructed multiphysical mathematical and computer models present separate interest in terms of the derived analytical expressions, mentioned as the direct problems in our work. The expressions obtained by various approaches, including the integral transforms, functional constructions and proving the posed lemmas and theorems could be utilized further in sense of the technical engineering or theoretical investigations.

REFERENCES

1 Ambarzumian, V. Über die Beziehung zwischen der Lösung und der Resolvente der Integralgleichung des Strahlungs-gleichgewichts // Z. Physik. – 1929. – Vol. 52, – P. 263–267

2 Carlos E. Puente, A universe of projections: may Plato be right? // Chaos, Solitons & Fractals. – 2004, Vol. 19, № 2, – P. 241–253.

3 Couprie, D.L. Aristotle's Arguments for the Sphericity of the Earth. In: When the Earth Was Flat. Historical & Cultural Astronomy. – Springer, Cham., 2018, – P. 241–260.

4 Claudia M. Schmidt, Kant's transcendental and empirical psychology of cognition // Studies in History and Philosophy of Science Part A. – 2008, Vol. 39, № 4, P. 462-472.

5 Strutt, J. The Theory of Sound. Cambridge Library Collection - Physical Sciences. – Cambridge: Cambridge University Press, 2011.

6 Hulin, G., Maneuvrier, C., Tabbagh, A., & Vincent, J. What exists beneath the place where Conrad Schlumberger carried out the first (1912) electrical prospection experiment: the Val-Richer Abbey // Near Surface Geophysics. – 2018. Vol. 16, № 4, – P. 445–460.

7 Hadamard J. Sur les problèmes aux dérivées partielles et leur signification physique. // Princeton university bulletin. – 1902. – P. 49–52.

8 Tikhonov A.N. On the solution of ill-posed problems and the method of regularization. // Doklady Akademii Nauk. – 1963. – Vol. 151б № 3. 1963.

9 Colaço M.J., Orlande H.R.B., Dulikravich G.S. Inverse and optimization problems in heat transfer // Journal of the Brazilian Society of Mechanical Sciences and Engineering. – 2006. Vol. 28, № 1. – P. 1–24.

10 S. Szénási, Z. Fried and I. Felde. Training of Artificial Neural Network to Solve the Inverse Heat Conduction Problem. // IEEE 18th World Symposium on Applied Machine Intelligence and Informatics (SAMI). – 2020. – P. 293–298.

11 Dooyoul L., Dongsu C. Analysis of the reliability of a starter-generator using a dynamic Bayesian network // Reliability Engineering & System Safety. – 2020. – Vol. 195.

12 Masanori M., Hirofumi A., Wei L., Yuhichi M., Jaffar A. H. An analytical solution for two-dimensional inverse heat conduction problems using Laplace transform // International Journal of Heat and Mass Transfer. – 2003. – Vol. 46, № 12. – P 2135–2148.

13 Ahmet S. E., Amir M., Ragnar L. An ML-based approach for inverse identification of heat flux in machining // Procedia CIRP. – 2022. – Vol. 115. – P. 208–213.

14 Trilok G., Vishweshwara P.S., Gnanasekaran N. Inverse estimation of heat flux under forced convection conjugate heat transfer in a vertical channel fully filled with metal foam // Thermal Science and Engineering Progress. – 2022. – Vol. 33.

15 Han-Taw C., Ming-Hsun H., Kai-Chen Y., Kuei-Hao C., Kuo-Chi L. Study of inverse natural convection-conduction heat transfer for in-line tube heat exchanger in a hot box with experimental data // Journal of the Taiwan Institute of Chemical Engineers. – 2022. – Vol. 141.

16 Nan C., Xiang L., Hui T. A Bayesian model to solve a two-dimensional inverse heat transfer problem of gas turbine discs // Applied Thermal Engineering. – 2022. – Vol. 214.

17 Michele C. Solution of an inverse heat conduction problem with third-type boundary conditions // International Journal of Thermal Sciences. – 2022. – Vol. 175.

18 Camila F. G., Rens N., Cees W. M. G., Hans G.M. K., Mustafa B., Bart P.M. E. Inaccuracies in the inverse heat conduction problem solution and their effect on the estimation of heat fluxes during quenching // International Journal of Heat and Mass Transfer. – 2022. – Vol. 194.

19 Mohammad A., Muhammad M. S. Inverse analysis of mould-casting interfacial heat transfer towards improved castings // Materials Today: Proceedings. – 2022. – Vol. 56, № 2. – P. 742–748.

20 Andrzej F., Agnieszka W., Michał C. Trefftz numerical functions for solving inverse heat conduction problems // International Journal of Thermal Sciences. – 2022. – Vol. 177.

21 Michael F. M, Sandip M. Inverse Radiative Heat Transfer. Radiative Heat Transfer (Fourth Edition). – Academic Press, 2022. – P. 859-885.

22 Shibin W., Kun W., Peng X., Yajin H. Numerical and experimental verification of the single neural adaptive PID real-time inverse method for solving inverse heat conduction problems // International Journal of Heat and Mass Transfer. – 2022. – Vol. 189.

23 Ardeshir B., Xiaobing Z., Yogesh J. Solution to inverse natural convection problem using experimental data // International Journal of Heat and Mass Transfer. – 2022. – Vol. 189.

24 Han-Taw C., Wei-Yen S., Yu-Jun Z., Tian-Shiang Y., Kuan-Xun C. Prediction of 3D natural convection heat transfer characteristics in a shallow enclosure with experimental data // Progress in Nuclear Energy. – 1970. – Vol. 153.

25 Oliveira A.V.S., Avrit A., Gradeck M. Thermocouple response time estimation and temperature signal correction for an accurate heat flux calculation in inverse heat conduction problems // International Journal of Heat and Mass Transfer. – 2022. – Vol. 185.

26 Changuk A., Chanhun P., Dong I.P., Jin-Gyun K. Optimal hybrid parameter selection for stable sequential solution of inverse heat conduction problem // International Journal of Heat and Mass Transfer. – 2022. – Vol. 183.

27 Tokuma H., Hitoshi F. Evaluating surface heat flux in planar water-jet cooling of moving hot solid by inversely solving steady-state heat conduction // International Journal of Heat and Mass Transfer. – 2022. – Vol 197.

28 Roberto B., Amit K., Anna C., Gianluca G., Nicola P., Andrea M., Giuseppe R. Thermal diffusivity from Fourier's inverse problem supervised by an optimization model: Theoretical analysis and experimental validation // Case Studies in Thermal Engineering. – 2022. – Vol. 40.

29 Obinna U., Hamidreza N. A novel solution for inverse heat conduction problem in one-dimensional medium with moving boundary and temperature-dependent material properties // International Journal of Heat and Mass Transfer. – 2022. – Vol. 182.

30 Naoko I., Fabio B., Luca P., Luca C., Pamela V., Matteo M., Sara R. Characterization of thermal behavior of a micro pulsating heat pipe by local heat transfer investigation // International Journal of Heat and Mass Transfer. – 2022. – Vol. 196.

31 Bapuji S., Subharthi S., Sivakumar R., Sekhar T.V.S. The effect of rotating fluid with Taylor column on forced convective heat transfer // International Communications in Heat and Mass Transfer. – 2022. – Vol. 137.

32 Ji Zh., Han Y., Ning M., Zhe Y. Estimation of solid concentration in solid–liquid two-phase flow in horizontal pipeline using inverse-problem approach // Particuology. – 2022. – Vol. 62. – P. 1-13.

33 Shawn S., Reid A. B., Karen A. T. Two-layer transient heat transfer using impulse response methods // International Journal of Heat and Mass Transfer. – 2022. – Vol. 187.

34 Bo Y., Geyong C., Shanhong R., Yanpeng G., Chunying D. An isogeometric boundary element method for transient heat transfer problems in inhomogeneous materials and the non-iterative inversion of loads // Applied Thermal Engineering. – 2022. – Vol. 212.

35 Lei L., Hao Z., Yu X., Wei L. Inverse modeling of thermal boundary conditions in commercial aircrafts based on Green's function and regularization method // Building and Environment. – 2022. – Vol. 217.

36 Baiyi L., Jixiong Z., Jipeng C., Hao Y., Hengfeng L. An analytical solution to periodical heat transfer problems of multilayer rocks for thermal energy storage in underground mines // Journal of Energy Storage. – 2022. – Vol. 50.

37 Kentaro Y., Shintaro Y., Kikuo F. Data-driven multifidelity topology design using a deep generative model: Application to forced convection heat transfer problems // Computer Methods in Applied Mechanics and Engineering. – 2022 Vol. 388.

38 Tobias K., Rico P., Jens W., Marc H. An experimental approach to determine local heat transfer characteristics in additively manufactured cooling configurations // International Journal of Heat and Mass Transfer. – 2022. – Vol. 185.

39 Miao C., Chunyun Zh., Bowen Zh., Bingbing X., Haifeng P., Xiao-wei G., Numerical solution of phase change heat transfer problems by effective heat capacity

model and element differential method // Journal of Computational Science. – 2022. – Vol. 60.

40 Theera H., Suradech S., Ratinun L., Bundit K. Study on heat transfer in two-layer porous media with heat generation in porous media // Energy Reports. – 2022. – Vol. 8. – P. 1565-1576.

41 Tian Zh., Wei A., Huan M., Zheng L., Qun C. Integral identification of fluid specific heat capacity and heat transfer coefficient distribution in heat exchangers based on multiple-case joint analysis // International Journal of Heat and Mass Transfer. – 2022. – Vol. 185.

42 Jaco D., Hannalie S., Josua P. M. The effect of circumferentially non-uniform heat flux on flow boiling heat transfer in a horizontal tube // International Journal of Heat and Mass Transfer. – 2022. – Vol. 185.

43 Saima B., Ghulam R., Nawa A., Ilyas K., Hajra K., Nawaf H. Numerical analysis of heat and mass transfer in micropolar nanofluids flow through lid driven cavity: Finite volume approach // Case Studies in Thermal Engineering. – 2022. – Vol. 37.

44 Oliveira A.V.S., Maréchal D., Borean J.L., Schick V., Teixeira J., Denis S., Gradeck M. Experimental study of the heat transfer of single-jet impingement cooling onto a large heated plate near industrial conditions // International Journal of Heat and Mass Transfer. – 2022. – Vol. 184.

45 Mohammad P., Ankur J. Eigenfunction-based solution for one-dimensional solid-liquid phase change heat transfer problems with advection // International Journal of Thermal Sciences. – 2022. – Vol. 172.

46 Jiachang T., Xiao L., Yong L., Qishui Y., Jianghong Y., Chengji M., Chunming F. A surrogate model based active interval densifying method for nonlinear inverse problems // Structures. – 2022. Vol. 45. – P. 695-706.

47 Massa L. Multiresolution Reconstruction of the Hypersonic Heat Flux // International Journal of Heat and Mass Transfer. – 2022. – Vol. 190.

48 Vanitha G. P, Mahabaleshwar U.S., Shadloo M.S. An impact of Richardson number on mixed convective flow of nanoparticles with heat and mass transfer // International Communications in Heat and Mass Transfer. – 2022. – Vol. 139.

49 Liu Y., Gao Y., Zhu P., Zou Y., Dong Z. Study on heat transfer model of roughness wall in supersonic two-phase flow of solid rocket motor // International Communications in Heat and Mass Transfer. – 2022. – Vol. 138.

50 Habib-ur-Rehman S., Adnan Q., Rabia S., Zahid A., Muhammad A., Muhammad F., Muhammad M. A., Shahid I., Hassan A., Yunus K. T.M., Fahad N., Hafiz M. A., Kalam M.A., Manzoore E. M. S. Heat transfer and pressure drop characteristics of ZnO/DIW based nanofluids in small diameter compact channels: An experimental study // Case Studies in Thermal Engineering. – 2022. – Vol. 39.

51 Fengyuan L., Xiaoshu C., Tianyi C. Inverse transfer function identification for high-frequency pressure probes using M-sequence pressure generators, Flow Measurement and Instrumentation. – 2022. – Vol. 87.

52 Mashhadi A., Sohankar A. Two- and three-dimensional simulations of flow and heat transfer around rectangular cylinders // Computers & Fluids. – 2022. – Vol. 249.

53 Hisham E., Xiaobing Z., Mohammednour G., Mozdalifah A. Numerical investigation of pentagonal V-shape ribs to enhance heat transfer in hydrogen rocket engine cooling channels // International Journal of Hydrogen Energy. – 2022. – Vol. 47, № 56. P. 23871–23886.

54 Pierre L.M., Nicolas B., Jean-Luc B., Nicolas L., Thierry G., Jean-Marc V. Development of an original overmoulding device to analyse heat transfer at polymer/polymer interface during overmoulding // Applied Thermal Engineering. – 2022. – Vol. 216.

55 Davydova M.A., Zakharova S.A. Multidimensional thermal structures in the singularly perturbed stationary models of heat and mass transfer with a nonlinear thermal diffusion coefficient // Journal of Computational and Applied Mathematics. – 2022. – Vol. 400.

56 Elliott J.W., Lebon M.T., Robinson A.J. Optimising integrated heat spreaders with distributed heat transfer coefficients: A case study for CPU cooling // Case Studies in Thermal Engineering. – 2022. – Vol. 38.

57 Basharat U., Bandar M. F., Basim M. M., Kottakkaran S. N., Hafiz A. W., Umar K. Heat transfer analysis in Darcy Forchheimer flow of hybrid nanofluid for multiple shape effects over a curved stretching surface // Case Studies in Thermal Engineering. – 2022. – Vol. 40.

58 Shahab M., Suhas S. J., Ali M. A computational model for interfacial heat and mass transfer in two-phase flows using a phase field method // International Journal of Heat and Mass Transfer. – 2022. – Vol. 197.

59 Avijit K., Sumanta A. Numerical simulation of falling film sensible heat transfer over round horizontal tubes // International Journal of Heat and Mass Transfer. – 2022. – Vol. 190.

60 Qingying L., Lu H., Weichen P., Senyun L., Tian B. Three-dimensional ice shape detection based on flash pulse infrared thermal wave testing // Case Studies in Thermal Engineering. – 2022. – Vol. 36.

61 Jérémie L., Marc M., Pascal L., Stéphane B., Christophe C., Frédéric T. Comprehensive correlation for the prediction of the heat transfer through a single droplet in dropwise condensation regime // Applied Thermal Engineering. – 2022. – Vol. 209.

62 Amir S., Mohammad G., Alireza M. N. Heat transfer enhancement in mini channel heat sinks utilizing corona wind: A numerical study // International Journal of Heat and Mass Transfer. – 2022. – Vol. 182.

63 Wen-Wei J., Geng-Hui J., Chen-Hao T., Kai Y., Xiao-Wei G. A new method for identifying temperature-dependent thermal conductivity in transient heat conduction problems based on element differential method // Engineering Analysis with Boundary Elements. – 2022. – Vol. 137. – P. 65–77.

64 Kelvin C., Renato M. C., Carolina P. N.C., Péricles C. P. Heat transfer analysis of compressible laminar flow in a parallel-plates channel via integral transforms // International Communications in Heat and Mass Transfer. – 2022. – Vol. 138.

65 Zbigniew M., Beata H., Agnieszka C. R. Inverse solutions to a vertical plate cooling in air – a comparative study // International Journal of Heat and Mass Transfer. – 2022. – Vol. 188.

66 Sehra, Sami U. H., Saeed U. J., Rubi B., Jawaher H. A., Ilyas K., Abeer A. Heat-mass transfer of MHD second grade fluid flow with exponential heating, chemical reaction and porosity by using fractional Caputo-Fabrizio derivatives // Case Studies in Thermal Engineering. – 2022. – Vol. 36.

67 Oulghelou M., Beghein C., Allery C. A surrogate optimization approach for inverse problems: Application to turbulent mixed-convection flows // Computers & Fluids. – 2022. – Vol. 241.

68 Aqiang L., Gaowen L., Ran C., Yan C., Qing F. Comprehensive evaluations of heat transfer performance with conjugate heat dissipation effect in high-speed rotating free-disk system of aero-engines // Fundamental Research. – 2022.

69 Sarra R., Walid H., Lioua K., Patrice E. Heat transfer by oil natural convection in an annular space under combined effects of carbon nanotubes and electric field // International Communications in Heat and Mass Transfer. – 2022. – Vol. 138.

70 Yingxiong L., Cheng S. Stochastic heat transfer analysis and reliability assessment under non-stationary random thermal load using the explicit time-domain method // International Journal of Heat and Mass Transfer. – 2022. – Vol. 194.

71 Sina S., Mohsen J., Hossein A., Hossein A. D. A. MHD heat and mass transfer nanofluid flow on a porous cylinder with chemical reaction and viscous dissipation effects: Benchmark solutions // Case Studies in Thermal Engineering. – 2022. – Vol. 40.

72 Rabie A. A. S., Farah R. A., Nadeen A. Effect of mesh refinement on the solution of the inverse uncertainty quantification problem for transient physics // Progress in Nuclear Energy. – 2022. – Vol. 152.

73 Mohsen S., Alan C., Michel V. A review on the heat transfer in asphalt pavements and urban heat island mitigation methods // Construction and Building Materials. – 2022. – Vol. 359.

74 Uday S. D., Amit R., Pavel A. P. Determination of temperature distribution in cold forging with the support of inverse analysis // Measurement. – 2022. – Vol. 187.

75 Hui W., Bingzhu L., Zhiguo Q., Pingwen M. Moving impingement heat transfer in a three-dimensional rarefied hydrogen gas jet based on the direct simulation Monte Carlo method coupled with the finite difference method // International Journal of Heat and Mass Transfer. – 2022. – Vol. 188.

76 Veera K. M. Numerical investigation on steady natural convective flow past a perpendicular wavy surface with heat absorption/generation // International Communications in Heat and Mass Transfer. – 2022. – Vol. 139.

77 Karchevsky A.L., Rysbayuly B.R. Analytical expressions for a solution of convective heat and moisture transfer equations in the frequency domain for layered media // Eurasian journal of mathematical and computer applications. – 2015. – Vol. 3, № 4. – P. 55–67.

78 Kulik L.M., Shapavalov G.E. Unsteady heat transfer through a multilayer flat plate // Izv. USSR Academy of Sciences, Energy and Automation. – 1961. Vol. 1, № 2. – P. 72–77.

79 Kogan M.G. Non-stationary thermal conductivity in layered media // JTP. – Vol. 27, № 3. – P. 522–533.

80 Robert E., Franca S., Patrick J. Hierarchical regularization of solution ambiguity in underdetermined inverse and optimization problems // Journal of Computational Physics: X. – 2022. – Vol. 13.

81 Huiqing L., Heping M. Error estimate of a Legendre-Galerkin Chebyshev collocation method for a class of parabolic inverse problem // Applied Numerical Mathematics. – 2021. – Vol. 170. – P. 179–189.

82 Toby S., Rodrigo B. P., Robert D. S. Effective new methods for automated parameter selection in regularized inverse problems // Applied Numerical Mathematics. – 2020. – Vol. 152. P. 29–48.

83 Abdelhak H., Hacene S. Integral equations method for solving a Biharmonic inverse problem in detection of Robin coefficients // Applied Numerical Mathematics. – 2021. – Vol. 160. – P. 436–450.

84 Chengzhi L., Xuli H., Li Z. Unconditional convergence of iterative approximation methods // Engineering Analysis with Boundary Elements. – 2021. – Vol. 126. – P. 161–168.

85 Gaurav M., Ankik K. G. Convergence rates for iteratively regularized Gauss–Newton method subject to stability constraints // Journal of Computational and Applied Mathematics. – 2022. – Vol. 400.

86 Yiqin L., Liang B., Qinghua W. On the convergence rate of an iterative method for solving nonsymmetric algebraic Riccati equations // Computers & Mathematics with Applications. – 2021. – Vol. 62. – P. 4178–4184.

87 Heydar A. K., Zangian M., Minuchehr A., Zolfaghari A. An improved convergence rate for the prompt α eigenvalue calculation in α-k iteration methods // Annals of Nuclear Energy. – 2018. – Vol. 118. P. 15–25.

88 Chun-Hua G., Wen W. L. Convergence rates of some iterative methods for nonsymmetric algebraic Riccati equations arising in transport theory // Linear Algebra and its Applications. – 2010. – Vol. 432, № 1. – P. 283–291.

89 Daniel M., Marino A. Nonlinear manifold learning for model reduction in finite elastodynamics // Computer Methods in Applied Mechanics and Engineering. – 2013. – Vol. 261–262. – P. 118–131.

90 Quang A. D., Quang L. D. A unified approach to study the existence and numerical solution of functional differential equation // Applied Numerical Mathematics. – 2021. – Vol. 170. – P. 208–218.

91 Fatemeh P. A. B., Mehdi N.–K., Lothar R. Iterative Tikhonov regularization of tensor equations based on the Arnoldi process and some of its generalizations // Applied Numerical Mathematics. – 2020. – Vol. 151. P. 425–447.

92 Petra W., Patryk W., Rico Z. Bounded weak solutions of time-fractional porous medium type and more general nonlinear and degenerate evolutionary integro-differential equations // Journal of Mathematical Analysis and Applications. – 2021. – Vol. 499, № 1.

93 Rysbaiuly B. R., Sinitsa A. V., Capsoni A. Analytical Inverse Analysis Methodological Approach for Thermo-Physical Parameters Estimation of Multilayered Medium Terrain with Homogenized Sampled Measurements // Symmetry. – 2022, № 14.

94 Sinitsa A.V., Capsoni A. Design of novel inverse analysis methodology for exact estimation of elasticity parameters in thermoelastic stress model // International Communications in Heat and Mass Transfer. – 2022. – Volume 135.

APPENDIX A - Notes for the conjugate problem derived for the thermoelastic stress analysis inverse methodology analytical solution

The conjugate model (A.1) – (A.4), deduced in the multilayered medium: $x \in \Omega$:

$$\rho c \frac{\partial \psi}{\partial t} + \frac{\partial}{\partial x}\left(\lambda_n \frac{\partial \psi}{\partial x}\right) = 0 \ . \tag{A.1}$$

$$\left(h_{out}\psi - \lambda_n \frac{\partial \psi}{\partial x}\right)|_{x=0} = 2\left(T - Tg_1(t)\right)|_{x=0}. \tag{A.2}$$

$$\left(h_{ins}\psi + \lambda_n \frac{\partial \psi}{\partial x}\right)|_{x=L} = 2\left(T - Tg_2(t)\right)|_{x=L}. \tag{A.3}$$

$$\psi|_{t=T_m} = \psi(x, T_m) = 0. \tag{A.4}$$

Further we utilize the Laplace transform towards the above model:

$$\mathcal{L}\left[\frac{\lambda}{\rho c_p}\frac{\partial^2 \psi}{\partial x^2}\right] = \frac{\lambda_n}{\rho c_p}\left[\begin{matrix} p^2\tilde{\psi}(p,t) - p\psi(0,t) - \\ -\frac{2p}{\lambda_n}\left(u[0,t] - Tg_1(t)\right) - h_{ins}\psi p \end{matrix}\right] = 0 \tag{A.5}$$

By applying the conjugate boundary conditions, we deduce that:

$$\tilde{\psi}(p,t) = \frac{\rho c_p \psi(0,t)}{\lambda_n p} - \frac{2\rho c_p}{\lambda_n^2 p}\left(u[0,t] - Tg_1(t)\right) - \frac{\rho c_p h_{ins}\psi}{\lambda_n p} \tag{A.6}$$

While the inverse Laplace transform has the following form:

$$\mathcal{L}^{-1}\left\{\frac{c\psi(0,t)}{\lambda_n p} - \frac{2\rho c_p}{\lambda_n^2 p}\left(u[0,t] - Tg_1(t)\right) - \frac{\rho c_p h_{ins}\psi}{\lambda_n p}\right\} =$$

$$= \mathcal{L}^{-1}\left\{\frac{c\psi(0,t)}{\lambda_n p} - \frac{2\rho c_p}{\lambda_n^2 p}\left(u[0,t] - Tg_1(t)\right) - \frac{c h_{ins}\psi}{\lambda_n p}\right\} =$$

$$= \left[\frac{c\psi(0,t)}{\lambda_n}\theta(x) - \frac{2c}{\lambda_n^2}\left(u[0,t] - Tg_1(t)\right)\theta(x) \ - \frac{c h_{ins}\psi}{\lambda_n}\theta(x)\right], \ x \in \Omega. \tag{A.7}$$

We have implemented the following properties of the Laplace transform:

$$\begin{cases} \mathcal{L}^{-1}\{af(s)+bg(s)\} = a\mathcal{L}^{-1}\{f(s)\}+b\mathcal{L}^{-1}\{g(s)\}, \\ \mathcal{L}^{-1}\left\{\frac{c}{s}\right\} = c\theta(t), \\ \mathcal{L}^{-1}\{1\} = \delta(t). \end{cases} \tag{A.8}$$

Here we have utilized the Heaviside step function and the Dirac delta function respectively:

$$\begin{cases} \theta(x) = \begin{cases} 0, x < 0, \\ 1, x \geq 0. \end{cases}' \\ \delta(x) = \lim_{b\to 0} \frac{1}{|b|\sqrt{\pi}} e^{-\left(\frac{x}{b}\right)^2}. \end{cases} \tag{A.9}$$

APPENDIX B - The title page for the firstly mentioned article reprint

International Communications in Heat and Mass Transfer 135 (2022) 106096

Contents lists available at ScienceDirect

International Communications in Heat and Mass Transfer

journal homepage: www.elsevier.com/locate/ichmt

Design of novel inverse analysis methodology for exact estimation of elasticity parameters in thermoelastic stress model

Artem V. Sinitsa [a,*], Antonio Capsoni [b]

[a] School of Mathematics and Cybernetics, Kazakh-British Technical University, Tole bi st., 59 050050 Almaty, Kazakhstan
[b] Department of Architecture, Built Environment and Construction Engineering, Polytechnic University of Milan, Piazza Leonardo da Vinci 32, 20133 Milan, Italy

ARTICLE INFO

Keywords:
Thermoelastic effect
Inverse problems
Analytical expressions
Thermodynamics of continuum

ABSTRACT

This paper presents general outlines of the research conducted in the applied mathematics field, – the theory of inverse problems, specifically utilized for the thermoelastic stress analysis model for exact estimation of thermo-elasticity parameters. We present formulation of the well posed direct mathematical model that depicts general interconnections between physically governed fields for thermally heated plate subjected to fixed constrains on the boundaries with small deformations from thermal expansion over the homogeneous multilayered medium domain. Applying elements of variational calculus, functional analysis and fractional order derivatives, we demonstrate the derivation of the conjugate problem and analytical expressions used for exact estimation of structural material thermoelastic properties. The novelty of proposed methodology lies in derivation of exact estimators that could be utilized for general homogenized thermoelastic model with finite amount of sampled temperature measurements on the domain outlets. It also opens curtains over the key issues and some important aspects aroused in the derivation procedures of exact estimators for general problem statement. There were posed and discussed necessary conditions in a form of a working hypothesizes. Results may be utilized as an experimental technique designed to obtain an essential information on the surface stress field along with the thermoelastic material properties.

1. Introduction of the problem statement

The subject area of interest is the novel theory of inverse problems with its prospective and promising opportunities utilized for the field of thermoelastic stress analysis modeling. In our paper we present the special case of application for such theory in terms of thermo-elasticity parameters estimation for structural materials. The necessity is dictated by the needs of design stage of construction service for any artificial structure. For such purpose, we investigate general structural elements' that are commonly used in the development process of engineering constructions. In modern practice it is crucial to operate with accurate data regarding the structural elements' material mechanical and physical properties that are relevant to model and simulate precise prime loads and major displacements distributions. Sufficiently small variations in such data may result in unpredictable outcomes with dramatic circumstances [1–4]. However, there is a majority of empirical methods prevailing in a modern practice useful to determine indicated material parameters' quantities. Most of commonly utilized empirical methods require the conduction of empirical estimation in laboratory conditions which consequentially leads to increase of time and cost of production services [5–7]. Thus, the development of suggested methodology eventually will lead to an increase of simulations accuracy level and decrease in a cost of production allowing us fully to eliminate or to keep the probability of numerical and measurements error occurrences at prescribed tolerance level. For this purpose, we start our investigation by setting up proper thermoelastic stress analysis model that will establish the stress-thermal relationship which is used further for estimation of the key material configuration parameters analytically applying key elements of the theory of inverse problems. To obtain corresponding posteriori estimators we construct appropriate mappings in terms of the functional relations supporting its relevance by numerical computations conducted delicately with respect to the build model. Implementation of investigated inverse theory approach for suggested model eliminates the necessity of empirical data sampling allowing us to escape the usage of laboratory experiments and providing us with possibility to determine the key material parameters of system configuration on site. It is still a matter of importance to set a relevant direct problem that will depict the general physical fields interconnections describing them in terms of a system of partial differential equations.

* Corresponding author.
E-mail address: a.sinitsa@kbtu.kz (A.V. Sinitsa).

https://doi.org/10.1016/j.icheatmasstransfer.2022.106096

Available online 7 May 2022
0735-1933/© 2022 Elsevier Ltd. All rights reserved.

APPENDIX C - The publication certificate of the MDPI editorial office for the second mentioned research paper

symmetry

an Open Access Journal by MDPI

CITESCORE 4.3

IMPACT FACTOR 2.940

CERTIFICATE OF PUBLICATION

Certificate of publication for the article titled:

Analytical Inverse Analysis Methodological Approach for Thermo-Physical Parameters Estimation of Multilayered Medium Terrain with Homogenized Sampled Measurements

Authored by:

Bolatbek Rysbaiuly; Artem Sinitsa; Antonio Capsoni

Published in:

Symmetry **2022**, Volume 14, Issue 11, 2248

MDPI Academic Open Access Publishing since 1996

Basel, October 2022